Controlling the Radical Polymerization of Polyacrylamide from the Surface of Activated Carbon for Flocculation Applications

A Thesis Submitted to the Committee on Graduate Studies in Partial Fulfillment of the Requirements for the Degree of Master of Science in the Faculty of Arts and Science

TRENT UNIVERSITY

Peterborough, Ontario, Canada

Materials Science M.Sc. Graduate Program

January 2025

Abstract

Controlling the Radical Polymerization of Polyacrylamide from the Surface of Activated Carbon for Flocculation Applications

Kyle Matthew D. Reyes

The oil sands industry is producing large volumes of tailings waste reaching 2 billion cubic meters by 2034.[1] In this study, the industrial standard flocculant, high molecular weight PAM, was grafted from the surface of activated carbon (AC). This material was designed to increase the flocculant's hydrophobicity and density. Different molecular weight PAM was grafted from AC with different AC contents and particle sizes (AC-PAMs). The AC-PAMs were synthesized by surface-initiated atom transfer radical polymerization (SI-ATRP). The AC-PAMs achieved molecular weights 107 – 5,600 kg/mol and AC content of 0.2 – 5.8% on <0.1 and 0.1 – 0.5 mm AC particle diameters. AC-PAM achieved higher solids contents up to 51 wt% using AC-PAM with 5.1 wt% AC due to the grafting from a hydrophobic AC core. To summarize, our work shows the successful grafting of PAM from AC and its potential as a flocculant for mature fine tailings.

Keywords

Activated carbon, polyacrylamide, surface-initiated polymerization, grafting-from, atom transfer radical polymerization, mature fine tailings, flocculation

Acknowledgments

Firstly, I would like to express my gratitude to my supervisor, Dr. Andrew J. Vreugdenhil, for his tremendous support, guidance, and patience throughout the completion of my thesis. The past few years have been a wonderful experience, and I am forever thankful for this opportunity. I also want to extend a special thanks to Oliver Strong and Dr. Kevin Scotland for all their help, advice, and technical expertise during my research. I am also grateful to everyone else at the Trent Inorganic Materials Research Laboratory, including Tyler Roy, Kelly Wright, Kyle Fisher, Elmira Nazari, Hamant France, Teagan Carr, Nethma Dissanayake, Tate Mazurkewich, Lora Vassiliadis, and Joshua Tapp. Additionally, I would like to thank Paul Pede from Carbonix Inc. for his support throughout my research. I would also like to acknowledge my committee members, Dr. Eric Keske and Dr. Olena Zenkina, for their valuable input over the course of this work. I am also thankful to my family for their unwavering support, even while being halfway across the world. Finally, I want to express my gratitude to my partner, Kyla Bruce, and my friends, who have provided me with encouragement and a sense of family while being away from home.

Table of Contents

Abstract ii

Keywords ii

Acknowledgments iii

List of Figures ix

List of Tables xii

List of Equations xiv

List of Abbreviations and Symbols xvi

Abbreviations xvi

Symbols xix

1. Introduction 1

1.1. Mature Fine Tailings 1

1.2. Dewatering Oil Sand Tailings 2

1.2.1. Consolidated Tailings 2

1.2.2. Paste Technology 3

1.2.2.1. Polymeric Flocculants 3

1.3. Polymer Brushes 7

1.4. Reversible-Deactivation Radical Polymerization (RDRP) 8

1.4.1. Features of a Reversible-Deactivation Radical Process (RDRP) 10

1.4.2. Atom Transfer Radical Polymerization (ATRP) 13

1.5. Activated Carbon (AC) 16

1.5.1. Surface Initiated Atom Transfer Radical Polymerization (SI-ATRP) of Polyacrylamide from the Surface of Activated Carbon 17

1.6. Thesis Objectives 18

2. Key Experimental Techniques 19

2.1. Key Characterization Techniques 19

2.1.1. Size Exclusion Chromatography (SEC) 19

2.1.2. Raman Spectroscopy 22

2.1.3. X-ray Photoelectron Spectroscopy 24

2.2. Key Techniques for Measuring Flocculation 25

2.2.1. Dean-Stark Extraction 25

2.2.2. Settling Rate 26

2.2.3. Capillary Suction Time 27

2.2.4. Supernatant Turbidity 28

2.2.5. Solids Content 28

3. Controlled Radical Polymerization of Polyacrylamide 29

3.1. Introduction 29

3.2. Materials and Methods 34

3.2.1. Materials 34

3.2.2. Activator Regenerated by Electron Transfer Atom Transfer Radical Polymerization (ARGET ATRP) of Polyacrylamide 35
3.2.3. Standard Atom Transfer Radical Polymerization (ATRP) of Polyacrylamide 35
3.2.4. Characterization 36
3.3. Results and Discussion 36
3.3.1. Raman spectroscopy of Polyacrylamide 36
3.3.2. Effect of feeding the reducing agent and temperature 37
3.3.3. Effect of halide salt and solvent 38
3.3.5. Increasing Degree of Polymerization (DP) 41
3.4. Conclusions 42
4. Surface Initiated Atom Transfer Radical Polymerization from Activated Carbon 43
4.1. Introduction 43
4.2. Materials and Methods 45
4.2.1. Materials 45
4.2.2. Preparation of Activated Carbon from Petroleum Coke 46
4.2.3. Preparation of oxidized activated carbon (AC-OH) 46
4.2.4. Preparation of initiator grafted activated carbon 47
4.2.5. Surface-initiated ATRP of acrylamide from AC-Init (AC-PAM) 48
4.2.5.1. Standard ATRP 48
4.2.5.2. ARGET ATRP 48

4.2.6. Hydrolysis of PAM from AC-PAM 48
4.2.7. Characterization 49
4.3. Results and Discussion 50
4.3.1. Characterization of AC-PAM 50
4.3.2. Molecular weight determination 55
4.3.3. Thermogravimetric analysis (TGA) 57
5. Flocculation performance of AC-PAM 59
5.1. Introduction 59
5.2. Materials and Methods 63
5.2.1. Materials 63
5.2.2. Preparation of AC-PAM 63
5.2.3. Dean-Stark Extraction 63
5.2.4. Settling Tests 63
5.2.5. Characterization 64
5.3. Results and Discussion 64
5.3.1. Dean-Stark Extraction 64
5.3.2. Flocculation Performance 65
5.4. Conclusions 71
6. Conclusions 73
6.1. General Conclusions 73

6.2. Future Work 74

6.3. Contributions to Science 76

6.3.1. Publications and Patents 76

6.3.2. Conferences 76

Appendix 77

Supplementary Figures 77

References 78

List of Figures

Figure 1.1 Structure of a) non-ionic PAM, b) cationic PAM (PAM-co-PDADMAC), c) anionic PAM (PAM-co-PAA), and d) hydrophobic PAM (PAM-c-P(t-BAAM). 4

Figure 1.2 Possible polymeric flocculant conformations following adsorption. (A) single point attachment; (B) loop adsorption; (C) flat multiple site adsorption; (D) high molecular weight random coil; (E) non-uniform segment distribution; and (F) multilayer adsorption. 4

Figure 1.3 Fabrication of polymer brushes using a) grafting-to, b) grafting-from, and c) grafting through strategy. 8

Figure 1.4 Reversible radical trapping through a deactivation/activation process. 9

Figure 1.5 Degenerative exchange process. 10

Figure 1.6 Features of RDRP: a) dependence of $\ln([M]_0/[M])$ over time and b) dependence of the number average molecular weight (M_n) on monomer conversion.[43] 11

Figure 1.7 ATRP Scheme 13

Figure 1.8 Potential oxygen and nitrogen functional groups on the surface of AC. 17

Figure 3.1 ATRP Scheme 30

Figure 3.2 Competing side reactions in aqueous ATRP of PAM 31

Figure 3.3 Monomer conversion of acrylamide to polyacrylamide (PAM) 37

Figure 3.4 Raman spectra of PAM synthesized in Runs A to O. Reaction conditions for Runs A to O are listed in Tables 3.1 to 3.4. 37

Figure 3.5 Normalized RID Signal vs molecular weight of PAM synthesized from Run A and Run K 41

Figure 4.1 Synthesis scheme for the preparation of initiator-modified ACs 45

Figure 4.2 FTIR of oxidized AC ($AC_{0.1\text{-}0.5\text{-}OH}$), alkyl bromide-modified AC ($AC_{0.1\text{-}0.5}$-Br), alkyl chloride-modified AC ($AC_{0.1\text{-}0.5}$-Cl), polyacrylamide grafted AC ($AC_{0.1\text{-}0.5}$-Br-$PAM_{20k,\ Std}$), and polyacrylamide (PAM). 51

Figure 4.3 High-resolution C 1s scans with synthetic components for activated carbon ($AC_{0.1\text{-}0.5}$), oxidized AC ($AC_{0.1\text{-}0.5}$-OH), alkyl-bromide functionalized AC ($AC_{0.1\text{-}0.5}$-Br), alkyl-chloride functionalized AC ($AC_{0.1\text{-}0.5}$-Cl), polyacrylamide grafted from AC ($AC_{0.1\text{-}0.5}$-Br-$PAM_{20k,\ Std}$).... 53

Figure 4.4 High-resolution (bottom) Cl 2p scan of alkyl chloride functionalized AC ($AC_{0.1\text{-}0.5}$-Cl) (top), Br 3d scan of alkyl bromide functionalized AC ($AC_{0.1\text{-}0.5}$-Br) (middle), and ($AC_{0.1}$-Br) (bottom) with synthetic components fitted. 53

Figure 5.1 Initial settling rates (ISR) of flocculated 5 wt% MFT with aluminum sulphate (alum), polyacrylamide (PAM), and polyacrylamide grafted from AC (AC-PAM)..... 67

Figure 5.2 From left to right, 5 wt% MFT treated with 2,500 ppm Free PAM, 15,000 ppm $AC_{0.1\text{-}0.5}$-Cl-$PAM_{5k,\ EtOH,\ NaCl}$, 2,500 ppm $AC_{<0.1}$-Br-$PAM_{20k,\ Std}$, 5,000 ppm $AC_{0.1\text{-}0.5}$-Br-$PAM_{20k,\ Std}$, 5,000 ppm $AC_{<0.1}$-Br-$PAM_{2k,\ Std}$, 5,000 ppm $AC_{0.1\text{-}0.5}$-Br-$PAM_{2k,\ Std}$, 5,000 ppm $AC_{<0.1}$-Br-$PAM_{20k,\ ARGET}$, 5,000 ppm $AC_{0.1\text{-}0.5}$-Br-$PAM_{20k,\ ARGET}$ after 10 minutes of settling..... 68

Figure 5.3 Capillary suction times (CST) of flocculated 5 wt% MFT with aluminum sulphate (alum), polyacrylamide (PAM), and polyacrylamide grafted from AC (AC-PAM) 68

Figure 5.4 Supernatant turbidities of flocculated 5 wt% MFT with aluminum sulphate (alum), polyacrylamide (PAM), and polyacrylamide grafted from AC (AC-PAM)..... 69

Figure 5.5 Solids contents of flocculated 5 wt% MFT with aluminum sulphate (alum), polyacrylamide (PAM), and polyacrylamide grafted from AC (AC-PAM)..... 70

Figure S0.1 FTIR spectra of oxidized AC ($AC_{<0.1}$-OH), bromine initiator grafted AC ($AC_{<0.1}$-Br), polyacrylamide grafted from AC ($AC_{0.1\text{-}0.5}$-Cl-$PAM_{5k,\ EtOH,\ NaCl}$, $AC_{<0.1}$-Br-$PAM_{20k,\ Std}$,

$AC_{<0.1}$-Br-$PAM_{2k,\ Std}$, $AC_{0.1\text{-}0.5}$-Br-$PAM_{2k,\ Std}$, $AC_{<0.1}$-Br-$PAM_{20k,\ ARGET}$, and $AC_{0.1\text{-}0.5}$-Br-$PAM_{20k,\ ARGET}$) 77

Figure S0.2 High resolution C 1s scans of activated carbon ($AC_{<0.1}$), oxidized AC ($AC_{<0.1}$-OH), bromine initiator grafted AC ($AC_{<0.1}$-Br), and polyacrylamide grafted ACs ($AC_{0.1\text{-}0.5}$-Cl-$PAM_{5k,\ EtOH,\ NaCl}$, $AC_{<0.1}$-Br-$PAM_{20k,\ Std}$, $AC_{<0.1}$-Br-$PAM_{2k,\ Std}$, $AC_{0.1\text{-}0.5}$-Br-$PAM_{2k,\ Std}$, $AC_{<0.1}$-Br-$PAM_{20k,\ ARGET}$, and $AC_{0.1\text{-}0.5}$-Br-$PAM_{20k,\ ARGET}$)..... 77

List of Tables

Table 3.1 The effect of feeding reducing agent and temperature to the monomer conversion, theoretical number average molecular weight (Mn, theo), experimental number and weight average molecular weight (Mn, exp and Mw, exp), and dispersity of the ARGET ATRP of PAM 38

Table 3.2 The effect of halide salt choice and concentration, and solvent choice on the monomer conversion, theoretical number average molecular weight ($M_{n,\ theo}$), experimental number, weight average molecular weight ($M_{n,\ exp}$ and $M_{w,\ exp}$), and dispersity of the ARGET ATRP of PAM ... 39

Table 3.3 The effect of halide salt concentration and ligand/metal catalyst complex to the monomer conversion, theoretical number average molecular weight ($M_{n,\ theo}$), experimental number and weight average molecular weight ($M_{n,\ exp}$ and $M_{w,\ exp}$), and dispersity of the ARGET ATRP of PAM 40

Table 3.4 Ultra-high molecular weight PAM (Degree of Polymerization = 20,000) and their monomer conversion, theoretical number average molecular weight ($M_{n,\ theo}$), experimental number and weight average molecular weight ($M_{n,\ exp}$ and $M_{w,\ exp}$), and dispersity of the ATRP of PAM 42

Table 4.1 Elemental composition in atomic % of standard, oxidized, bromine-initiator, and chlorine-initiator functionalized ACs with particle diameters <0.1 mm and 0.1-0.5 mm from XPS survey scans 52

Table 4.2 Weight %, the concentration of Br and Cl on the surface of AC, and mass required to reach DP =[M]/[I]= 20k 54

Table 4.3 Mass recovery, number (M_n) and weight (M_w) average molecular weight of AC-PAM synthesized using different ATRP conditions of Run M, N, and O from Chapter 3, particle size, and degree of polymerization..... 55

Table 4.4 Residual weight % at 1,000ºC and AC content of PAM and different AC-PAMs..... 58

Table 5.1 The composition of MFT determined from Dean-Stark extraction 65

Table 5.2 PAM and AC-PAM with different AC content, M_n, and M_w evaluated for flocculation of 5 wt% MFT..... 66

List of Equations

Equation 1 Rate of polymerization 10

Equation 2 Persistent radical effect 10

Equation 3 Degree of polymerization 11

Equation 4 Dispersity 12

Equation 5 Electron transfer between metal complexes 14

Equation 6 Heterolytic cleavage of the metal halide bond 14

Equation 7 Electron affinity of the halogen 14

Equation 8 Bond dissociation energy of the propagating chain end and alkyl halide initiator 14

Equation 9 ATRP equilibrium 14

Equation 10 Rate of polymerization due to activator-deactivator ratios 15

Equation 11 Number average molecular weight 20

Equation 12 Weight average molecular weight 20

Equation 13 Dispersity 20

Equation 14 Elution volume of the analyte 20

Equation 15 Refractive index of a dilute solution 21

Equation 16 Concentration of the sample in solution 21

Equation 17 Monomer conversion 24

Equation 18 Binding energy 24

Equation 19 Relation of the degree of polymerization to monomer conversion 33

Equation 20 Theoretical number average molecular weight 33

Equation 21 Experimental dispersity 34

Equation 22 Conversion to weight percent from atomic percent 54

Equation 23 Concentration of halide on the surface of AC in moles per gram of AC..... 54

Equation 24 Amount of AC initiator required to reach a specified degree of polymerization.... 54

Equation 25 Volume of aluminum sulphate required..... 63

List of Abbreviations and Symbols

Abbreviations

AA	acrylic acid
AC	activated carbon
AC-Br	bromine initiator grafted activated carbon
AC-Cl	chlorine initiator grafted activated carbon
AC-PAM	polyacrylamide grafted activated carbon
AC-OH	oxidized activated carbon
Alum	aluminum sulfate
AMPS	2-acrylamide-2-methyl-1-propanesulfonic acid
APS	ammonium persulfate
ARGET	attenuated total reflectance
ATR	activators regenerated by electron transfer
BE	binding energy
BiBB	α-bromoisobutyrylbromide
BPY	bipyridine
CPC	2-chloropropionyl chloride
CST	capillary suction time
CTA	chain transfer agent
DADMAC	diallyl dimethyl ammonium chloride
DCM	dichloromethane
DMAP	4-dimethylaminopyridine

DMC/DAC	acryloyloxyethyl trimethylammonium chloride
DP	degree of polymerization
EBiB	ethyl α-bromoisobutyrate
ECP	ethyl 2-chloropropionate
EDL	electrical double layer
FTIR	fourier transform infrared spectroscopy
H_2SO_4	sulfuric acid
HADE	poly(N-acryloyl-1,2-diaminoethane hydrochloride)
ISR	initial settling rate
KE	kinetic energy
KOH	potassium hydroxide
MAA	methacrylic acid
MAAMBO	5-methacrylomido-1,2-benzoboroxole
Me6TREN	tris[2-(dimethylamino)ethyl]amine
MFT	mature fine tailings
NIPAM	N-isopropyl acrylamide
NMP	nitroxide-mediated polymerization
NTU	nephelometric turbidity units
OSPW	oil sands process-affected water
PAM	polyacrylamide
PAM-co-PAA	poly(acrylamide-co-acrylic acid)
PAM-co-PDADMAC	poly(acrylamide-co-diallyl dimethyl ammonium chloride)
PAM-co-P(t-BAAM)	poly(acrylamide-co- N-tert-butyl acrylamide)

Petcoke	petroleum coke
PMDETA	N,N,N′,N″,N″-Pentamethyldiethylenetriamine
PIMP	photoiniferter-mediated polymerization
PPM	mg of flocculant per kg of suspended solids
PRE	persistent radical effect
RDRP	reversible-deactivation radical polymerization
RID	refractive index detector
RP	radical polymerization
SEC	size exclusion chromatography
SI-ATRP	surface-initiated atom transfer radical polymerization
t-BAAM	N-tert-butyl acrylamide
TGA	thermogravimetric analysis
THF	tetrahydrofuran
TEA	triethylamine
TEABr	triethylammonium bromide
VOC	volatile organic compounds
XPS	x-ray photoelectron spectroscopy

Symbols

Đ	Dispersity
$P_n^{\cdot}$	Propagating radicals
X	Persistent radical
$\mathbf{R_p}$	Rate of polymerization
[M]	Monomer concentration
k_p	Propagation rate constant
$[M]_0$	Monomer concentration at time 0
$[M]_t$	Monomer concentration at time t
k_p^{app}	Apparent propagation rate constant
$[P^{\cdot}]$	Propagating radicals concentration
M_n	Number average molecular weight
$[I]_0$	Initiator concentration at time 0
[I]	Initiator concentration and dormant chain ends
[D]	Deactivator concentration
P_n-X	Dormant species in the form of an initiating alkyl halide
Cu(I)L	Transition metal complex in their lower oxidation state
k_{act}	Activation rate constant
L	Ligand
Cu(II)L-X	Transition metal in its higher oxidation state coordinated with the halide ligand from the dormant species
k_{deact}	Deactivation rate constant
K_{ATRP}	ATRP equilibrium constant

K_{ET}	Equilibrium constant for the electron transfer between the metal
K_X	complexes
K_{EA}	Equilibrium constant for the heterolytic cleavage of the Cu(II)L-X
	bond
K_{BD}	Equilibrium constant for the electron affinity of the halogen
M_w	Equilibrium constant for the bond dissociation energy of the
V_e	propagating chain end and Alkyl halide initiator
V_i	Weight average molecular weight
V_p	Analyte's elution (retention) volume
K_d	Interstitial volume of the column
V_0	Pore volume of the packing
n_0	Distribution coefficient
n’	Void volume
c	Refractive index of the solvent
v_1, v_2, …	Refractive index of the sample
hv_1, hv_2, …	Concentration of the sample in solution
hv	Vibrational energy levels
ϕ	Photon energy levels
Xnl_j	Energy of the photon
	Work function
	X is the element, n is the principal quantum number (n = 1, 2, 3,
M_i	…), l is the orbital angular momentum number denoted as s, p, d, f,
N_i	

$M_{n, theo}$	corresponding to l = 0, 1, 2, …, n – 1, and j is the total angular
$[M]_0/[I]_0$	momentum
$M_{n, exp}$	Molecular weight of a chain
$M_{w, exp}$	Number of chains of a specific molecular weight
	Theoretical number average molecular weight
	Ratio of monomer to initiator at t = 0
	Experimental number average molecular weight
	Experimental weight average molecular weight

1. Introduction

1.1. Mature Fine Tailings

Canada is home to the third largest oil reserve in the world in the form of oil sand deposits, with an estimated volume of 28.3 billion cubic meters.[2] The Clark hot water process extracts bitumen from oil sands, which mixes crushed oil sand ores with hot alkaline water. Then, the bitumen is separated by a flotation process. This process extracts ~90% of the bitumen and requires 2.5 m^3 of water at 40-80ºC for each barrel of bitumen extracted.[3] This process produces large volumes of oil sand tailings, which are collected in tailing ponds.

Over time, tailing ponds will form three regions due to the sand, silt, and clay particles settling by gravity. The top layer comprises the supernatant water contaminated with polycyclic hydrocarbons, heavy metals, and naphthenic acids. The next layer underneath consists of fine clay and silt particles with less than 15 wt % solids called fluid fine tailings.[4] Finally, a layer of mature fine tailings (MFT) consists of approximately ~30-35 wt % solids, ~65 wt % water, and ~3-5 wt % residual bitumen.[5] The majority of the solids have a particle size of either 2-44 μm (78 %, fine silt) or <2 μm (19 %, fine clay), while only 4% are >44 μm (coarse sand).[6] These solids are mostly kaolinite, illite, and mixed-layer clays, such as interstratified illite-smectite and kaolinite-smectite. Due to their strong negative zeta potential, these solids are responsible for the colloidal stability of MFTs.[7] Additionally, the residual bitumen binds clay particles that trap water by constricting interparticle pathways. Together, they form a gel-like suspension that could take several decades to settle and release the captured water.[8]

The inability to separate the water from the MFTs produces a large volume of tailings, projected at current rates to reach 2 billion cubic meters by 2034.[1] These tailings are stored in

artificial ‘ponds’ that cover an area approximately one-and-a-half times the size of Vancouver (176 km^2).[9] Hence, these tailings challenge the oil sands mining industry with two major problems. First, the ponds occupy large areas of land that cannot be used and must be rehabilitated. Second, the water in the MFT remains trapped and unusable for further bitumen extraction.

1.2.Dewatering Oil Sand Tailings

The treatment of tailings requires the solids to settle in a reasonable time and to recover the maximum volume of water possible that reaches the quality standards so that it can be reused in the bitumen extraction process.[10] The two leading large-scale dewatering technologies currently being developed to achieve these are consolidated and paste technologies.

1.2.1. Consolidated Tailings

The consolidated tailings process mixes coarse sand from fresh tailings with mature fine tailings and a coagulant to form a non-segregating mixture. The coarse sand is expected to aggregate with the fine clay particles in the MFT, creating a denser solids phase and releasing particle-free water.[11] The coagulant facilitates consolidation by reducing the repulsive forces between the negatively charged clays via charge neutralization.[5] Inorganic coagulants are typically employed, with gypsum proven to be the most effective and accessible. However, adding inorganic coagulants results in high concentrations of divalent ions (e.g. Ca^{2+} and SO_4^{2-}) in the recovered water.[11] These divalent ions lower the efficiency of bitumen extraction and oil recovery by diminishing the long-range repulsive force and enhancing the adhesion force between silica and bitumen.[12] Therefore, better alternatives to the consolidated tailings process, such as paste technology, are being explored.

1.2.2. Paste Technology

The current paste technology uses a polymer flocculant to rapidly thicken the fluid fine tailings into a paste, increasing the solids content from approximately 15 wt% to 30 wt %.[9] It is generally accepted that the polymer flocculant forms bridges between the suspended particles in the tailings. This achieves a denser solid aggregate, releasing water and increasing the solids' content. Compared to the consolidated tailings process, divalent cations detrimental to bitumen extraction are not leached into the reclaimed water. However, paste technology has been limited to only thickening FFTs and not treating MFTs since the flocculated MFT still contains large volumes of water that cannot be easily removed. This prevents the complete reclamation of land and water from the tailings, resulting in the continued need for tailings ponds.[13] Despite these disadvantages, paste technology has been successfully applied in other mining industries to obtain sediments with solids content between 50-70 wt%.[14] Hence, more polymeric flocculants are currently being explored to push the development of paste technology for the remediation of MFTs.

1.2.2.1. Polymeric Flocculants

Polyacrylamide or polyacrylamide copolymers are currently used as commercial polymeric flocculants (Figure 1.1). Segments of these polymer flocculants are diffusively transported to the solid-water interface, where irreversible solid-polymer attachment can occur via van der Waals or electrostatic attraction.

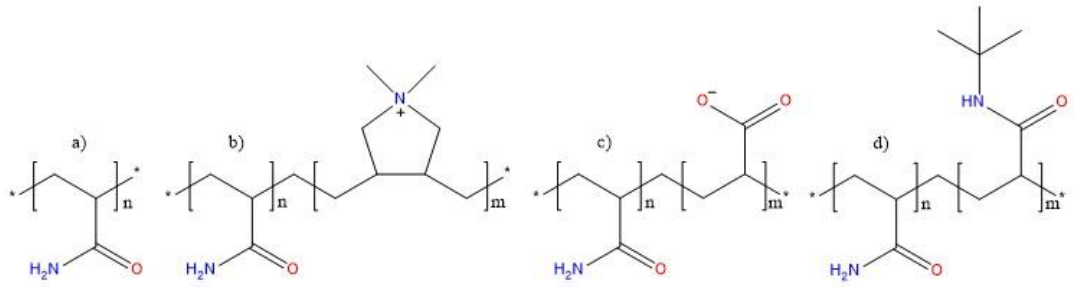

Figure 1.1 Structure of a) non-ionic PAM, b) cationic PAM (PAM-co-PDADMAC), c) anionic PAM (PAM-co-PAA), and d) hydrophobic PAM (PAM-c-P(t-BAAM).

The primary constraint of polymers in flocculating is their ability to adsorb multiple suspended solid particles in a single chain. This requires the extended polymer chain segment to be at least twice the length of the fine clay particles' electrical double layer (EDL). Polymer chain segments can have different possible conformations, which can improve or hinder particle bridging (Figure 1.2).[15]

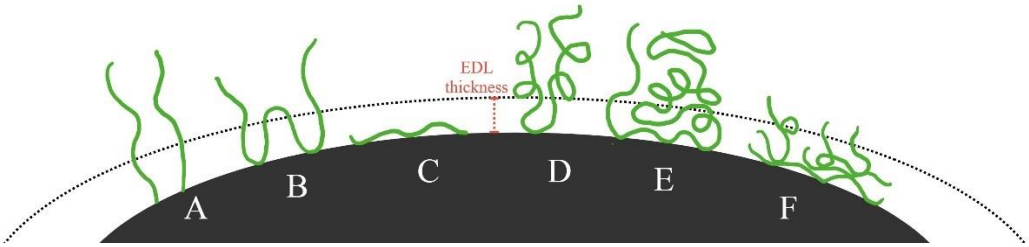

Figure 1.2 Possible polymeric flocculant conformations following adsorption. (A) single point attachment; (B) loop adsorption; (C) flat multiple site adsorption; (D) high molecular weight random coil; (E) non-uniform segment distribution; and (F) multilayer adsorption.

The adsorbed polymer conformation depends on five essential characteristics:[16]

1. Polymer chain length: At a fixed adsorption density, the polymer chain could reach a length where it starts to coil (D, E, and F). This could reduce its adequate adsorption capacity due to self-interaction. However, the polymer chain should not be shorter than two times the EDL of the suspended solids.

2. Polymer-solids interaction: Strong polymer-solids interaction causes the polymer to collapse on the clay's surface (C, E, and F). The polymer should be weak enough to extend from its anchor point on the clay surface.
3. Polymer-water interaction: Hydrophilicity allows the polymer to maximize its contact with water and access more clay particles (A, B, and D). Consequently, hydrophilicity increases water retention in flocs, decreasing net water release and solids content.
4. Polymer self-interaction: Favorable attraction between functional groups on the polymer chain causes self-collapse and the formation of loops and coils, which hinder particle bridging (D, E, and F).
5. Polymer chain stiffness: Stiffer polymers will be more resistant to changes in their conformation (A and C). Polymers should achieve a balance between surviving fluid shear and reorienting their chains to form denser flocs.

Polyacrylamide (PAM) based flocculants typically reach high molecular weights of up to 10^{6-7} g/mol.[17] PAM achieves a good polymer-solid interaction through hydrogen bonding between its amide functionality and the clay's silica/silanol groups.[18] PAM is also very hydrophilic and not stiff. Hence, it is typically used as a flocculant in the mining industry.[6]

However, polyacrylamide has a high polymer self-interaction due to its amide functionality, making it inefficient for the flocculation of fine clay particles (< 2 μm) as it forms a gel-like network via hydrogen bonding that retains large volumes of water.[19] The inability to separate fine clay particles (< 2 μm) is detrimental to the infrastructure used in the oil extraction process since the primary use of the separated water is in the extraction process. The floc's retention of large volumes of water leads to a low resulting solids content. This makes it challenging to achieve the target 75 wt% solids content required for reclamation.[6]

Given these limitations, new approaches to polymer flocculation are being sought, primarily through developing new polymeric flocculants. Research has mainly focused on developing new polyacrylamide-based polymers due to PAM's accessibility and functionality. PAM can be modified by changing its molecular weight, chemical composition, and architecture (branched or linear) through copolymerization.

Charged polymers can extend their polymer segments in solution due to electrostatic repulsion between different chains and within polymer chain segments. Polyacrylamide (PAM) can be charged by copolymerizing with an ionizable monomer. A cationic polyacrylamide can be synthesized by copolymerization with acryloyloxyethyl trimethylammonium chloride (DMC/DAC),[20] and diallyl dimethyl ammonium chloride (DADMAC) monomers to neutralize the negatively charged clay particles.[21] However, the favorable charge pair between cationic PAM and the suspended solids causes the polymer to collapse onto the solid's surface, unable to extend into the solution for bridging. On the other hand, anionic polyacrylamide can be utilized to flocculate negatively charged particles. This occurs through divalent metal ions, bridging the flocculant and particles.[22] Due to the heterogeneous distribution of charges on the surface of the suspended solids, local positively charged areas also adsorb the negatively charged polymer.[23] A lower affinity for polymer-solid adsorption allows the anionic PAM to conform to a more extended morphology capable of bridging more particles. Because of this, multiple studies have found that anionic PAM with 22-30% of its polymer backbone charged and high MW (10^{6-7}) linear chains were the most efficient flocculants for treating oil sands tailings.[23–26] Anionic PAM has been made with acrylic acid (AA), methacrylic acid (MAA), and 2-acrylamide-2-methyl-1-propanesulfonic acid (AMPS).[27] Despite flocculating well, anionic PAM is still unable to effectively dewater oil sands tailings due to the polymer's high hydrophilicity.

Therefore, research into functionalities that could enhance dewaterability is being explored. This has been achieved by copolymerizing PAM with hydrophobic monomers such as N-tert-butyl acrylamide (t-BAAM)[28], N-isopropyl acrylamide (NIPAM),[29] and 5-methacrylomido-1,2-benzoboroxole (MAAMBO).[30] Reports have shown that increasing the hydrophobic segment can increase the rate of dewatering from the aggregates by up to a factor of five.[31]

In addition to linear polymers, branched polymers have also been investigated as an attempt to extend more polymer segments into the solution. For example, PAM has been copolymerized with a cationic hyperbranched oligomer, poly(N-acryloyl-1,2-diaminoethane hydrochloride) (HADE). It showed improved flocculation performance compared to its linear counterpart with similar molecular weights, charge density, and intrinsic viscosity. This was attributed to the extended conformation of the charged hyperbranched polymer due to the added steric hindrance, allowing the cationic terminal groups on the branches to be better exposed in solution.[32] Conversely, research into hybrid grafted polymeric brush flocculants has been limited.

1.3.Polymer Brushes

Polymers have previously been grafted on many substrates, including graphene, metals, and proteins, to tailor the substrate's chemical and physical properties, including surface wettability, adsorption capacity, and thermal stability.[33–38] Polymers covalently attached to a surface are commonly called polymer brushes. There are three approaches to forming polymer brushes: grafting-to, grafting-through, and grafting-from (Figure 1.3). The grafting-to approach reacts end-functionalized polymer chains with an appropriate surface functional group on the substrate.[39,40] A grafting-from approach, in which polymer chains are directly grown from an initiator functionalized surface, can achieve higher grafting densities.[41] A grafting-through approach grows polymer brushes with polymerizable groups functionalized on the substrate's

surface. This process also produces non-grafted polymer chains, which are challenging to separate from the grafted material. Because of the perceived benefits of a higher grafting density, a grafted-from approach is typically used to functionalize surfaces with polymers. However, depending on the application, this may or may not be desirable.

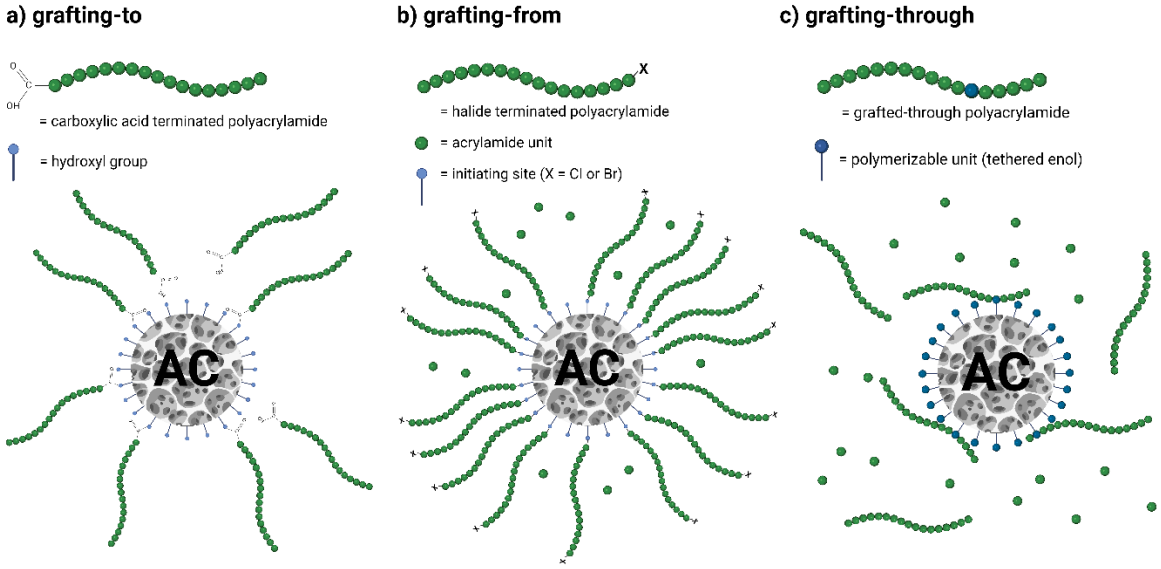

Figure 1.3 Fabrication of polymer brushes using a) grafting-to, b) grafting-from, and c) grafting through strategy.

1.4.Reversible-Deactivation Radical Polymerization (RDRP)

A bottom-up approach, such as forming a grafted-from polymer brush, mainly uses a surface-initiated reversible-deactivation radical polymerization (RDRP) capable of forming polymers with relatively low molecular weight dispersity (Đ). It allows for exact control over the polymer's molecular weight, architecture, and composition.[42] There are three main RDRP processes: atom transfer radical polymerization (ATRP),[42–50] reversible addition-fragmentation chain transfer (RAFT) polymerization,[51–54] and nitroxide-mediated polymerization (NMP).[55–59]

All three RDRP processes establish a dynamic equilibrium between propagating radicals and various dormant species.[60] ATRP and NMP reversibly trap radicals in a deactivation/activation process. (Figure 1.4)

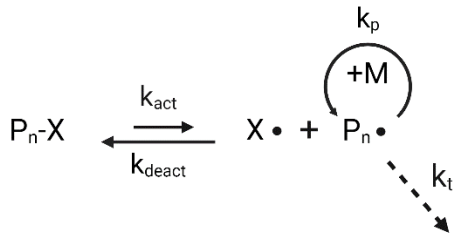

Figure 1.4 Reversible radical trapping through a deactivation/activation process.

This approach relies on a self-regulating kinetic feature named the persistent radical effect (PRE).[61] Propagating radicals ($P_n^{\cdot}$) are rapidly trapped in the deactivation process by species (X), which is a stable radical such as a nitroxide (in NMP).[57] Conversely, conventional radical polymerization (RP) uses an initiation-termination process to produce growing radicals. In ATRP and NMP, the propagating ($P_n^{\cdot}$) and the persistent (X) partners form and disappear at equal rates. Suppose the reversible processes were the only reactions and no radicals were initially present. In that case, Pn· and X concentrations increase equally in time and reach equal steady-state values in equilibrium. The propagating radical ($P_n^{\cdot}$) continues to grow and eventually decays by irreversible bimolecular self-terminations. The persistent radicals (X) cannot terminate with each other but only (reversibly) cross-couple with the growing species. Hence, each radical-radical termination causes an irreversible accumulation of the persistent radical (X). Consequently, the concentration of propagating radicals ($P_n^{\cdot}$) and the probability of termination decreases with time since the propagating radicals predominantly react with the higher concentration of X.

In comparison, RAFT employs a "reversible transfer" using a chain transfer agent (CTA), which is also called a degenerative exchange process (Figure 1.5).

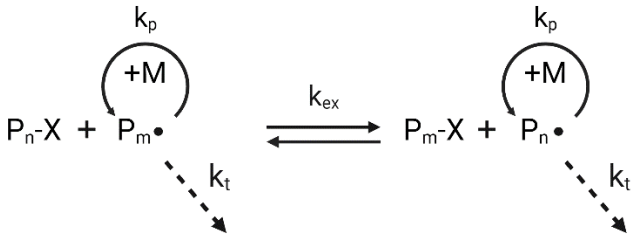

Figure 1.5 Degenerative exchange process.

This system also relies on a slow initiation and fast termination process typical of radical polymerization (RP). However, RAFT employs a higher chain transfer agent (CTA) concentration than radical initiators. A small concentration of radicals consumes the monomer, which can terminate but also degeneratively exchange with the dormant species, CTA.[51]

1.4.1. Features of a Reversible-Deactivation Radical Process (RDRP)

An RDRP process should display first-order kinetic behavior, a predeterminable molecular weight, a narrow molecular weight distribution, and preserved polymer chain end functionalities. The polymerization rate (R_p) in RDRP is linearly dependent on the log of the monomer concentration ([M]) over time (Equation 1). This is due to the persistent radical effect (PRE) leading to a constant concentration of active propagating radical species (Equation 2).

$$R_p = -\frac{d[M]}{dt} = k_p[P^{\cdot}][M] \quad (1)$$

Equation 1 Rate of polymerization

$$\ln\frac{[M]_0}{[M]_n} = k_p[P^{\cdot}]t = k_p^{app}t;\ (\text{if } [P^{\cdot}] \text{ is constant}) \quad (2)$$

Equation 2 Persistent radical effect

Where k_p is the propagation rate constant, [P·] is the concentration of propagating radicals, $[M]_0$ is the monomer concentration at t = 0, $[M]_t$ is the monomer concentration at time t, and k_p^{app} is the apparent propagation rate constant.[43]

The semilogarithmic plot of Equation 2 presents the linear dependence of the log of the monomer concentration over time and possible deviations from a constant [P·] (Figure 1.6a). Deviations in this plot are due to its sensitivity to any change in the concentration of the active propagating species [P·]. An early negative deviation from linearity occurs due to the slow initiation of the dormant species. At the same time, a late negative deviation from linearity occurs due to termination reactions. Chain transfer does not affect the [P·].[43]

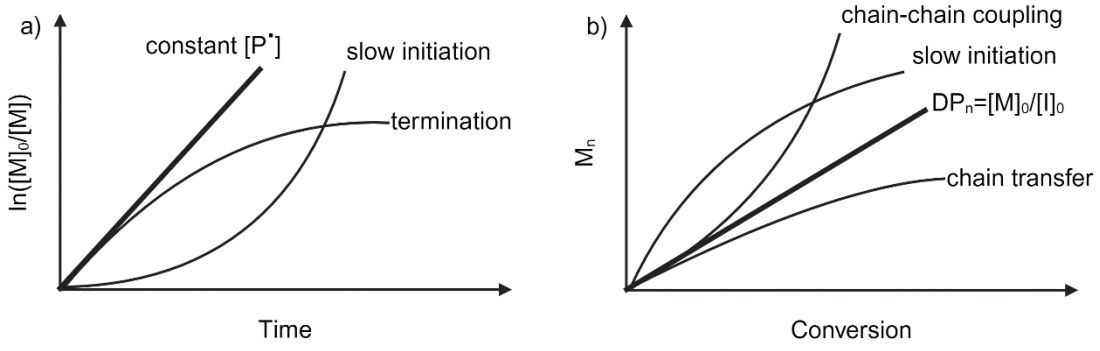

Figure 1.6 Features of RDRP: a) dependence of ln($[M]_0$/[M]) over time and b) dependence of the number average molecular weight (M_n) on monomer conversion.[43]

The pre-determinable degree of polymerization (DP) in an RDRP process describes the number average molecular weight (M_n) as a linear function of monomer conversion (Equation 3).

$$DP_n = \frac{M_n}{M_0} = \frac{\Delta[M]}{[I]_0} = \frac{[M]_0}{[I]_0}(\text{conversion}) \quad (3)$$

Equation 3 Degree of polymerization

Where $[I]_0$ is the initiator concentration at t = 0. This results from maintaining a constant number of chains throughout the polymerizations. Moreover, the number of chains in the polymerization is sensitive to slow initiation, chain coupling, and chain transfer processes. This is summarized in

a plot of the number average molecular weight (M_n) vs the monomer conversion (Figure 1.6b). A slow initiation leaves out initiators in the RDRP process, resulting in a higher M_n than the projected theoretical M_n. Chain-coupling processes decrease the number of chains while increasing the total M_n. Lastly, chain transfer reactions increase the number of chains, so the total M_n decreases even at high monomer conversions.[43]

A narrow molecular weight distribution is not necessarily a result of controlled polymerization since it ignores the effect of the initiation, exchange, and propagation rate. Therefore, the following requirements should be met to achieve a narrow molecular weight distribution polymer. First, the rate of initiation should be faster than the rate of propagation so all chains simultaneously grow. Second, the reversible rate of deactivation between species of different reactivity is faster than the rate of propagation. This ensures all active chain ends are equally susceptible to growing uniform polymer lengths. Third, there should be negligible chain transfer or termination. Lastly, the rate of depropagation is substantially lower than propagation.[43] For systems with a slower reversible deactivation process, the molecular weight distribution or dispersity (Đ) can be defined by the following Equation 4,

$$Đ = \frac{M_w}{M_n} = 1 + \left(\frac{k_p[I]_0}{k_{deact}[D]}\right)\left(\frac{2}{\text{conversion}} - 1\right) \quad (4)$$

Equation 4 Dispersity

where M_w is the weight, M_n is the normal average molecular weight, k_p is the rate of propagation, k_{deact} the rate of deactivation, [I] is the concentration of initiator and dormant chain ends, and [D] is the concentration of the deactivator. Hence, it is possible to fine-tune the Đ by targeting lower conversions or increasing the concentration of the deactivator.[44]

Lastly, the polymer chains should have preserved end-functionalities due to the negligible irreversible chain transfer and termination. Therefore, propagation could resume upon the addition of more monomers. Together, these features provide the best opportunity to control a material's bulk properties through the array of choices in composition, functionality, and topology attainable at the molecular level.

1.4.2. Atom Transfer Radical Polymerization (ATRP)

The most common and effective RDRP is Atom Transfer Radical Polymerization (ATRP).[35,42–44,46–50,60,62–77] ATRP is controlled by an equilibrium between propagating radicals and a dormant species in the form of an initiating alkyl halide (P_n-X).[42] The dormant species (P_n-X) periodically reacts with a transition metal complex in their lower oxidation state such as [L_mCu(I)], acting as an activator with the rate constant of activation (k_{act}) (L_m representing the ligand). This reaction intermittently produces radicals (P_n·), and the transition metal in its higher oxidation state coordinated with the halide ligand from the dormant species [L_mCu(II)-X] (Figure 1.7).[42]

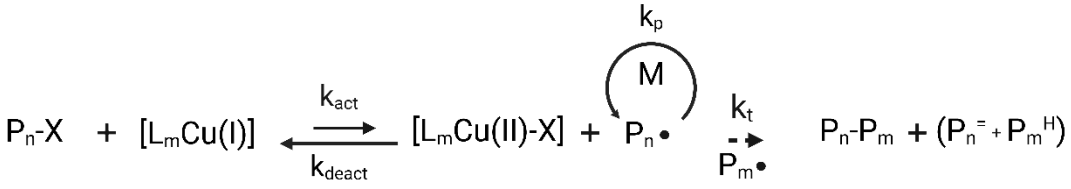

Figure 1.7 ATRP Scheme

The [L_mCu(II)-X] deactivator reacts with the propagating radical with the deactivation rate constant (k_{deact}) to reform the dormant species and the activator. ATRP limits termination processes including chain coupling and disproportionation that yields P_n-P_m, $P_n^=$, and P_m where P is the polymer chain and H is the transferred hydrogen atom. In the case of a surface-initiated

ATRP or SI-ATRP, the surface of the substrate is functionalized with an alkyl halide initiating group.

The ATRP equilibrium must be understood and controlled to execute a successful ATRP process. The ATRP equilibrium constant (K_{ATRP}) is expressed as the ratio between the activation rate constant (k_{act}) and the deactivation rate constant (k_{deact}). It can also be expressed as a combination of several contributing reversible reactions shown in Equations 5-8 and summarized in Equation 9.[66,74]

$$[L_m Cu(I)] \overset{K_{ET}}{\longleftrightarrow} [L_m Cu(II)]^+ + e^- \tag{5}$$

Equation 5 Electron transfer from the metal complex

$$X^- + [L_m Cu(II)]^+ \overset{K_X}{\leftrightarrow} [L_m Cu(II) - X] \tag{6}$$

Equation 6 Heterolytic formation of the metal halide bond

$$X^{\cdot} + e^- \overset{K_{EA}}{\longleftrightarrow} X^- \tag{7}$$

Equation 7 Electron affinity of the halogen

$$P_n - X \overset{K_{BD}}{\longleftrightarrow} P_n^{\cdot} + X^{\cdot} \tag{8}$$

Equation 8 Bond dissociation energy of the propagating chain end and alkyl halide initiator

$$K_{ATRP} = \frac{k_{act}}{k_{deact}} = K_{ET} K_{EA} K_{BD} K_X \tag{9}$$

Equation 9 ATRP equilibrium

Where K_{ATRP} is expressed as the product of the equilibrium constants for electron transfer between the metal complexes (K_{ET}), heterolytic cleavage of the [L_mCu(II)-X] bond (K_X), electron affinity of the halogen (K_{EA}), and bond dissociation energy of the propagating chain end and alkyl halide initiator (K_{BD}).[78–80]

The equilibrium constants K_{EA} and K_X are very solvent-dependent.[81] K_{EA} increases in protic solvents as halide anions are stabilized through solvation, while K_X is affected by the change in solvent polarity.[81] The K_X of a typical ATRP catalyst consisting of [L_mCu(II)-Br] with L_m = bipyridine (bpy), N,N,N′,N″,N″-pentamethyldiethylenetriamine (PMDETA), or tris[2-(dimethylamino)ethyl]amine (Me_6TREN) was approximately five orders of magnitude greater in organic solvent CH_3CN, than in aqueous solvents.[82] The changes in K_{EA} and K_X values in protic solvents increase the K_{ATRP} value (Equation 9). This also decreases the amount of [L_mCu(II)-X] present in the reaction, which increases the rate of polymerization defined by the following seen in Equation 10. Therefore, controlling the ATRP of a hydrophilic polymer such as polyacrylamide (PAM) requires protecting the deactivator [L_mCu(II)-X] (Details in Chapter 3).[81]

$$R_p = k_p K_{ATRP} \frac{[P_n X][L_m Cu(I)]}{[L_m Cu(II) - X]} [M] \quad (10)$$

Equation 10 Rate of polymerization due to activator-deactivator ratios

Polyacrylamide brushes have been grafted for different surfaces and applications explicitly through atom transfer radical polymerization. These surfaces can contribute to the effect of a desired application. Polyacrylamide has been grafted from the surfaces of microporous polysulfone membranes, polyethylene terephthalate, silica, silicon, and gold films for anti-microbial coatings and sensing.[83–89] Poly(N-isopropyl acrylamide) (PNIPAM) was grafted from the surfaces of cellulose, superparamagnetic cobalt, gold, and silica nanoparticles toward the development of drug delivery systems, detection assays, bioseparations, and sensing.[90–93] The molecular weight of these polymer brushes has remained low at less than 10^5 g/mol. However, to remain practically applicable, the flocculation of oil sands tailings requires higher molecular weights and a more economical hydrophobic core.

Additionally, a grafting-from process can produce polymer brushes with control over their conformation. In 2016, Lilge et al. investigated the polyacrylamide brush thickness with varying surface initiator fractions.[86] They found that the polymer brush thickness increases as the initiator density increases independent of the polymer brush molecular weight. The increase is due to the polymer's extended conformation instead of a coil or loop. Extending the polymer into the solution may improve the particle bridging capacity of a single chain.

1.5.Activated Carbon (AC)

Activated carbon (AC) is a porous carbonaceous material extensively used to extract gaseous and liquid contaminants.[94–98] ACs are produced by carbonizing a wide range of raw materials, followed by activation to develop their porous structure.[99] The carbonization step removes most of the non-carbon elements in the raw material and arranges the residual carbon atoms into a microcrystalline structure composed of disordered aromatic sheets.[100] The disordered aromatic sheets give rise to AC's porous structure.[101]

Carbonaceous precursors are typically renewable sources such as nutshells, fruit pits, paper mill waste, wood, charcoal, coal, lignite, bone, and peat.[99] The resulting AC has a variety of functional groups on its surface due to the presence of residual heteroatoms, such as oxygen and nitrogen, that form from its precursor (Figure 1.8).[102] These influence AC's properties, including hydrophobicity, surface charge, electron density, and sites for further surface modifications.[102–104]

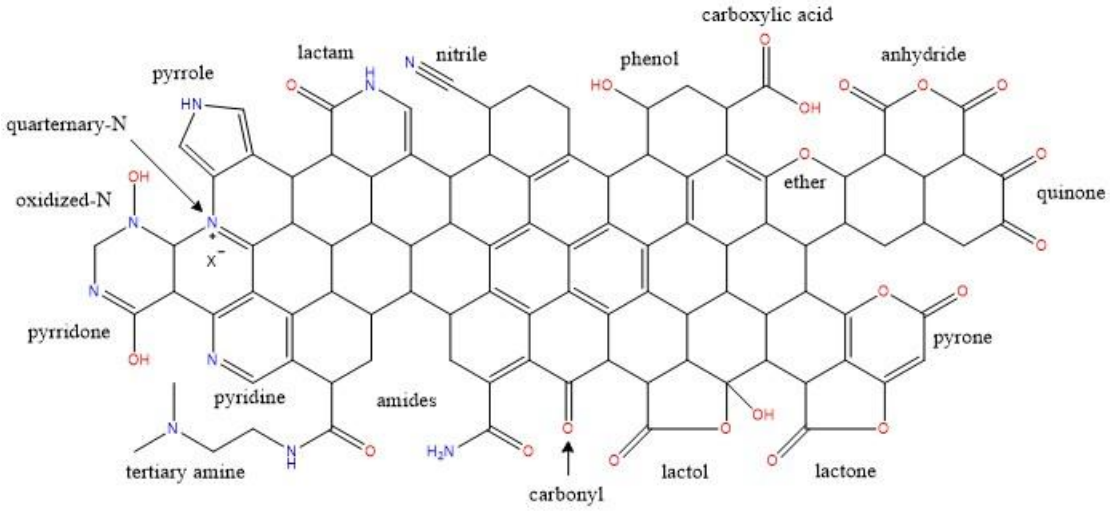

Figure 1.8 Potential oxygen and nitrogen functional groups on the surface of AC.

This research investigated the petroleum coke (petcoke) based activated carbon as a macroinitiator or hydrophobic core for the PAM brushes. Petcoke is a substantial byproduct of the Alberta oil sand mining industry, which has generated over 72 million tonnes as of 2011.[105] Petcoke typically has>85% carbon with 5-7% sulphur content, which hinders more traditional applications as a fuel source in steel production.[106] Activating petroleum coke is a convenient and cost-effective method for producing sustainable adsorbents for naphthenic acids and heavy metals in oil sands process-affected water.[107–109]

Covalently attaching the flocculant PAM from the surface of activated carbon could prevent polymer leaching into the treated process water, provide a hydrophobic core to improve dewatering, and release process water with reduced naphthenic acids and metals.

1.5.1. Surface Initiated Atom Transfer Radical Polymerization (SI-ATRP) of Polyacrylamide from the Surface of Activated Carbon

Activated carbon (AC) is modified with polymer brushes to impart a high density of desired functional groups and improve the adsorption of a specific gaseous or liquid contaminant. The

Surface Initiated Atom Transfer Radical Polymerization (SI-ATRP) from the AC surface has been limited to poly(tert-butyl acrylate)[110] and poly(hydroxyethyl acrylate)[111] to impart high hydroxyl groups for wastewater treatment. More recently, in 2023, polyacrylamide was grafted from the surface of activated carbon by SI-ATRP to develop a hybrid oil sand tailings flocculant.[112] The reported polyacrylamide grafted activated carbon (AC-PAM) had brushes with a low molecular weight of 176,000 g/mol, a high dispersity of 2.1, and a low polyacrylamide content of 11%. However, the reported AC-PAM could flocculate dilute (5 wt%) oil sand tailings at a high dose of 20,000 ppm (mg of flocculant per kg of suspended solids). Further development of the material should focus on controlling the polymerization of polyacrylamide to achieve higher molecular weights and evaluate the effect of the polymer brush molecular weight on the flocculation of mature fine tailings (MFTs).

1.6. Thesis Objectives

Due to the increasing amount of tailings waste generated by the oil sands industry and the significant use of polyacrylamide (PAM) in recovering the land and water they occupy; researchers are exploring new flocculants. A promising option is polyacrylamide grafted from petroleum coke-activated carbon surface (AC-PAM). This process repurposes the petroleum coke waste from the oil sands industry into a product that addresses their tailings waste. In addition, the activated carbon (AC) provides extra hydrophobicity to assist in water recovery. However, only PAM brushes with molecular weights $< 10^6$ g/mol have been studied, necessitating a high dosage of AC-PAM to treat mature fine tailings (MFT). Therefore, this thesis aims to create AC-PAM with higher molecular weight PAM brushes and assess their flocculation performance. This was accomplished by completing the following objectives:

1. Develop an aqueous atom transfer radical polymerization (ATRP) method for synthesizing high-molecular-weight polyacrylamide (PAM) with molecular weights > 10^6 g/mol, by exploring ATRP parameters such as the use of a reducing agent, cosolvent, halide salt, and different catalyst systems.
2. Synthesize different molecular weight PAM brushes grafted from activated carbon (AC) surfaces (AC-PAM) with varying AC content and particle sizes using the developed ATRP procedure.
3. Evaluate the flocculation performance of the AC-PAM with different molecular weight brushes, AC content, and particle sizes in comparison to ungrafted/free PAM by conducting settling tests on diluted mature fine tailings (MFT).

2. Key Experimental Techniques

2.1. Key Characterization Techniques

2.1.1. Size Exclusion Chromatography (SEC)

Polymers are complex multicomponent materials that have several important distributed properties. The performance and characteristics of these materials are highly dependent on various distributed properties, including molar mass, chemical composition, and end-group functionality, among others. Polymers typically express their molar masses as averages based on chain length or weight. These averages include number-average molar mass (M_n) and weight-average molar mass (M_w). M_n is the statistical average molar mass of all the polymer chains and is described by Equation 11,[113]

$$M_n = \frac{\Sigma N_i M_i}{\Sigma N_i} \quad (11)$$

Equation 11 Number average molecular weight

where M_i is the molecular weight of a chain, and N_i is the number of chains of that molecular weight. M_n is the value at which equal numbers of molecules are on either side of the M_n in the molar mass distribution. Alternatively, M_w appears when there are equal masses of molecules on each side of the M_w in the molar mass distribution and is described by Equation 12.[113] The molar mass distribution can also be represented by its dispersity (Đ). The dispersity describes the broadness of a molar mass distribution and is defined by Equation 13.[113] When M_w equals M_n, the polymer is said to be monodisperse. While a value greater than 1 indicates a broader molar mass distribution.[113]

$$M_w = \frac{\Sigma N_i {M_i}^2}{\Sigma N_i M_i} \quad (12)$$

Equation 12 Weight average molecular weight

$$Đ = \frac{M_w}{M_n} \quad (13)$$

Equation 13 Dispersity

Size exclusion chromatography (SEC) is one of the most critical methods for analyzing the molar mass distribution of polymers.[2] The analyte molecules selectively distribute between a stationary and mobile phase in SEC based on the chromatographic process. Equation 14 can describe the separation process of any chromatography,

$$V_e = V_i + V_p K_d \quad (14)$$

Equation 14 Elution volume of the analyte

where V_e represents the analyte's elution (retention) volume, V_i is the interstitial volume of the column, V_p is the pore volume of the packing, and K_d is the distribution coefficient. The distribution coefficient is the ratio of the analyte concentration in the mobile and the stationary phase.[113]

SEC separates polymers by their hydrodynamic volume in a dilute solution using a stationary phase with a characteristic pore size distribution. The polymers may have access to the pores depending on their hydrodynamic volumes. Large molecules cannot enter the pores and are excluded. Hence, they have a K_d equal to 0 and are eluted first at the interstitial volume V_i. At the same time, small molecules have access to all the pores of the stationary phase, having a K_d equal to 1 and eluting at the void volume (V_0).[113]

Various detectors are capable of detecting samples as they elute from the column. In GPC, a refractive index detector (RID) is typically used. RID measures the difference in the refractive index between the mobile phase and the pure solvent held in a reference cell. The refractive index of a dilute solution is calculated using Equation 15,

$$n = n_0 + (n' - n_0)c \tag{15}$$

Equation 15 Refractive index of a dilute solution

Where n_0 is the refractive index of the solvent, n' is the sample's refractive index, and c is the concentration of the sample in solution. This equation can be rearranged to form Equation 16,

$$\mathrm{c} = \frac{\mathrm{n} - \mathrm{n_0}}{\mathrm{n'} - \mathrm{n_0}} \tag{16}$$

Equation 16 Concentration of the sample in solution

which demonstrates that the difference in the RI between the solvent and the sample solution is proportional to the sample concentration.

The SEC column must be calibrated with monodisperse polymers with known peak molecular weights (M_p). The calibration of the column is achieved by taking a linear regression of the logarithmic plot of the standards' M_p and the elution volumes of their peak maxima. The molar mass distribution can be calculated using this calibration. The calibration standards should also be chemically like those of the analyzed samples. The macromolecule's chemical composition, topology, solvent, and more affect the hydrodynamic volume of a polymer. Polyethylene oxide/polyethylene glycol standards are most used to analyze aqueous linear polymers.

The molar mass and molar mass distributions in this work were determined by SEC using Agilent Technologies 1220 Infinity LC equipped with an Agilent Technologies 1260 Infinity RID. The SEC column used was a PL aquagel-OH MIXED-H 8 μm, 300 x 7.5 mm column with a molar mass lower limit of 6,000 g/mol and upper limit of 10,000,000 g/mol. The eluent was an aqueous solution of 0.2 M $NaNO_3$ and 0.01 M NaH_2PO_4 adjusted to pH 7 using 0.1 M NaOH. Samples were diluted to 0.1 % (w/v%) and were injected at a volume of 20 μL. The column was operated at room temperature with a 1 mL/min flow rate while the detector was set at 35ºC. The column was calibrated using polyethylene oxide/polyethylene glycol standards with monodisperse molar mass distributions at M_n values in the 106 – 1,522,000 g/mol (Agilent Technologies).

2.1.2. Raman Spectroscopy

Raman spectroscopy relies on the physical phenomena of Raman scattering, an inelastic light scattering process. A molecule with vibrational energy levels v_1, v_2, … with corresponding energies of hv_1, hv_2, …, respectively, interacts with a photon of energy hv (where h is Plank's constant, and v is the frequency of the incident radiation). The scattered radiation energy hv' is

collected. Much of the collected radiation will be from Rayleigh scattering, which has the same energy as the incident light. A small fraction of this scattered radiation will have energy of $h(v \pm v_1)$ (termed Stokes or anti-Stokes scattering). This inelastic component of the scattered radiation is the Raman scattering.[114] Raman scattering is plotted into the intensity of scattered radiation as a function of the frequency shift between incident and scattered radiation.

Raman spectra of all the samples were acquired on a Renishaw inVia Raman Microscope. The spectrometer is equipped with a laser operating at 633 nm and an 1800 line/mm diffraction grating. Samples were acquired by taking aliquots from the polymerization reaction and examining them on a silicon wafer. A laser power of the maximum allowable 100 mW and five scans were used for each acquisition. The resulting spectra were transferred from the Renishaw WiRE 3.4 software to an individual PC. Data analysis of the spectra was conducted on OriginPro 10.0.5.157, allowing multiple spectra to be displayed at user-defined magnifications, perform arithmetic operations, background subtraction, and integrate peaks within a spectrum. Monomer conversion was calculated using Equation 17, where $[P]_t$ is the concentration of polymer at time t, determined by the peak integral at ~2930 cm^{-1} associated with the symmetrical stretching of CH_2 in the polymer. While $[M]_t$ is the concentration of monomer at time t, determined by the peak integral at ~1285 cm^{-1} associated with the bending of CH in acrylamide. Both peak integrals are normalized to the peak integral at ~1430-1460, which is associated with the bending of CH_2 in both polymer and monomer. The broadening of the CH_2 bending peak at 1430 cm^{-1} is a blue shift of the CH_2 bending peak as the acrylamide is polymerized.[115] When calculating monomer conversion, the broadened 1430 cm^{-1} peak is integrated to account for the CH_2 bending in PAM and AM. This peak is used as the internal standard for quantifying the monomer conversion.

$$\text{Monomer Conversion} = \frac{[\text{P}]_\text{t}}{[\text{M}]_\text{t} + [\text{P}]_\text{t}} \times 100\% \quad (17)$$

Equation 17 Monomer conversion

2.1.3. X-ray Photoelectron Spectroscopy

X-ray photoelectron spectroscopy (XPS) is a characterization technique used to determine the elemental composition and speciation of solid substrate's outer 1-10 nm. The physical basis of XPS experiments relies on the photoelectron emission process. The sample is irradiated with x-rays of known energy and ejects an inner-shell electron initially bound to an atom/ion. The kinetic energy (KE) of that emitted electron is then measured.[116] This measurement is helpful since it is discrete and a function of the electron binding energy (BE), which is element- and chemical-environment-specific. A precise estimate of the binding energy (BE) can be obtained using the Einstein relation shown in Equation 18,[117]

$$\text{BE} = \text{hv} - \phi - \text{KE}. \quad (18)$$

Equation 18 Binding energy

where hv is the energy of the photon, and ϕ is the work function of the instrument. This represents the minimum energy required to remove an electron from the instrument, assuming a conductive sample in physical contact with the instrument is analyzed.[116]

The plot of the intensity in counts per second vs the binding energy can determine the relative abundance of the various elements in the sample. Most XPS peaks are due to electrons originating from specific core levels, which did not suffer energy losses from inelastic collisions. They are described using a spectroscopic notation of the form "X nl_j," where X is the element, n is the principal quantum number (n = 1, 2, 3, …), l is the orbital angular momentum number denoted as s, p, d, f, corresponding to l = 0, 1, 2, …, n – 1, and j is the total angular momentum

High-resolution scans of these peaks can be used to determine the chemical speciation of the specific element since the binding energy depends on the electron's chemical environment. This is due to the differences in charge density on an atom. The higher negative charge density results in the photoelectrons with higher kinetic energy, hence, the lower binding energy of corresponding peaks in the spectrum. This work uses the XPS peaks of C1s, O1s, N1s, and Br2p.

XPS measurements were acquired on a Kratos AXIS supra spectrometer using a monochromatic A1 K(alpha) source (15mA, 15kV). The instrument work function was calibrated to a binding energy (BE) of 83.96 eV for the Au 4f7/2 line for metallic gold, and the spectrometer dispersion was adjusted to a BE of 932.6 eV for the Cu 2p3 eV line of metallic copper. The Kratos charge neutralizer system was used on all samples. Survey scan analyses were performed with an analysis area of 300 x 700 microns and a pass energy of 160 eV. High-resolution analyses were performed with an analysis area of 300 x 700 microns and a pass energy of 20 eV. Data processing of the survey and high-resolution scans were analyzed using CASA XPS (version 2.31). The spectra were corrected to the main line of the C1s spectrum at 284.85 eV, and baseline corrections were made using a Shirley-type background correction.

2.2. Key Techniques for Measuring Flocculation

2.2.1. Dean-Stark Extraction

To have a complete evaluation of the flocculation performance, the colloid composition must be characterized and kept consistent throughout the flocculation tests. The received Mature Fine Tailing (MFT) samples have variable compositions from batch to batch. Therefore, a Dean-Stark extraction determined the MFT batch's solid, water, and bitumen content. A Dean-Stark apparatus comprises a round bottom flask, thimble, condenser, and a water trap. The sample (~50

g of MFT) is placed in a pre-weighed thimble and held above the reflux flask containing aromatic toluene (~200 mL). By heating the system, toluene and water vapours rise to the condenser and are collected by the water trap. The toluene and water are separated into two layers, with the toluene on the top layer. Excess toluene in the trap reaches the side arm and flows back into the thimble containing the sample. The toluene dissolves the bitumen in the sample and drips back into the reflux flask containing the toluene. This cycle is continued by refluxing for approximately 24 hours until the toluene dripping from the sample does not visibly contain any bitumen. After refluxing, the thimble is dried in an oven at 110ºC overnight and weighed to determine the solid content of the sample. The toluene/bitumen solution is placed in a 250 mL volumetric flask and topped with fresh toluene. 5 mL of the solution was pipetted onto a pre-weighed filter paper, and the toluene was allowed to evaporate in an oven at 110ºC overnight. After drying, the filter paper is weighed to determine the bitumen mass in the 5 mL sample. Finally, the mass of the bitumen in the sample is calculated from the mass of bitumen in 5 mL by multiplying by 20. [118]

2.2.2. Settling Rate

A flocculant's effectiveness in industrial applications is typically assessed based on specific parameters that reflect how well the polymer can flocculate certain solid suspensions. Settling tests measure how quickly a flocculant can settle a given suspension. This test indirectly represents the kinetics of the process involved in the flocculation, such as adsorption and charge neutralization. The colour-separating interface called the mudline is monitored as a function of time after the treatment of the flocculant to the suspension, producing a settling profile. The initial linear region of the settling profile is called the initial settling rate (ISR), which measures the initial flocculation kinetics.

The ISR is obtained by first performing a settling test with MFT slurry diluted to 5 wt% solids with deionized water. 100.0 g of 5 wt% MFTs is poured into a 250 mL beaker and is mixed at 600 rpm using a three-blade propeller. While mixing, the flocculant was added to the suspended slurry. The mixture was left to mix at 600 rpm for 2 minutes, followed by 200 rpm for 8 minutes. Approximately 5 mL of the mixture was analyzed for its capillary suction time (CST), see Section 2.2.3. The rest was transferred into a 100 mL graduated cylinder, and the change in mudline height was recorded over time. The settling profile was obtained by plotting the mudline height vs time. Additionally, linear regression is fitted in the initial linear region of the settling profile to obtain the ISR value. The treated MFTs are left in the graduated cylinder for 24 hours to allow further separation of solids from the supernatant to measure the supernatant turbidity (see Section 2.2.4.).

2.2.3. Capillary Suction Time

The treated tailings should be easily filtered. Capillary suction time (CST) measures the filterability and ease of removing water from sediments. The flow restriction is caused by the development of interparticle networks within the sediment, reducing dewaterability.[119] Therefore, the CST value can also be used to show a difference in floc structure between applied flocculants.[120] The CST apparatus consists of a cylindrical steel funnel on filter paper fitted between two Perspex plates with electrode sensors across the top plate. The sample is poured into the steel reservoir, allowing its moisture to flow uniformly into the filter paper through capillary action. The instrument measures the time it takes for the water to travel a specific distance between two electrodes on top of the filter paper. A higher CST value indicates the treated tailings' lower dewatering or high-water retention.[18]

The CST of the flocculant-treated MFT is measured right before performing the settling tests using a Type 304M Capillary Suction Timer (Triton Electronics Ltd.). It includes 7x9 cm CST papers with a 9 sec/100 mL/ square inch porosity sandwiched between two Perspex plates with four electrode probes. The CST measurement is taken directly after treating the MFTs with flocculant. Approximately 5 mL of each sample is poured into the 1.8 cm steel funnel placed on the CST paper and electrodes.

2.2.4. Supernatant Turbidity

The supernatant is defined as the liquor left on top of the settled sediments after completing the flocculation. The supernatant quality is assessed by its turbidity, which results from the presence of suspended solid particles. In this work, turbidity was measured using an attenuation method using a DR/890 Portable Colorimeter (Hach). A sample cuvette is filled with the supernatant after settling for 24 hours. The sample is irradiated with light, and as it passes through the sample, it loses intensity due to scattering and absorption by the suspended solids. The intensity of the light beam after it passes through the sample is measured and expressed in nephelometric turbidity units (NTU).[121–123]

2.2.5. Solids Content

The ability of a flocculant to dewater sludge can be determined by measuring the solids content of the sediment formed after treatment.[124,125] The solids content is measured by calculating the (dry mass)/(wet mass) ratio.[126] Once the supernatant turbidity is measured, the settled MFTs are passed through a 1 mm mesh sieve. The collected sediment is weighed and is denoted as the wet mass. Afterward, the collected sediment is dried in a 110ºC oven overnight to weigh the dry mass.

3. Controlled Radical Polymerization of Polyacrylamide

3.1.Introduction

Polyacrylamide (PAM) has many applications but is most known for flocculation. In that role it is found in many other fields including municipal water treatment, reverse osmosis membranes, drag reduction, oil recovery, paper manufacturing, and soil conditioning. The global PAM market was valued at USD 5.8 billion in 2022 and is estimated to reach USD 9.1 billion in 2030.[127] The potential toxicity of PAM is typically neglected. Still, its natural and chemical degradation product, acrylamide, is a toxic chemical that endangers the local ecosystem and human health.[128–130] Therefore, alternatives to reduce the required PAM in water-based applications are being explored. A popular candidate is to graft PAM from a substrate that could impart additional properties and limit the leaching of PAM.[112,131–135] PAM has typically been prepared via free radical polymerization for more than two decades due to the numerous available methods (using free radical initiators, electrochemical initiation, ultrasonic waves, photochemical sensitizers, ultraviolet radiation, ionizing radiation, and aqueous redox systems) that can reach complete conversion in large-scale reactions.[136] However, free radical polymerization cannot grow polymer brushes exclusively from a substrate, which is one of the primary goals of this thesis. Therefore, reversible deactivation radical polymerization (RDRP) techniques were investigated. RDRP techniques, including atom transfer radical polymerization (ATRP), nitroxide-mediated polymerization (NMP), photoiniferter-mediated polymerization (PIMP), and reversible addition-fragmentation chain transfer (RAFT), have all been reported to graft different polymers from different substrates.[50,137] This is made possible by the modification of the substrate with functional groups that can initiate a polymerization reaction; grafted initiators include alkyl halides for ATRP, alkoxy amines for NMP, photoiniferters for PIMP, and

chain transfer agents for RAFT.[3] Out of all these RDRP techniques, ATRP has become the most extensively used technique to modify surfaces with grafted polymers due to its compatibility with a wide array of monomers and substrates.[137]

All four RDRP processes establish a dynamic equilibrium between propagating radicals and various dormant species.[4] In ATRP, the dormant species (P_n-X) periodically reacts with a transition metal complex in its lower oxidation state such as ([L_mCu(I)]), acting as an activator with the rate constant of activation (k_{act}) (with L representing the ligand). This reaction intermittently produces propagating radicals ($P_n\cdot$), and the transition metal in its higher oxidation state coordinated with the halide ligand from the dormant species ([L_mCu(II)L-X]) (Figure 3.1). The potential of ATRP to control the polymerization process is a promising aspect of this research.[42]

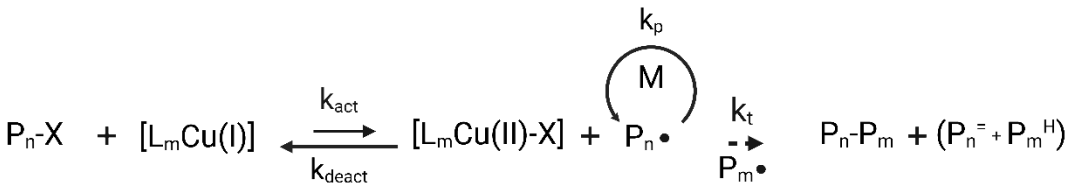

Figure 3.1 ATRP Scheme

The copper-mediated ATRP in water can undergo side reactions that derail the ATRP equilibrium and result in poor levels of control. These side reactions are shown in Figure 3.2 and are listed below as challenges I to IV.[138]

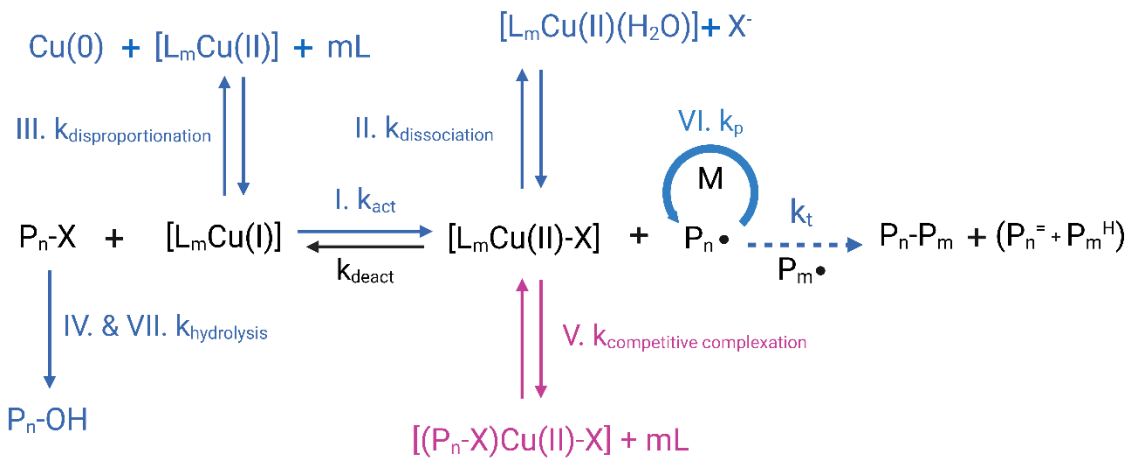

Figure 3.2 Competing side reactions in aqueous ATRP of PAM

I. The ATRP equilibrium constant is large in aqueous media, generating higher radical concentrations that lead to an increased rate of termination.[72]

II. The deactivator, [L_mCu(II)-X], experiences partial dissociation of the anionic halide ligand, leading to the inefficient deactivation of the propagating radicals.[65]

III. The typical [L_mCu(I)] complexes for ATRP can disproportionate into Cu(0) and [L_mCu(II)].[65]

IV. The chain-end functionality (P_n-X) can be hydrolyzed, resulting in lower conversions.[65]

In addition to these concerns, the targeting of high molecular weight polyacrylamide also has the following challenges: [139]

V. Polyacrylamide competitively complexes the transition-metal cations through the amide group, effectively stopping the deactivation from occurring.

VI. A faster rate of polymerization of PAM than the rate of initiation produces a higher dispersity.

VII. The chain-end halide atom can undergo nucleophilic displacement by the amide group of the acrylamide units.

Faced with these challenges, investigation of the aqueous ATRP of PAM has been limited to molecular weights of at most 10^5 g/mol. Appel et al. developed a procedure that controllably polymerizes various acrylamides with a number average molecular weight (M_n) of $3.55 \cdot 10^5$ g/mol using ethanol as a cosolvent to decrease the polarity of the solvent.[49] Wever et al. formed higher molecular weight PAM of up to $5.20 \cdot 10^5$ g/mol via aqueous ATRP using Me_6TREN as a ligand, which has a higher complexation constant and a chlorine-based initiator but produced limited control with a PDI > 1.5.[140]

Therefore, the principal goal discussed in this chapter is the control of the ATRP of polyacrylamide in the formation of high molecular weight 10^5-10^6 g/mol products. This includes a thorough investigation of the following:

1. Testing ATRP variations, such as Activators Regenerated by Electron Transfer (ARGET) ATRP, which uses a reducing agent to regenerate the activator (transition metal complex at the lower oxidation state) and comparing the use of a single injection vs. a controlled feeding of the reducing agent to lower the equilibrium constant by keeping the activator/deactivator ratio low (Challenge I).
2. Investigating the addition of halide salts to stabilize the deactivator, [L_mCu(II)-X], from partial dissociation of the halide ligand (Challenge II) efficiently.
3. Evaluate using cosolvents to reduce the polarity of the solvent (Challenge II).

4. Test bromine/chlorine end-functionalized initiators to investigate their stability against nucleophilic displacement by the penultimate amide group of the formed PAM (Challenges IV, VI, and VII).
5. To investigate the ligand's ability to stabilize the catalyst complex against disproportionation and competitive complexation with the formed PAM while maintaining strong reducing properties (Challenge III and V).

Each parameter is evaluated against two features of a controlled radical polymerization: 1) pre-determinable degree of polymerization (DP) and 2) designed narrow molecular weight distribution. The following equations 19 and 20 define the first feature:

$$\mathrm{DP_n} = \frac{\mathrm{M_{n,theo}}}{\mathrm{M_0}} = \frac{[\mathrm{M}]_0}{[\mathrm{I}]_0} \cdot \text{monomer conversion} \tag{19}$$

Equation 19 Relation of the degree of polymerization to monomer conversion

where $\mathrm{M_{n,theo}}$ is the theoretical number average molecular weight, $\mathrm{M_0}$ is the molar mass of the monomer, $\frac{[\mathrm{M}]_0}{[\mathrm{I}]_0}$ is the ratio of monomer to initiator at t = 0, and monomer conversion is determined by Raman Spectroscopy, detailed in Chapter 2.1.2.

Equation 1 can be rearranged to calculate $\mathrm{M_{n,theo}}$ shown in equation 2:

$$\mathrm{M_{n,theo}} = \mathrm{M_0} \cdot \frac{[\mathrm{M}]_0}{[\mathrm{I}]_0} \cdot \text{monomer conversion} \tag{20}$$

Equation 20 Theoretical number average molecular weight

The $\mathrm{M_{n,theo}}$ can be evaluated against the experimental number average molecular weight ($\mathrm{M_{n,exp}}$) determined by size exclusion chromatography (SEC).

A narrow molecular weight distribution (Đ) indicates the absence of chain transfer and termination reactions in the polymerization. It is calculated by dividing the experimental weight average molecular weight ($M_{w,exp}$) by the experimental number average molecular weight ($M_{n,exp}$) (Equation 21).

$$Đ = \frac{M_{w,exp}}{M_{n,exp}} \quad (21)$$

Equation 21 Experimental dispersity

This chapter aims to synthesize high molecular weight PAM reaching 10^5-10^6 g/mol using aqueous ATRP. The ATRP conditions that produce high molecular weight PAM with a good correlation between $M_{n,theo}$ and $M_{n,exp}$, a narrow molecular weight dispersity (Đ < 1.5), and a decent monomer conversion will be used to graft PAM from the surface of AC in the next chapter.

3.2. Materials and Methods

3.2.1. Materials

Acrylamide, ethanol, $CuCl_2$, triethylammonium bromide (TEABr), sodium chloride, tris[2-(dimethylamino)ethyl]amine (Me_6TREN), ethyl α-bromoisobutyrate (EBiB), and ethyl 2-chloropropionate (ECP) were purchased from Sigma Aldrich and used as received. CuCl was purchased from Sigma Aldrich and was washed with glacial acetic acid. $CuBr_2$ was purchased from Alfa Aesar and was used as received. N,N,N',N",N"-pentamethyldiethylenetriamine (PMDETA) was purchased from TCI America and was used as received. Ascorbic acid was purchased from Bio Basic and was used as received.

3.2.2. Activator Regenerated by Electron Transfer Atom Transfer Radical Polymerization (ARGET ATRP) of Polyacrylamide

3.2.2.1.Single Addition of Ascorbic Acid

10.662 g of acrylamide (0.15 mol), 27 mg of ascorbic acid ($1.5x10^{-4}$ mol), and 39 mL of Millipore water were added to a round bottom flask and sparged with N_2 for 1 hour. 0.5 mL of the catalyst stock solution containing $CuBr_2/CuCl_2$ ($1.5x10^{-5}$ mol) and PMDETA/Me_6TREN ($1.5x10^{-4}$ mol) sparged with N_2, and the initiator ECP/EBiB ($3x10^{-5}$ mol for DP = 5,000 and $7.5x10^{-6}$ mol for DP = 20,000) was injected into the flask using a N_2 purged syringe needle and the reaction was sealed under N_2. Reactions proceeded for the desired times and were stopped by exposing the reaction to air. A sample was taken to analyze using Raman Spectroscopy, while the rest was precipitated with 250 mL methanol. The precipitated polymer was separated from the solution and was washed with another 10 mL of methanol before drying in a vacuum oven at 40 ºC overnight.

3.2.2.2.Feeding of Ascorbic Acid

Samples were treated as in section 3.2.2.1. However, with the change, 30 mL of 7.2 mM ascorbic acid was added to the reaction flask using a syringe pump at a 1.25 mL/hr rate.

3.2.3. Standard Atom Transfer Radical Polymerization (ATRP) of Polyacrylamide

10.662 g of acrylamide (0.15 mol), 80 µl of Me_6TREN ($3x10^{-4}$ mol), initiator ECP/EBiB ($3x10^{-5}$ mol for DP = 5,000 and $7.5x10^{-6}$ for DP = 20,000) and 39 mL of Millipore water were added to a round bottom flask and sparged with N_2 for 1 hour at room temperature. In a 50 mL Schlenk flask, 30 mg of CuCl ($3x10^{-4}$ mol) was added, vacuumed and backfilled with N_2 thrice. The sparged monomer, ligand, and initiator solution were transferred into the Schlenk flask containing CuCl using an N_2-purged syringe to initiate the polymerization. Reactions proceeded

for the desired time and were stopped by exposing the reaction to air. A sample was taken to analyze using Raman spectroscopy, while the rest was precipitated with ~5x v/v methanol. The precipitated polymer was separated from the solution and was washed with another 10 mL of methanol before drying in a vacuum oven at 40 ºC overnight.

3.2.4. Characterization

The polymer's molecular weight and molecular weight distribution were assessed by size exclusion chromatography (SEC) using an Agilent Technologies 1220 Infinity LC equipped with a refractive index detector (RID, Agilent Technologies 1260 Infinity). A PL aquagel-OH MIXED-H 8 μm, 300 x 7.5 mm column was used with an aqueous solution of 0.2 M $NaNO_3$ and 0.01 M NaH_2PO_4 at pH 7 as the mobile phase. Each injected sample was 20 μL with a concentration of 0.10 % (g/mL%). Chromatography proceeded at room temperature, with a 1 mL/min flow rate, with the detector set at 35 ºC. The column was calibrated with PEO/PEG standard samples with narrow molecular weight distributions in the range of 106 – 1,522,000 g/mol (Agilent Technologies). All Raman spectra were acquired using a Renishaw inVia Raman Microscope with 633 nm excitation and an 1800 line/mm diffraction grating. Laser power at the source was 100 mW. Samples were analyzed on a silicon wafer, and five scans were co-added to achieve appropriate signal-to-noise in the 100 to 3400 cm^{-1} range.

3.3.Results and Discussion

3.3.1. Raman spectroscopy of Polyacrylamide

Raman spectroscopy was used to monitor the monomer conversion of acrylamide to PAM (Figure)under different ATRP conditions. As shown in Figure 3.3, the PAM from runs A to O contains the peaks corresponding to the CH_2 symmetrical stretching in the polymer at 2930 cm^{-1},

CH bending in acrylamide (AM) at 1285 cm^{-1}, and CH_2 bending in both AM and PAM at 1430-1460 cm^{-1}. The broadening of the CH_2 bending peak at 1430 cm^{-1} is a blue shift of the CH_2 bending peak as the acrylamide is polymerized.[115] When calculating monomer conversion, the broadened 1430 cm^{-1} peak area is integrated to account for the CH_2 bending in PAM and AM.

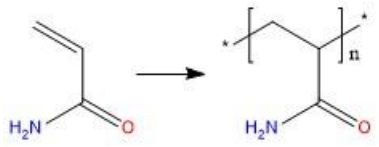

Figure 3.3 Monomer conversion of acrylamide to polyacrylamide (PAM)

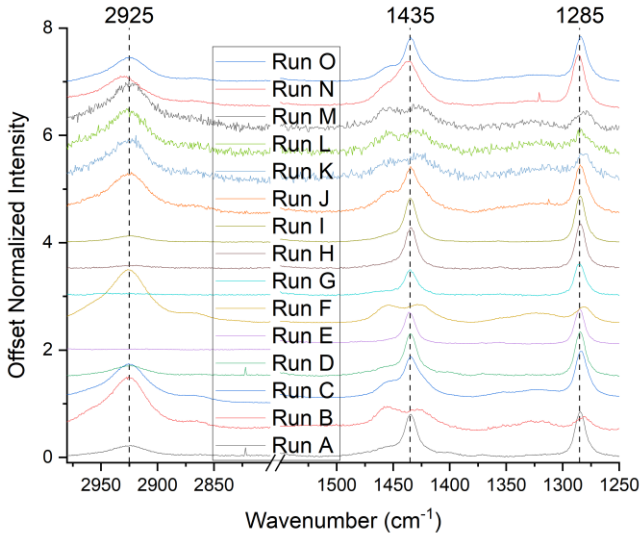

Figure 3.4 Raman spectra of PAM synthesized in Runs A to O. Reaction conditions for Runs A to O are listed in Tables 3.1 to 3.4.

3.3.2. Effect of feeding the reducing agent and temperature

PAM was initially polymerized to a DP = 5,000, which should reach 355,400 g/mol at 100% monomer conversion. The baseline (Run A) used an ARGET ATRP procedure to polymerize PAM, poly(methyl methacrylate), and poly(t-butyl acrylate) from the surface of AC.[112,141] This resulted in a high dispersity of 4, indicating a loss of control in the reaction, likely due to challenges outlined in the introduction (Table 3.1). Challenge I was to reduce the large

ATRP equilibrium constant in aqueous ATRP. This was addressed by incrementally feeding the ascorbic acid to maintain a lower activator/deactivator ratio and reducing the concentration of propagating radicals, leading to a decreased rate of termination. Combined with a decrease in reaction temperature, which also lowers the ATRP equilibrium, this achieved a lower dispersity of 2.04 (Run D).

Table 3.1 The effect of feeding reducing agent and temperature to the monomer conversion, theoretical number average molecular weight (Mn, theo), experimental number and weight average molecular weight (Mn, exp and Mw, exp), and dispersity of the ARGET ATRP of PAM

Run	Ascorbic acid feed (µmol/minute)	Temperature (ºC)	Time (minutes)	Monomer Conversion (%)	$M_{n,\ theo}$ (kg/mol)	$M_{n,\ exp}$ (kg/mol)	$M_{w,\ exp}$ (kg/mol)	Đ
A	A single Injection of 300 µmol	60	15	50±18	180±64	250±40	1000± 159	4.0±0.2
B	30	60	15	77±1	274±3	220±17	940± 82	4.3±0.3
C	30	40	60	60±12	220±44	190±16	610± 40	3.2±0.1
D	30	RT	60	35±9	120±31	210±17	430± 24	2.04± 0.05
E	15	RT	60	7±2	27±8	220±26	490± 25	2.2±0.2

ARGET ATRP with DP = [M]/[I] = 5000, [M] = 3M, moles(M) = 0.15, [I]:[Cu]:[L] = 1:1:10, PMDETA as the ligand, $CuBr_2$ as the catalyst, and water as the solvent. Each experiment was run in triplicate.

3.3.3. Effect of halide salt and solvent

Further improvements in the polymerization were achieved by using ethanol as a cosolvent, reducing the solvent's polarity and stabilizing the deactivator from halide ligand dissociation (Challenge II). This achieved a high monomer conversion of up to 81% and a dispersity of 1.9. Further stabilization of the deactivator was achieved with the addition of halide salts TEABr/NaCl, reaching the lowest dispersity of 1.4 (Runs G-I). The lower dispersity came

at the cost of poor monomer conversions not greater than 30% even after 4 hours. The slower rate of polymerization could be due to a higher concentration of deactivator, [$L_mCu(II)$-X], by the formation of inactive [$L_mCu(II)$-X], or substitution of Me_6TREN ligand with halide anions.[69]

Table 3.2 The effect of halide salt choice and concentration, and solvent choice on the monomer conversion, theoretical number average molecular weight ($M_{n,\,theo}$), experimental number, weight average molecular weight ($M_{n,\,exp}$ and $M_{w,\,exp}$), and dispersity of the ARGET ATRP of PAM

Run	Halide Salt (M)	Solvent	Time (hours)	Monomer Conversion (%)	$M_{n,\,theo}$ (kg/mol)	$M_{n,\,exp}$ (kg/mol)	$M_{w,\,exp}$ (kg/mol)	Đ
D	None	water	1	35±9	120±31	210±17	430±24	2.04±0.05
F	None	70:30 water: ethanol	Instant	81±1	287±5	382±6	700±12	1.9±0.2
G	0.1M TEABr	70:30 water: ethanol	4	14±7	50±15	48±1	72±1	1.49±0.03
H	1M NaCl	70:30 water: ethanol	4	12±6	40±20	49±3	73±3	1.49±0.04
I	1M TEABr	70:30 water: ethanol	4	30±9	100±34	13±4	19±9	1.4±0.2

ARGET ATRP with DP = [M]/[I] = 5000, [M] = 3M, moles(M) = 0.15 mol, [I]:[Cu]:[L] = 1:1:10, PMDETA as the ligand, $CuBr_2$ as the catalyst, at room temperature and ascorbic acid was fed at a rate of 1 mole to the metal per minutes. Each experiment was run in triplicate.

3.3.4. Effect of catalyst and ligand complex

Challenges III, IV, V, VI, and VII were addressed by replacing the alkyl bromide initiator (EBiB) with an alkyl chloride initiator (ECP) and the catalyst complex to CuCl/Me_6TREN in Run K. This resulted in a decent monomer conversion and a low dispersity of 1.6 (Table 3.3, Figure 3.4). The alkyl chloride initiator and CuCl stabilized the dormant species from hydrolysis.[67,69] The ligand Me_6TREN replaced PMDETA since it has a lower disproportionation rate constant when complexed with Cu(I).[68] Lastly, a standard ATRP replaced the previous ARGET ATRP procedure since the feeding of ascorbic acid could not polymerize PAM from the

surface of AC in a separate experiment, likely due to the slower production of propagating radicals and their trapping by the variety of oxygen functional groups on the surface of AC in the feeding of ascorbic acid. Therefore, Run K was the ideal candidate to test high molecular weight PAM polymerization with molecular weights of up to 10^6 g/mol. This was achieved by targeting a higher DP of 20,000, which should be 1,421,600 g/mol at 100% monomer conversion.

Table 3.3 The effect of halide salt concentration and ligand/metal catalyst complex to the monomer conversion, theoretical number average molecular weight ($M_{n,\,theo}$), experimental number and weight average molecular weight ($M_{n,\,exp}$ and $M_{w,\,exp}$), and dispersity of the ARGET ATRP of PAM

Run	Reaction Conditions	Time (minutes)	Monomer Conversion (%)	$M_{n,\,theo}$ (kg/mol)	$M_{n,\,exp}$ (kg/mol)	$M_{w,\,exp}$ (kg/mol)	Đ
H[1]	EBiB initiator, [$CuBr_2$] = 3, [PMDETA] = 30 mM, 1M NaCl, 30% ethanol	4	12±6	40±20	49±3	73±3	1.49±0.04
J	ECP initiator, [CuCl] = [Me_6TREN] = 3 mM, 30% ethanol	4	54±7	190±20	100±20	220±50	2.2±0.2
K	ECP initiator, [CuCl] = [Me_6TREN] = 3 mM, 0.1M NaCl, 30% ethanol	1	69±1	246±4	107±4	180±20	1.6±0.1
L	ECP initiator, [CuCl] = [Me_6TREN] = 3 mM, 0.5M NaCl, 30% ethanol	1	70±11	260±39	91±6	360±40	4.0±0.2

[1]ARGET ATRP with ascorbic acid was fed at a rate of 1 mole to the metal per minute,DP = [M]/[I] = 5000, [M] = 3M, moles(M) = 0.15, and conducted at room temperature. Each experiment was run in triplicate.

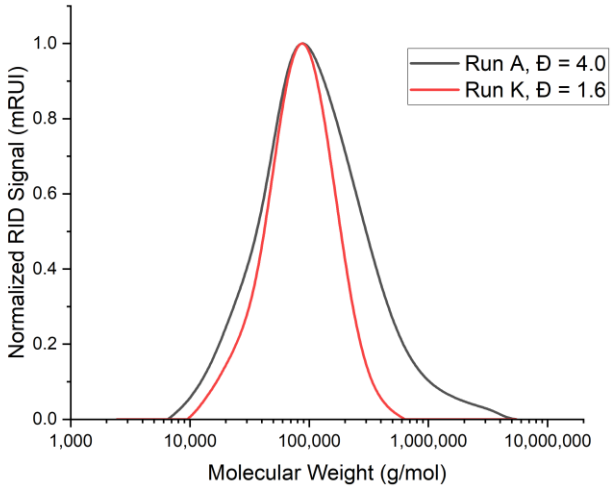

Figure 3.5 Normalized RID Signal vs molecular weight of PAM synthesized from Run A and Run K

3.3.5. Increasing Degree of Polymerization (DP)

With the same reaction conditions as run K, run M increased its degree of polymerization to 20,000 by reducing the concentration of the initiator. However, it only reached a low M_n value of 180 kg/mol even though its theoretical M_n is 1,000 kg/mol. This could indicate that acrylamide polymerizes outside the provided alkyl chloride initiator, translating to unattached/free PAM when using an AC macroinitiator. Higher molecular weights were achieved using an alkyl bromide initiator with a higher activation rate constant than alkyl chloride and removing the additional halide salt and ethanol cosolvent.[67] Run N used a standard ATRP procedure, achieving higher than expected M_n, likely due to termination reactions such as chain coupling. On the other hand, Run O, which used an ARGET ATRP procedure, achieved a better correlation between theoretical and experimental M_n, likely due to a higher initial concentration of deactivator, $CuCl_2$, which mediated the concentration of propagating radicals, preventing termination events.

Table 3.4 Ultra-high molecular weight PAM (Degree of Polymerization = 20,000) and their monomer conversion, theoretical number average molecular weight ($M_{n,\,theo}$), experimental number and weight average molecular weight ($M_{n,\,exp}$ and $M_{w,\,exp}$), and dispersity of the ATRP of PAM

Run	Reaction Conditions	Monomer Conversion (%)	$M_{n,\,theo}$ (kg/mol)	$M_{n,\,exp}$ (kg/mol)	$M_{w,\,exp}$ (kg/mol)	Đ
M[1]	ECP initiator, [CuCl] = [Me_6TREN] = 3 mM, 0.1M NaCl, 30% ethanol	70 ± 12	1,000 ± 200	180 ± 65	280 ± 70	2.6 ± 0.5
N[2]	[CuCl] = [Me_6TREN] = 1.2 mM, water	50 ± 13	700 ± 200	1,900 ± 600	3,000 ± 2,000	1.7 ± 0.3
O[2]	[$CuCl_2$] = 1.2 mM, [Me_6TREN] = [Ascorbic Acid] = 6 mM, water	60 ± 11	900 ± 200	700 ± 200	1,000 ± 300	1.4 ± 0.2

[1]DP = [M]/[I] = 5000, [M] = 3M, moles(M) = 0.15, and conducted at room temperature for 1 hour. [2]DP = [M]/[I] = 20000, [M] = 3M, moles(M) = 0.15, and conducted at room temperature for 1 hour. Each experiment was run in triplicate.

3.4.Conclusions

In this chapter, I have described the successful synthesis of polyacrylamides with three different molecular weights, 100, 700, and 1900 kg/mol, with molecular weight dispersities 1.4-1.7, via aqueous ATRP. Lower molecular weights of 100 kg/mol with low molecular weight dispersities were attained using ethanol as a cosolvent, additional halide salt, an alkyl chloride initiator, and CuCl/Me_6TREN catalyst (Run K). Ultra-high molecular weight PAM with higher molecular weights of 700 and 1,900 kg/mol were attained via standard and ARGET ATRP using Me_6TREN as a ligand and an alkyl bromide initiator (Run N and O). The next chapter uses the ATRP conditions in Run K, Run N, and Run O to graft PAM brushes on activated carbon with different molecular weights via SI-ATRP.

4. Surface Initiated Atom Transfer Radical Polymerization from Activated Carbon

4.1. Introduction

Activated carbon (AC) is a versatile material owing to its unique porous and carbonaceous structure composed of disordered aromatic sheets.[101] Depending on the carbonaceous precursor, the resulting AC could have a variety of functional groups on its surface due to residual heteroatoms such as oxygen and nitrogen.[102] These influence the AC's properties, including hydrophobicity, surface charge, electron density, and sites for further surface modifications.[102–104] The combination of AC's carbonaceous porosity and surface functional groups allows it to be extensively used as a solid-state adsorbent for gaseous and liquid contaminants.[94–98,107,109]

Research has uncovered a promising and cost-effective method for waste remediation in the oil sand industry: the transformation of petcoke byproducts into AC. This method, with its potential to adsorb naphthenic acids and heavy metals present in oil sand process-affected water, offers hope for the future of waste remediation in the oil sand industry.[107–109] Continuing the effort to apply petcoke AC to remediate waste produced by the oil sand industry, this research investigates the use of petcoke AC as a substrate for grafting polyacrylamide. This is significant as it offers a potential solution for the large-scale flocculation of over a trillion litres of tailings, a primary environmental concern in the oil sand industry.

Surface modification through polymer grafting has become a powerful approach to modifying interfaces' chemical and physical properties.[137] Depending on the specific polymer, it can impart a high density of different functional groups and morphologies. This can alter the substrate's properties, including adsorption capacity, colloidal stability, surface wettability, and

electronic properties.[137] There are three approaches to polymer grafting: grafting-to, -through, or -from. A grafting-from method is usually employed to modify substrates because it can achieve higher grafting densities since polymer chains are directly grown from an initiator functionalized surface.[76,86,142,143] A grafting-from approach uses a surface-initiated reversible-deactivation radical polymerization (SI-RDRP) capable of forming polymers with precise molecular weight, architecture, and composition control.[44,137]

Previously in our laboratory, an AC-modified PAM (AC-PAM) was synthesized via a grafting-from method using surface-initiated activators generated by electron transfer atom transfer radical polymerization (SI-AGET-ATRP). With its remarkable ability to flocculate dilute mature fine tailings (MFT) with 5 wt% solids, this AC-PAM outperformed free PAM with the same molecular weight and dose of 20,000 ppm. The potential application of this AC-PAM in large-scale flocculation of over a trillion litres of tailings is a promising area for further research.[112]

Ungrafted/free polyacrylamide requires a higher molecular weight of $2x10^6$ g/mol to flocculate tailings effectively.[18] At this molecular weight, the polymer's length is much greater than twice the double-layer length of the suspended clays in the tailings, allowing it to induce bridging flocculation.[18] Additionally, the PAM forms a gel-like network in water via hydrogen bonding that hinders its ability to release water during flocculation.[19] The introduction of hydrophobic segments in PAM is currently being researched to improve the water release during flocculation. This has been seen in the literature by the copolymerizing of PAM with hydrophobic monomers such as N-tert-butyl acrylamide (t-BAAM)[28], N-isopropyl acrylamide (NIPAM),[29] and 5-methacrylomido-1,2-benzoboroxole (MAAMBO).[30] These reports have shown

that increasing the hydrophobic segment can improve the rate of dewatering from the aggregates by up to a factor of five.[31]

This chapter discusses synthesizing high molecular weight PAM brushes from the surface of hydrophobic petcoke-based AC to evaluate their effect on the flocculation of dilute mature fine tailings (MFT). The AC is modified into a macroinitiator for SI-ATRP using an adapted procedure from Begin et al. (Figure 4.1).[112] The polymer brushes are grown from the surface of the initiator-modified AC using the ATRP conditions developed in the previous chapter.

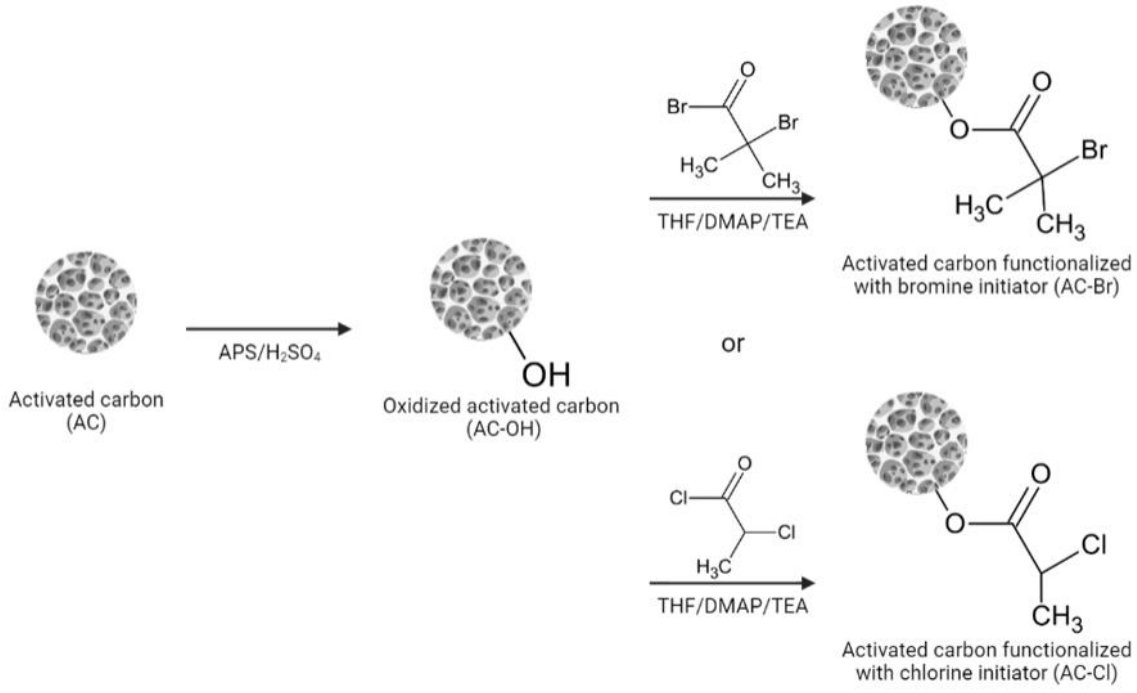

Figure 4.1 Synthesis scheme for the preparation of initiator-modified ACs

4.2. Materials and Methods

4.2.1. Materials

Potassium hydroxide (KOH), ammonium persulfate (APS), sulfuric acid (H_2SO_4), 4-N,N-dimethylaminopyridine (DMAP), α-bromoisobutyrylbromide (BiBB), and 2-chloropropionyl chloride (CPC) was purchased from Sigma Aldrich and was used as received.

Dichloromethane (DCM) and tetrahydrofuran (THF) were purchased from Sigma Aldrich and were dried using 4 Å molecular sieves. Triethylamine (TEA) was purchased from Alfa Aesar and was dried using 4 Å molecular sieves. Suncor Energy Inc. (Alberta, Canada) supplied petroleum coke.

4.2.2. Preparation of Activated Carbon from Petroleum Coke

Petroleum coke was first heat treated at 400 ºC for 30 minutes to remove impurities. Approximately 3.0 g of petroleum coke and 3.0 g of KOH were ground thoroughly and placed in a stainless-steel crucible. The mixture was then ramped at 40 ºC/min to 430 ºC, where it was held for 30 minutes, followed by ramping at 90 ºC/min to 900 ºC, where it was held for 15 minutes, all under N_2. The sample was allowed to cool to a minimum of 250 ºC under N_2 flow before being removed from the oven. The sample was ground with a mortar and pestle and stirred with 60 mL of deionized water for 1 hour, then vacuum filtered and washed with 60 mL of deionized water at 80 ºC for another hour. The sample was finally stirred with 0.1 M HCl (10 mL/g of AC) at 80 ºC for 1 hour, then recovered by vacuum filtration. The recovered AC)was dried in an oven at 110 ºC overnight. The dried AC was separated by diameter using US Standard Sieve No. 35 and 140, resulting in ACs with diameters >0.5mm, 0.1 – 0.5 mm, and <0.1 mm.

4.2.3. Preparation of oxidized activated carbon (AC-OH)

Approximately 4.0 g of activated carbon (<0.1 mm and 0.1 – 0.5 mm diameter), 22.2 g ammonium persulfate (97.3 mmol), and 2.72 mL (50.0 mmol) of concentrated H_2SO_4 were added to 35 mL of deionized water. The mixture was stirred at 300 rpm at 60 ºC for 4 hours. The mixture was cooled to room temperature and filtered by vacuum filtration. The product was washed with deionized water until the washings were neutral, then dried in an oven overnight at 110 ºC.

4.2.4. Preparation of initiator grafted activated carbon

4.2.4.1. Bromine initiator grafted activated carbon (AC-Br)

Approximately 2.5 g of AC-OH (<0.1 mm and 0.1 – 0.5 mm diameter), 0.147 g of DMAP (1.20 mmol), 50 mL of dry tetrahydrofuran (THF), and 2.80 mL of triethylamine (20.1 mmol) were added to a 100 mL round bottom flask. The mixture was dispersed in an ultrasonic bath for 30 minutes, then transferred to an ice-salt bath and sparged with N_2 for 30 minutes. In a separate round bottom flask in an ice-salt bath, 14 mL of dry THF was sparged with N_2 for 30 minutes. Once sparged, 1.076 mL of α-bromoisobutyryl bromide (BiBB) (8.705 mmol) was charged. The initiator solution with BiBB was charged dropwise into the AC-OH solution for an hour. The mixture was stirred in an ice-salt bath for 3 hours, then at room temperature for 48 hours. The mixture was filtered and washed with deionized water and then acetone. The resulting product was dried in a vacuum oven at 40 ºC.

4.2.4.2. Chlorine initiator grafted activated carbon (AC-Cl)

Approximately 2.5 g of AC-OH, 0.147 g of DMAP (1.20 mmol), 50 mL of dry DCM and 2.80 mL of TEA (20.1 mmol) were added to a 100 mL round bottom flask. The mixture was dispersed in an ultrasonic bath for 30 minutes, then transferred to an ice-salt bath and sparged with N_2 for 30 minutes. In a separate round bottom flask in an ice-salt bath, 14 mL of dry DCM was sparged with N_2 for 30 minutes. Once sparged, 1.529 mL of 2-chloropropionyl chloride (CPC) (15.80 mmol) was charged. The initiator solution with BiBB was added dropwise into the AC-OH solution for an hour. The mixture was stirred in an ice-salt bath for 3 hours, then at room temperature for 48 hours. The mixture was filtered and washed with deionized water and then acetone. The resulting product was dried in a vacuum oven at 40ºC.

4.2.5. Surface-initiated ATRP of acrylamide from AC-Init (AC-PAM)

4.2.5.1. Standard ATRP

10.67 g of acrylamide (15.00 mmol), 15/150 mg of AC-Br (<0.1 mm and 0.1 – 0.5 mm diameter), and 39 mL of Millipore water were added to a Schlenk flask and sparged with N_2 for 1 hour. After sparging, the Schlenk flask was put under positive nitrogen before adding CuCl (0.015 mmol) and Me_6TREN (0.015 mmol). The reaction was sealed, then vacuumed and filled with N_2 three times. The reaction was stirred at 300 rpm for 24 hours. Afterward, the AC-PAM was precipitated from the reaction using 250 mL of methanol, collected, and washed with another 50 mL of methanol before drying in a vacuum oven at 60ºC overnight.

4.2.5.2. ARGET ATRP

10.67 g of acrylamide (15.00 mmol), 27 mg of ascorbic acid (0.15 mmol), 15/150 mg of AC-Br/Cl (<0.1 mm and 0.1 – 0.5 mm diameter), and 34 mL of Millipore water were added to a round bottom flask and sparged with N_2 for 1 hour. $CuBr_2$/$CuCl_2$ (0.015mmol) and PMDETA/Me_6TREN (0.15 mmol) were added into a vial fitted with a septum containing 5 mL of water. The catalyst solution was sparged with N_2 and injected into the flask containing the monomer solution using an N_2-purged syringe needle, and the reaction was sealed under N_2 flow. The reaction was stirred at 300 rpm for 24 hours. Afterward, the AC-PAM was precipitated from the reaction using 250 mL of methanol, collected, and washed with another 50 mL of methanol before drying in a vacuum oven at 60 ºC overnight.

4.2.6. Hydrolysis of PAM from AC-PAM

The polymer was cleaved off the surface of AC through acid-catalyzed hydrolysis to determine the molecular weight of the grafted polymer. 0.1 g of AC-PAM was added into 5 mL

of 0.1 M hydrochloric acid (HCl), and the mixture was refluxed at 100 ºC for 3 hours. Upon completion, the solution was cooled to room temperature and neutralized to pH 7 using dilute NaOH, and the PAM was collected using a 0.45 μm syringe filter. The filtrate was precipitated in excess methanol (~ x5 filtrate volume) and vacuum filtered to recover the cleaved polymer, which was dried in a vacuum oven at 60 ºC overnight.

4.2.7. Characterization

Fourier transform infrared spectroscopy (FTIR) was used to determine the functional groups on the surface of the different AC samples. All samples were analyzed using a Nicolet 380 FTIR spectrometer with a diamond crystal attenuated total reflectance (ATR) accessory. 128 scans per analysis within the 4000-400 cm^{-1} range were performed. The functionalized activated carbon samples' elemental composition and chemical speciation were measured by X-ray photoelectron spectroscopy (XPS), as described in Chapter 2.1.5. The polymer's molecular weight and molecular weight distribution were assessed by size exclusion chromatography (SEC) using an Agilent Technologies 1220 Infinity LC equipped with a refractive index detector (RID, Agilent Technologies 1260 Infinity). A PL aquagel-OH MIXED-H 8 μm, 300 x 7.5 mm column was used with an aqueous solution of 0.2M $NaNO_3$ and 0.01 M NaH_2PO_4 at pH 7 as the mobile phase. Each sample injected was 20 μL with a concentration of 0.10 % (g/mL%). Chromatography proceeded at room temperature, with a 1 mL/min flow rate, with the detector set at 35ºC. The column was calibrated with PEO/PEG standard samples with narrow molecular weight distributions in the range of 106 – 1,522,000 g/mol (Agilent Technologies). Thermogravimetric analysis (TGA) was employed to determine the weight percent of the grafted material on the surface of the functionalized activated carbon samples. TGA was performed

using a TA instruments Q600 SDT thermal analyzer. The samples were heated from room temperature to 1000 ºC at 10 ºC/min under argon with a 20 mL/min flow rate.

4.3. Results and Discussion

4.3.1. Characterization of AC-PAM

Polyacrylamide was grafted from an activated carbon initiator with particle sizes <0.1 mm and 0.1-0.5 mm, denoted as $AC_{0.1}$ and $AC_{0.1\text{-}0.5}$. The AC initiator was synthesized by first oxidizing the activated carbon ($AC_{0.1}$-OH and $AC_{0.1\text{-}0.5}$-OH). The ATRP initiators, α-bromoisobutyryl bromide and 2-chloropropionyl chloride, were grafted to the oxidized AC surface to form the AC macroinitiators ($AC_{0.1}$-Br, $AC_{0.1\text{-}0.5}$-Br, $AC_{0.1}$-Cl, and $AC_{0.1\text{-}0.5}$-Cl). Polyacrylamide was grafted from these AC macroinitiators using standard and ARGET SI-ATRP at a Degree of Polymerization (DP) of 20,000, 5,000, or 2,000 based on Runs K, N, and O, denoted with the subscript $PAM_{5k,\ EtOH,\ NaCl}$, $PAM_{20k,\ Std}$, $PAM_{2k,\ Std}$, or $PAM_{20k,\ ARGET}$.

FTIR was used to monitor the addition of new functional groups after every modification on AC. Figure 4.2 shows the FTIR of the modified $AC_{0.1\text{-}0.5}$. The oxidized AC contains various oxygen-containing functional groups, evident from the band at 1716 cm^{-1} corresponding to C=O stretching vibrations of ketones, aldehydes, carboxyl or lactone groups, and the band at 1210 cm^{-1} assigned to C-O stretching vibrations in acids, phenols, esters and ethers (Figure 4.2). After initiator functionalization, both AC-Br and AC-Cl had an additional small peak at 1643 cm^{-1} corresponding to the C=O stretching vibration of alkyl bromide and alkyl chloride. Additionally, peaks corresponding to PAM were observed after grafting the PAM from the surface of AC ($AC_{0.1\text{-}0.5}$-Br-$PAM_{20k,\ Std}$). These included an NH_2 asymmetric stretching at 3339 cm^{-1}, NH_2 symmetric stretching at 3185 cm^{-1}, sp^3 CH_2 symmetric stretching at 2926 cm^{-1}, sp^3 CH_2

asymmetric stretching at 2860 cm^{-1}, C=O stretching at 1647 cm^{-1}, N-H bending at 1604 cm^{-1}, sp^3 CH_2 bending at 1446 cm^{-1}, and C-N stretching at 1415 cm^{-1}. The FTIR spectra for modified AC particle sizes <0.1 mm and the rest of AC-PAM showed similar results (Supplementary Figure S1).

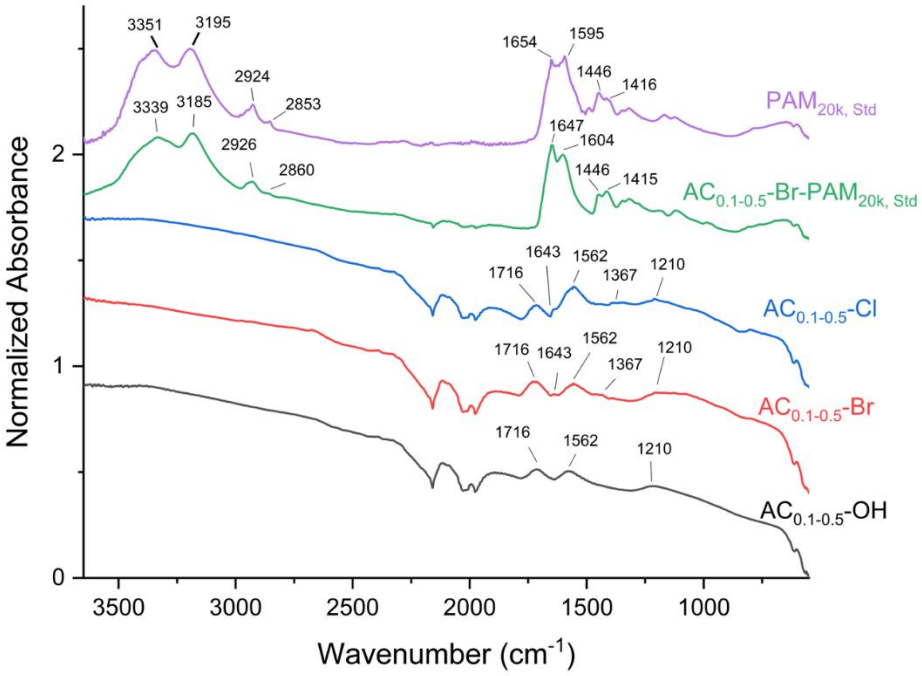

Figure 4.2 FTIR of oxidized AC ($AC_{0.1\text{-}0.5\text{-}OH}$), alkyl bromide-modified AC ($AC_{0.1\text{-}0.5}$-Br), alkyl chloride-modified AC ($AC_{0.1\text{-}0.5}$-Cl), polyacrylamide grafted AC ($AC_{0.1\text{-}0.5}$-Br-$PAM_{20k,\ Std}$), and polyacrylamide (PAM).

The elemental composition and speciation of the various modified ACs were determined using XPS. The elemental composition was determined from each sample's survey scans and is summarized in Table 4.1 below. Oxidation of the AC increased the total oxygen content in the sample from 16.13 and 15.88 At % to 20.69 and 18.81 At % while reducing the oxygen-containing silicates from 1.74 and 1.71 At% to 0.54 and 0.40 At%. Functionalization with the initiator increased the bromine content to 1.11 and 1.38 At %, while functionalization with the alkyl chloride initiator increased the chlorine content to 1.30 At%.

Table 4.1 Elemental composition in atomic % of standard, oxidized, bromine-initiator, and chlorine-initiator functionalized ACs with particle diameters <0.1 mm and 0.1-0.5 mm from XPS survey scans

Sample Name	Elemental Composition (At %)					
	C	O	Br	Cl	N	Others
Standard Activated Carbon ($AC_{<0.1}$)	81.32	16.13	0.00	0.00	0.30	Si(1.74), Fe(0.34), Ti(0.17)
Standard Activated Carbon ($AC_{0.1-0.5}$)	80.05	15.88	0.26	0.00	0.30	Si(1.71), Fe(0.33), Al(1.30), Ti(0.17)
Oxidized AC ($AC_{<0.1}$-OH)	78.31	20.69	0.00	0.44	0.01	S(0.54)
Oxidized AC ($AC_{0.1-0.5}$-OH)	79.84	18.81	0.00	0.00	0.88	Si(0.40), Fe(0.04), Ti(0.03)
Bromine-initiator functionalized AC ($AC_{<0.1}$-Br)	79.75	16.97	1.11	0.00	2.06	Si(0.12)
Bromine-initiator functionalized AC ($AC_{0.1-0.5}$-Br)	81.98	14.79	1.38	0.00	1.29	Si(0.56)
Chlorine-initiator functionalized AC ($AC_{0.1-0.5}$-Cl)	72.82	19.18	0.00	1.30	2.44	Si(2.05), Al(0.99), S(0.56), Ca(0.66)

Peak fitting of the high-resolution C 1s scan of the oxidized AC indicated successful oxidation due to the increase in % area of carbon-oxygen components C-OH/C-O-C (286.3-286.5 eV), C=O (287.7-287.9 eV), and O=C-O (288.8-289.0 eV) shown for $AC_{0.1\text{-}0.5}$ in Figure 4.3 while the C 1s scan of $AC_{<0.1}$ and the rest of the synthesized AC-PAMs are in Figure S2. Additionally, the "living" halide-ends of the alkyl halide initiators tethered on the surface of AC were preserved after initiator functionalization, as evident from the high % area of both C-Br and C-Cl from the peak fittings of high-resolution Br 3d scan and Cl 2p scan (Figure 4.4). Finally, ATRP of acrylamide conducted on free alkyl halide initiator forming PAM and from the surface of AC-Cl/AC-Br showed an increase in % area of carbon-oxygen component N-C=O (287.8-288.0 eV).

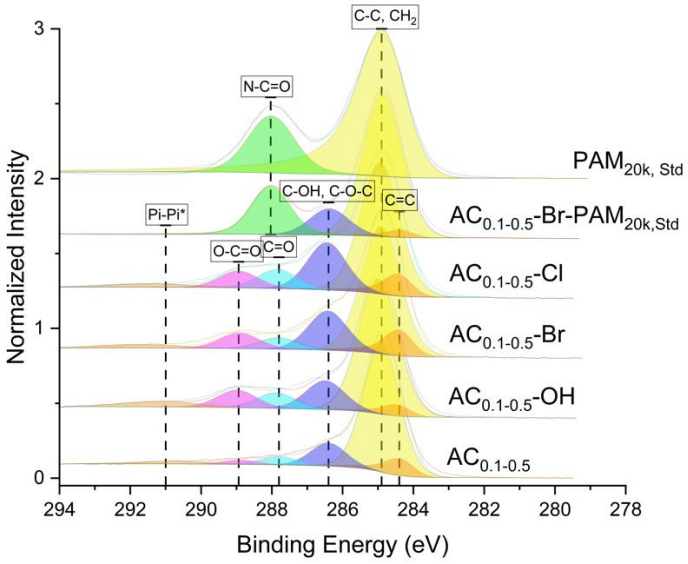

Figure 4.3 High-resolution C 1s scans with synthetic components for activated carbon ($AC_{0.1\text{-}0.5}$), oxidized AC ($AC_{0.1\text{-}0.5}$-OH), alkyl-bromide functionalized AC ($AC_{0.1\text{-}0.5}$-Br), alkyl-chloride functionalized AC ($AC_{0.1\text{-}0.5}$-Cl), polyacrylamide grafted from AC ($AC_{0.1\text{-}0.5}$-Br-$PAM_{20k,\ Std}$)

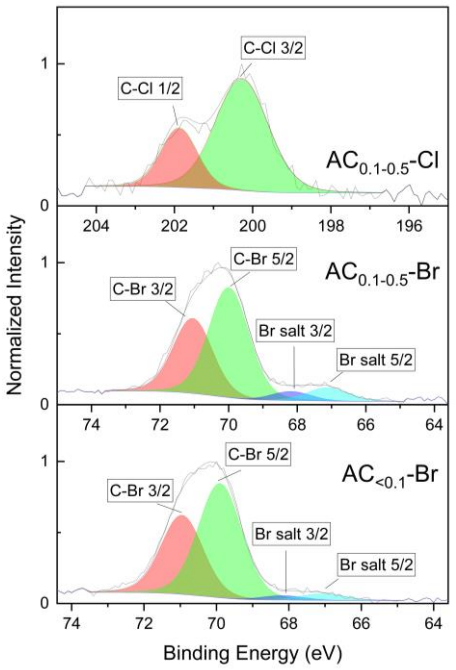

Figure 4.4 High-resolution (bottom) Cl 2p scan of alkyl chloride functionalized AC ($AC_{0.1\text{-}0.5}$-Cl) (top), Br 3d scan of alkyl bromide functionalized AC ($AC_{0.1\text{-}0.5}$-Br) (middle), and ($AC_{0.1}$-Br) (bottom) with synthetic components fitted.

The amount of initiator bound to the surface of activated carbon can also be estimated using the elemental composition of both AC-Br and AC-Cl from their respective XPS survey scans. The Br/Cl atomic % from the XPS survey scan can be converted to weight % using Equation 22. The Br/Cl weight % was used to estimate the concentration of Br/Cl as moles per gram of AC, which is 1:1 to the moles of initiating groups grafted per gram of AC using Equation 23. Finally, the mass of AC-Br and AC-Cl required to reach DP = 20,000 is calculated using Equation 24 and summarized in Table 4.2. A high DP of 20,000 was targeted to produce a molecular weight of 1,421.6 kg/mol if 100% monomer conversion and initiator efficiency were achieved. A lower DP of 2,000 was attempted to achieve a higher AC to PAM content.

$$\mathrm{Wt\%\ (Br)} = \frac{\frac{\mathrm{Wt\%(Br)}}{\mathrm{At\%(Br)}}}{\sum \frac{\mathrm{Wt\%(Br, C, O, \dots)}}{\mathrm{At\%(Br, C, O, \dots)}}} \tag{22}$$

Equation 22 Conversion to weight percent from atomic percent

$$[\mathrm{Br}]\left(\frac{\mathrm{moles}}{\mathrm{gram\ of\ AC}}\right) = \frac{\mathrm{moles\ (Br)}}{\mathrm{grams\ of\ AC}} = \frac{\mathrm{Wt\%(Br)}}{100 \cdot \mathrm{molar\ mass\ (Br)}} \tag{23}$$

Equation 23 Concentration of halide on the surface of AC in moles per gram of AC

$$\mathrm{AC_{<0.1}Br\ (g)} = \frac{\mathrm{moles\ of\ monomer}}{\mathrm{DP} \cdot [\mathrm{Br}]} = \frac{0.15}{20{,}000 \cdot 0.0008} = 0.009\ \mathrm{g} \tag{24}$$

Equation 24 Amount of AC initiator required to reach a specified degree of polymerization

Table 4.2 Weight %, concentration of Br and Cl on the surface of AC, and mass required to reach DP =[M]/[I]= 20k

Sample	Br/Cl Wt %	Concentration (mmoles of Br/Cl per gram of AC)	Mass required to reach DP = 20k (mg)
$AC_{0.1\text{-}0.5}$-Cl	3.3	0.90	8
$AC_{<0.1}$-Br	6.6	0.80	9
$AC_{0.1\text{-}0.5}$-Br	8.1	1.0	8

4.3.2. Molecular weight determination

Using the synthesized AC macroinitiators, seven different AC-PAMs were synthesized using different ATRP conditions (using Run K, N, and O from Chapter 3), AC particle size, and degrees of polymerization (DP). Their molecular weights and dispersity were determined by first cleaving the polymer brushes from the surface of AC using acid-catalyzed hydrolysis. The cleaved polymer was then analyzed using size exclusion chromatography calibrated by PEO/PEG standards as described in Chapter 3.

Table 4.3 Mass recovery, number (M_n) and weight (M_w) average molecular weight of AC-PAM synthesized using different ATRP conditions of Run M, N, and O from Chapter 3, particle size, and degree of polymerization

Sample	Reaction Conditions	Mass Recovery (%)	$M_{n,exp}$ (kg/mol)	$M_{w,exp}$ (kg/mol)
$AC_{0.1\text{-}0.5}$-Cl-$PAM_{5k,\ EtOH,\ NaCl}$	[CuCl] = [Me_6TREN] = 3 mM, 0.1M NaCl, 30% ethanol	60 ± 15	110 ± 10	280 ± 70
$AC_{<0.1}$-Br-$PAM_{20k,\ Std}$	[CuCl] = [Me_6TREN] = 0.9 mM	7 ± 2	5,600 ± 600	9,700 ± 900
$AC_{0.1\text{-}0.5}$-Br-$PAM_{20k,\ Std}$	[CuCl] = [Me_6TREN] = 0.9 mM	5 ± 2	4,900 ± 900	9,000 ± 2,000
$AC_{<0.1}$-Br-$PAM_{2k,\ Std}$	[CuCl] = [Me_6TREN] = 0.9 mM	24 ± 8	3,800 ± 600	7,000 ± 1,000
$AC_{0.1\text{-}0.5}$-Br-$PAM_{2k,\ Std}$	[CuCl] = [Me_6TREN] = 0.9 mM	17 ± 6	3,300 ± 700	6,000 ± 1,000
$AC_{<0.1}$-Br-$PAM_{20k,\ ARGET}$	[$CuCl_2$] = [Me_6TREN] = [Ascorbic Acid] = 3mM	22 ± 7	3,000 ± 1,000	6,000 ± 3,000
$AC_{0.1\text{-}0.5}$-Br-$PAM_{20k,\ ARGET}$	[$CuCl_2$] = [Me_6TREN] = [Ascorbic Acid] = 3mM	37 ± 2	1,400 ± 800	2,000 ± 2,000

Like Run M, $AC_{0.1\text{-}0.5}$-Cl-$PAM_{20k,\ EtOH,\ and\ NaCl}$ achieved high mass recoveries but low molecular weights, indicating chain transfer reactions that polymerize acrylamide outside the initiators tethered on the surface of AC (Table 4.3). Reducing the polarity using ethanol, increasing the stability of the deactivator using NaCl, and using a more stable alkyl chloride initiator have been shown to decrease the value of the ATRP equilibrium and improve the

control over the polymerization.[69,72] However, higher M_n was achieved when ethanol and NaCl were removed, and an alkyl bromide initiator was used. This shows that a higher ATRP equilibrium is preferred when grafting high-molecular-weight PAM.

Grafting from the surface of AC could hinder the polymerization of higher molecular weight PAM due to the diffusional limits imposed by AC's porosity. A higher ATRP equilibrium produces more propagating radicals on the surface of AC, which could be required to allow acrylamide to diffuse into the pores of AC and polymerize into higher molecular weight PAM. Whereas at a lower ATRP equilibrium, the propagating radical on the surface of AC could be deactivated before acrylamide diffuses into the pores to polymerize from the surface. Instead, the acrylamide would rather polymerize from a free propagating radical started by a chain transfer reaction or an unknown initiating side reaction. Hence, $AC_{0.1\text{-}0.5}$-Cl-$PAM_{5k,\ EtOH,\ and\ NaCl}$ produced lower molecular weight chains even at high mass recoveries.

The standard ATRP procedure ($AC_{<0.1}$-Br-$PAM_{20k,\ Std}$ and $AC_{0.1\text{-}0.5}$-Br-$PAM_{20k,\ Std}$) achieved the highest M_n, reaching 5,600 and 4,900 kg/mol. Higher than expected molecular weights at DP of 20,000 and low mass recoveries of 5-7% are likely due to chain termination events, specifically, chain coupling. At a higher ATRP equilibrium due to the polarity of the reaction medium, there is a higher concentration of propagating radicals. Combined with the high molecular weight target, it could produce propagating polyacrylamide brushes long enough to reach other propagating polyacrylamide brushes either on the same AC particle surface or others.

Decreasing the DP to 2,000 ($AC_{<0.1}$-Br-$PAM_{2k,\ Std}$ and $AC_{0.1\text{-}0.5}$-Br-$PAM_{2k,\ Std}$) improved the mass recoveries to 24 and 17% while still achieving higher than expected M_n of 3,800 and 3,300 kg/mol. The M_n was expected to be 142.16 kg/mol at a DP of 2,000 with 100% initiator

efficiency. This shows that the alkyl halide initiators tethered on the surface of AC have low initiator efficiencies, producing fewer chains with a higher molecular weight.

Using an ARGET SI-ATRP method improved mass recoveries to 22 and 37% with a slightly lower M_n of 3,000 and 1,400 kg/mol than the standard SI-ATRP method. This indicates fewer chain termination events, including chain coupling reactions. A higher initial concentration of deactivating [Cu(II)/L]-X in the solution could control the concentration of propagating radicals enough to limit chain termination while allowing the polymerization of higher molecular weight polymers, unlike adding ethanol and NaCl. Lastly, changing AC particle diameter between <0.1 mm and 0.1-0.5 mm consistently showed no significant differences in mass recovery, M_n, or M_w.

4.3.3. Thermogravimetric analysis (TGA)

Thermogravimetric analysis (TGA) was used to estimate the amount of grafted PAM from the surface of activated carbon. The increase in the residual weight percent at 1,000ºC of the AC-PAMs from PAM was assigned as the weight percent of activated carbon (AC) (Table 4.4). The AC content of the AC-PAM is influenced by the amount of AC initiator added in the reaction (i.e., degree of polymerization (DP)) and the mass recovered after polymerization. Therefore, $AC_{0.1\text{-}0.5}$-Cl-$PAM_{5k,\ EtOH,\ NaCl}$ had the lowest AC content of 0.2 wt % because they had the highest mass recovery of 60 %. Whereas $AC_{<0.1}$-Br-$PAM_{2k,\ Std}$ and $AC_{0.1\text{-}0.5}$-Br-$PAM_{2k,\ Std}$ had the highest AC content of 5.1 and 5.8 wt % since it had a low DP of 2,000 and a low yield of 24 and 17 %. The ability to graft PAM brushes from such a low AC content means that SI-ATRP can graft densely packed high molecular weight PAM brushes from the surface of AC.

Table 4.4 Residual weight % at 1,000ºC and AC content of PAM and different AC-PAMs

Sample	Residual Wt% at 1,000ºC	AC content (wt%)
PAM	8.45 ± 0.05	
$AC_{0.1\text{-}0.5}$-Cl-$PAM_{5k,\ EtOH,\ NaCl}$	8.7 ± 0.5	**0.2 ± 0.5**
$AC_{<0.1}$-Br-$PAM_{20k,\ Std}$	11.0 ± 0.9	**2.5 ± 0.9**
$AC_{0.1\text{-}0.5}$-Br-$PAM_{20k,\ Std}$	12 ± 1	**3.2 ± 1.0**
$AC_{<0.1}$-Br-$PAM_{2k,\ Std}$	13.5 ± 0.4	**5.1 ± 0.4**
$AC_{0.1\text{-}0.5}$-Br-$PAM_{2k,\ Std}$	14.3 ± 0.6	**5.8 ± 0.6**
$AC_{<0.1}$-Br-$PAM_{20k,\ ARGET}$	9.3 ± 0.8	**0.9 ± 0.8**
$AC_{0.1\text{-}0.5}$-Br-$PAM_{20k,\ ARGET}$	9.0 ± 0.6	**0.5 ± 0.6**

4.4. Conclusion

In this chapter, polyacrylamide was successfully grafted from activated carbon using a surface-initiated ATRP with a range of molecular weights, AC content, and AC particle diameters. Both FTIR and XPS of AC-PAM contained numerous peaks corresponding to the functional groups present in PAM. Both standard and ARGET SI-ATRP could synthesize high-molecular weight PAM brushes with M_n greater than 10^6 g/mol measured by SEC. For both AC particle diameters, <0.1 mm and 0.1-0.5 mm, and high DP of 20,000 ($M_{n.theo}$ = 1,421.6 kg/mol), the use of ethanol, NaCl, and alkyl chloride initiator, which showed improved control over the polymerization of free PAM in the last chapter was unable to polymerize PAM with higher molecular weights. Meanwhile, standard SI-ATRP provided poor control over the polymerization, resulting in low mass recoveries of 5 and 7%, but achieved higher experimental M_n of 4,900 and 5,600 g/mol. Finally, ARGET SI-ATRP provided better control, achieving higher mass recoveries of 22 and 37 wt%, with M_n of 3,000 and 1,400 kg/mol at the same DP of 20,000, closer to the expected M_n. The following chapter will examine the flocculation performance of the AC-PAMs with different molecular weight brushes, AC content, and AC particle size fabricated in this chapter to the flocculation performance of PAM.

5. Flocculation performance of AC-PAM

5.1. Introduction

As described previously, oil extraction from the Alberta oil sands has and continues to generate massive amounts of water-based tailings comprising sand, silt, clay, and residual bitumen. The sheer volume of this waste underscores the scale of the environmental challenge and the urgent need for effective management solutions.[1] These tailings are stored in tailings ponds, which use gravity to separate the solids from water. Over time, the coarse sand and some finer particles settle to the bottom of the pond, while some of the entrapped water is released and collected at the top of the pond to be recycled.[10] After several years of consolidation, a stable suspension of tailings forms between the coarse sand and supernatant water, referred to as mature fine tailings (MFT).[1] The MFT contains 30-35 wt% solids, mainly fine clays, that remain dispersed and do not naturally undergo consolidation for decades due to the electrostatic repulsion between the negatively charged particles.[144] Due to the slow consolidation of MFTs and high oil demand, the inventory of tailings ponds in Canada is estimated to reach 2 billion m^3 in 2034.[1]

Additionally, these tailings ponds contain large volumes of oil sands process-affected water (OSPW), which contains elevated levels of naphthenic acids, volatile organic compounds (VOCs), and heavy metals that have the potential to seep into the surrounding groundwater.[145] The Energy Resource Conservation Board in Alberta addressed these concerns by establishing tailings management regulations for oil sands operators. These regulations require that all tailings produced during a project's lifetime be ready to be reclaimed within ten years of its operation.[146] However, current dewatering technologies can only recover about 70% of the water from the oil sands tailings, leaving about 3.3 m^3 of tailings still being produced per 1 m^3 of

bitumen extracted.[10] To achieve tailings management regulations, current dewatering technologies must be improved.

Currently, commercial methods such as paste technology, a widely used technique for dewatering MFTs, are employed. These methods rely on polymer flocculants, typically long-chain water-soluble polymers that can promote settling suspended fine particles.[147] Depending on the polymer's charge and molecular weight, it can induce aggregation and water release through depletion, charge patch, and bridging flocculation.

Depletion flocculation requires that the continuous phase be saturated with a higher dose of low molecular weight neutral polymer. The polymer pushes the particles together until they approach closely enough that no polymer coils can fit, generating an osmotic force that removes the solvent between particles.[148] On the other hand, charge patch flocculation adsorbs a polymer with densely charged counter-ions on the surface of a particle, creating an area of localized charge inversion that can attract other particles. Both mechanisms tend to create coagulated rather than flocculated aggregates, according to the Derjaguin-Landau-Verwey-Overbeek (DLVO) theory, where reduction of inter-particle repulsion allows the particles to approach close enough to be held together by van der Waals forces.[148,149]

Bridging flocculation relies on adding a very high-molecular-weight polymer that can adsorb two or more particles per polymer. It is usually exceptionally rapid and gives rise to denser aggregates with lower content and porosity than depletion and charge-patch flocculation.[148,150] Most commercially available bridging flocculants are polyacrylamide (PAM) based. They are water-soluble and can easily be synthesized to reach high molecular weights.[7] Adsorption occurs through the formation of hydrogen bonds between the PAM's acrylamide protons and the oxygen atoms on the clay particles' surfaces.[7] However, PAM has high polymer self-interaction due to its

dense amide functionality. This forms a gel-like network via hydrogen bonding that retains large volumes of water, making it inefficient to flocculate fine particles (< 2μm).[19]

Developing new polyacrylamide-based flocculants by modifying molecular weight, chemical composition, and architecture opens exciting possibilities for improving dewatering technologies. When copolymerized with ionic monomers, acrylamide forms ionic PAM, which can extend its polymer chains in solution due to the electrostatic repulsion between chain segments with similar charges. Cationic PAM is synthesized by copolymerization with acryloyloxyethyl trimethylammonium chloride (DMC/DAC),[20] and diallyl dimethyl ammonium chloride (DADMAC) monomers.[147] However, very high molecular weight cationic PAM can also cause the polymer to collapse onto the solid's surface due to the favourable charge pair between cationic PAM and the negatively charged surface of the suspended particles, limiting its extended polymer chain segment length for bridging flocculation.

On the other hand, anionic PAM with a 22-30% charge density at very high molecular weights of 10^{6-7} g/mol was found to be more efficient in flocculating MFTs.[23–26] The heterogeneous distribution of negatively charged areas allows the anionic PAM to extend its polymer chain segments while maintaining adsorption sites for clay adsorption. Anionic PAM can be made with acrylic acid (AA), methacrylic acid (MAA), and 2-acrylamide-2-methyl-1-propanesulfonic acid (AMPS).[27] However, an anionic PAM can still not effectively dewater oil sands tailings due to the polymer's high hydrophilicity.

Therefore, further research into introducing hydrophobic monomer groups is being explored to enhance the dewaterability of PAM. Hydrophobic PAM has been synthesized by copolymerizing acrylamide with hydrophobic monomers such as N-tert-butyl acrylamide (t-BAAM),[29] N-isopropyl acrylamide (NIPAM),[151] and 5-methacrylomido-1,2-benzoborozole

(MAAMBO).[30] Increasing the PAM's hydrophobic segment has been shown to increase the dewatering rate by up to a factor of 5.[31]

Branched polymers have also been investigated to extend the PAM segments into the solution and increase its bridging capacity. In 2018, Xu et al. copolymerized PAM with a cationic hyperbranched oligomer, poly(N-acryloyl-1,2-diaminoethane hydrochloride) (HADE) to form a cationic hyperbranched PAM-HADE.[32] The steric hindrance due to branching forces an extended polymer configuration, improving flocculation performance compared with its linear counterpart, which has similar molecular weights, charge density, and intrinsic viscosity.[32] Extended polyacrylamide configuration can be achieved by grafting a surface with dense polymer chains. Das et al. demonstrated that PAM grafted on hydroxypropyl methylcellulose showed a larger hydrodynamic radius when its grafting efficiency increased, achieving lower supernatant turbidities and faster settling rates.[152]

Therefore, this chapter explores the flocculation performance of activated carbon polyacrylamide (AC-PAM) hybrids (synthesized in Chapter 4), the result of the PAM with different molecular weights and concentrations grafted from the surface of activated carbons at different concentrations and with different particle size distributions. PAM was grafted from the surface of activated carbon (AC) to impart a high density of PAM brushes on the surface, extend the polymer into the tailing solution, increase the density of flocs, and introduce hydrophobicity through the carbon substrate. It is hypothesized that the flocculation performance of PAM can be improved by grafting from an activated carbon substrate.

5.2. Materials and Methods

5.2.1. Materials

Suncor Energy Inc. (Alberta, Canada) supplied the mature fine tailings (MFT) used for the settling tests. Aluminum sulphate was procured from Kemira Chemicals Inc.

5.2.2. Preparation of AC-PAM

Polyacrylamide grafted from activated carbon was synthesized by oxidizing AC, followed by the attachment of the ATRP initiator, as outlined in Chapters 4.2.3. and 4.2.4. The polyacrylamide was grafted from the surface of AC-Br by ATRP, as summarized in Chapter 4.2.5.

5.2.3. Dean-Stark Extraction

The Dean-Stark extraction, described in Chapter 2.2.1, determined the supplied MFT sample's solids, moisture, and bitumen content.

5.2.4. Settling Tests

Settling tests were conducted by weighing 90.0 g of MFT slurry (diluted to 5.55 wt% solids in deionized water) into a 250 mL beaker. Flocculant dosages are reported as mg of flocculant per kg of solids in the MFT. Both flocculants, PAM and AC-PAM, were pre-dissolved in deionized water to a concentration of 1 wt% solids to water content for at least 48 hours. Each test is conducted with 950 ppm of aluminum sulphate (alum) calculated using the following equation 25:

$$\mathrm{V(mL)} = \frac{\mathrm{D} \cdot \mathrm{m_w}}{10^6 \cdot \mathrm{C} \cdot \mathrm{G}} \tag{25}$$

Equation 25 Volume of aluminum sulphate required

Where V(mL) is the volume of alum, D is the dosage of alum, m_w is the mass of water in the MFT slurry (95 g), C is the concentration of alum (44.78%), and G is the specific gravity of alum (1.33 g/ml). The slurry was presheared at 600 rpm using a three-blade propeller for 10 seconds. Then, 950 ppm of alum and the flocculant were added simultaneously. Afterward, the suspension was sheared at 600 rpm for 2 minutes, followed by 200 rpm for 8 minutes. 5 mL of the treated MFT slurry was transferred into a capillary suction time (CST) funnel (Chapter) while the rest was transferred to a 100 mL graduated cylinder to monitor the change in mudline height over time. A settling profile was obtained by plotting the mudline height vs. time, and the initial settling rate (ISR) was reported as the slope of the initial linear section of the profile. The slurry was allowed to consolidate for 24 hours, the supernatant was carefully pipetted, and the turbidity was measured using a DR/890 Portable Colorimeter (Hach). The consolidated flocs were drained using 1 mm sieves for 24 hours while covered at room temperature. The weight of the drained floc was determined and then dried for another 24 hours at 110 ºC. The solids content was calculated by dividing the weight of the dried floc by the drained floc times 100 %.[10,18,147,153]

5.2.5. Characterization

PAM and AC-PAMs were characterized using FTIR and XPS, as described in Chapter 4. Size exclusion chromatography, as described in Chapter 4, determined their molecular weights.

5.3. Results and Discussion

5.3.1. Dean-Stark Extraction

The flocculation performance of a flocculant depends on the composition of the suspension. Hence, it is essential to guarantee that the composition of this suspension is characterized and held constant throughout the flocculation tests. A Dean-Stark extraction was

used to determine the solid, water, and bitumen content of the given MFT sample since the composition of the received samples varies between batches. The extraction was repeated in triplicate (Table 5.1) and showed that the MFT sample contained 68 ± 3 wt% water, 27 ± 1 wt% solids, and 4 ± 1 wt% bitumen. These results were used to dilute the MFT to 5.55 wt% solids for the settling tests.

Table 5.1 The composition of MFT determined from Dean-Stark extraction

Composition (wt%)	Trial 1	Trial 2	Trial 3	Average
Water	64.8	71.5	70.2	68 ± 3
Solids	28.0	25.9	26.3	27 ± 1
Bitumen	5.5	4.6	3.3	4 ± 1

5.3.2. Flocculation Performance

The flocculation performance of AC-PAM with varying PAM brush molecular weight, AC content, and AC particle size was investigated by conducting settling tests to measure the initial settling rate, capillary suction time, supernatant turbidity, and solids content. Each test was conducted with a fixed dosage of 950 ppm of coagulant, aluminum sulphate, as prescribed by a lab-scale screening method for polymers that aim to replace the currently used PAM flocculant in industry.[154] The results were also compared to the flocculation performance with only the coagulant and PAM with a similar molecular weight to the grafted PAM from the surface of AC (AC-PAM). PAM was synthesized under the same conditions as Run M (described in Chapter 3). AC-PAMs were synthesized with different molecular weight brushes to determine the optimal polymer brush length to induce bridging flocculation. AC content was changed to evaluate the effect of hydrophobicity on the dewatering of MFT. AC particle sizes were separated to

determine if a smaller or larger particle size could obtain better flocculation performance. AC-PAMs of different molecular weight brushes, AC content, and AC particle sizes were synthesized under the same conditions of Runs K, M, N, and O, as described in Chapter 4. Table 5.2 summarizes each candidate's AC content, experimental number, and weight average PAM brush molecular weights.

Table 5.2 PAM and AC-PAM with different AC content, M_n, and M_w evaluated for flocculation of 5 wt% MFT

Sample	AC Content (%)*	$M_{n,exp}$ (kg/mol)	$M_{w,exp}$ (kg/mol)
$PAM_{20k,\ Std}$		1,900 ± 600	3,000 ± 2,000
$AC_{0.1\text{-}0.5}$-Cl-$PAM_{5k,\ EtOH,\ NaCl}$	0.2 ± 0.5	107 ± 4	180 ± 20
$AC_{<0.1}$-Br-$PAM_{20k,\ Std}$	2.5 ± 0.9	5,600 ± 600	9,700 ± 900
$AC_{0.1\text{-}0.5}$-Br-$PAM_{20k,\ Std}$	3.2 ± 1.0	4,900 ± 900	9,000 ± 2,000
$AC_{<0.1}$-Br-$PAM_{2k,\ Std}$	5.1 ± 0.4	3,800 ± 600	7,000 ± 1,000
$AC_{0.1\text{-}0.5}$-Br-$PAM_{2k,\ Std}$	5.8 ± 0.6	3,300 ± 700	6,000 ± 1,000
$AC_{<0.1}$-Br-$PAM_{20k,\ ARGET}$	0.9 ± 0.8	3,000 ± 1,000	6,000 ± 3,000
$AC_{0.1\text{-}0.5}$-Br-$PAM_{20k,\ ARGET}$	0.5 ± 0.6	1,400 ± 800	2,000 ± 2,000

Settling tests were conducted from a low dose of 1,000 ppm up to a higher dose of 15,000 ppm since this is known to affect the flocculation performance of a given polymer significantly. The polymer dosage usually increases the flocculation efficiency of a specific polymer up to a certain dosage wherein the flocculation is optimized. This occurs due to the partial coverage of the suspended particle surface with the flocculant, leaving sufficient unoccupied area for the adsorption of another polymer attached with other particles, hence facilitating bridging flocculation.[10] The particle surface becomes fully covered past this optimal polymer dosage, decreasing flocculation performance. Flocculation applications ideally look for lower optimized polymer dosages and a wider effective polymer dose range, indicating robustness.

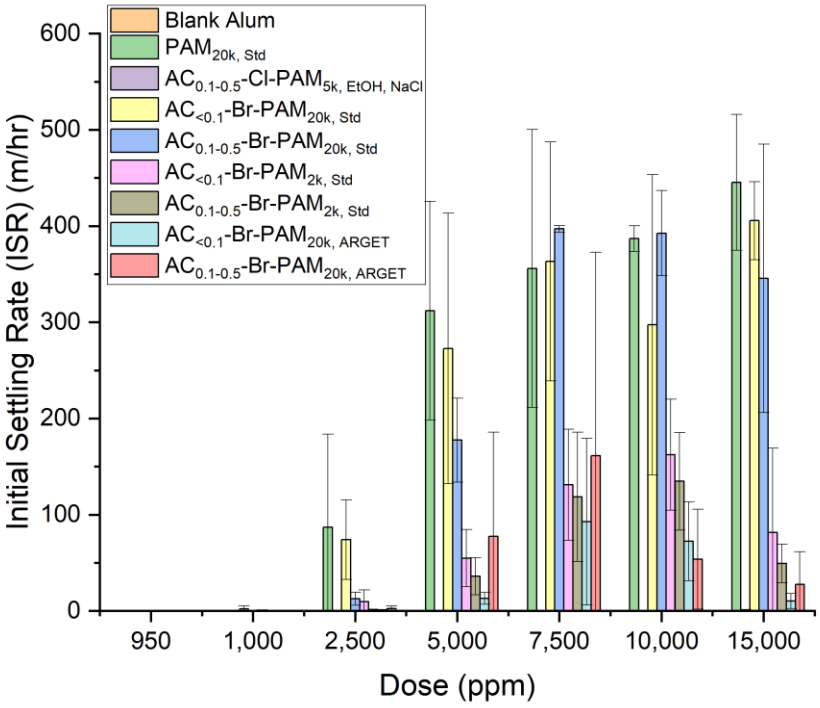

Figure 5.1 Initial settling rates (ISR) of flocculated 5 wt% MFT with aluminum sulphate (alum), polyacrylamide (PAM), and polyacrylamide grafted from AC (AC-PAM)

The initial settling rate (ISR) is measured after shearing the diluted MFTs with the flocculant. Higher initial settling rates indicate denser aggregate formation by a given flocculant.[148] Treatment with only aluminum sulphate (alum) only achieves an ISR of 0.07 m/hr due to the formation of less dense aggregates typical of a coagulation process (Figure 5.1).[148] Grafting the polyacrylamide from an AC substrate required a higher molecular weight polymer brush ($AC_{<0.1}$-Br-$PAM_{20k,\ Std}$, M_n = 5,600 kg/mol) to flocculate at a lower polymer dose of 2,500 ppm. In contrast, free polyacrylamide achieved high ISRs at a wider effective polymer dose range from 2,500 to 15,000 ppm with only a M_n of 1,900 kg/mol. The higher AC-PAM dose required might be due to the localization of dense PAM brushes on single AC particles, whereas free PAM could disperse in the suspension as single PAM brushes. Moreover, $AC_{0.1\text{-}0.5}$-Cl-$PAM_{5k,\ EtOH,\ NaCl}$ with lower molecular weight polymer brushes (M_n = 107 kg/mol) was unable to

form dense aggregates only reaching an ISR of 1.0 ± 0.5 m/hr. Even after 10 minutes, $AC_{0.1\text{-}0.5}$-Cl-$PAM_{5k,\ EtOH,\ NaCl}$ was the only flocculant that caused the least settling (Figure 5.2). This is likely due to the polymer's length being too short to be able to bridge suspended particles together.

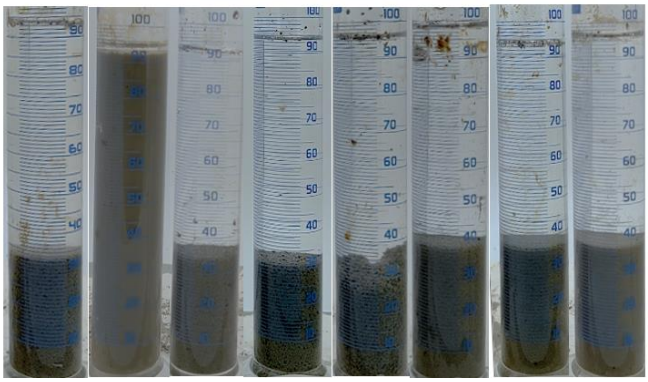

Figure 5.2 From left to right, 5 wt% MFT treated with 2,500 ppm Free PAM, 15,000 ppm $AC_{0.1\text{-}0.5}$-Cl-$PAM_{5k,\ EtOH,\ NaCl}$, 2,500 ppm $AC_{<0.1}$-Br-$PAM_{20k,\ Std}$, 5,000 ppm $AC_{0.1\text{-}0.5}$-Br-$PAM_{20k,\ Std}$, 5,000 ppm $AC_{<0.1}$-Br-$PAM_{2k,\ Std}$, 5,000 ppm $AC_{0.1\text{-}0.5}$-Br-$PAM_{2k,\ Std}$, 5,000 ppm $AC_{<0.1}$-Br-$PAM_{20k,\ ARGET}$, 5,000 ppm $AC_{0.1\text{-}0.5}$-Br-$PAM_{20k,\ ARGET}$ after 10 minutes of settling

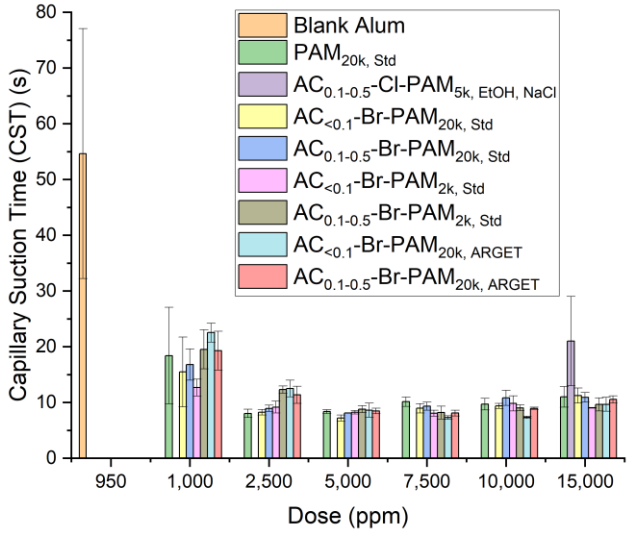

Figure 5.3 Capillary suction times (CST) of flocculated 5 wt% MFT with aluminum sulphate (alum), polyacrylamide (PAM), and polyacrylamide grafted from AC (AC-PAM)

The capillary suction time (CST) is taken immediately after shearing with the flocculant to determine the filterability of water through the formed flocs—the inability to form flocs results in a higher CST due to filtration resistance from suspended particles. In contrast, floc formation releases water from the suspension, allowing water to be filtered, decreasing the CST. Ideally, CST values are close to 8 seconds since this is the CST of deionized water. The addition of high molecular weight PAM, either grafted or free, had no impact on their optimal polymer dosage since all PAM and AC-PAM flocculants with molecular weights greater than 10^6 g/mol had comparably similar optimal flocculant dosages of 2,500 – 15,000 ppm with CST values of 15 seconds or less, except for $AC_{0.1\text{-}0.5}$-Cl-$PAM_{5k,\ EtOH,\ NaCl}$ with a lower molecular weight PAM brush, which was unable to achieve low CST values even at a high dosage of 15,000 ppm (Figure 5.3).

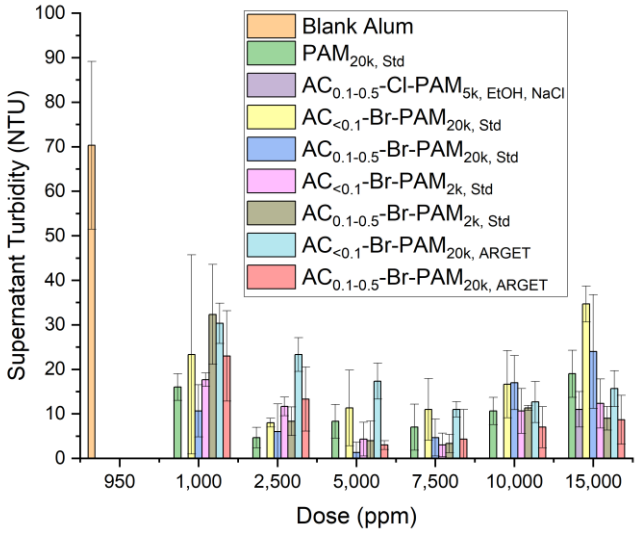

Figure 5.4 Supernatant turbidities of flocculated 5 wt% MFT with aluminum sulphate (alum), polyacrylamide (PAM), and polyacrylamide grafted from AC (AC-PAM)

The supernatant turbidity measures the clarity of the leftover supernatant after the flocs have settled for 24 hours. Higher supernatant turbidities indicate inefficient flocculation of

suspended particles in the diluted MFTs. All synthesized PAM and AC-PAM flocculants showed improved supernatant turbidites than the diluted MFT treated with the coagulant, even at a low dose of 1,000 ppm (Figure 5.4). Settling suspended particles after 24 hours using high molecular weight polymers at less-than-optimal dosage indicates incomplete or partial bridging of particles; hence, they cannot form heavy enough aggregates to reach higher initial settling rates. However, low molecular weight flocculants incapable of bridging flocculation typically relies on a second mechanism, depletion flocculation. The high concentration of low molecular weight AC-PAM at a dose of 15,000 ppm could push particles closely enough that no polymer coils can fit, generating enough osmotic force to release the water between particles and bring them together.[148] Hence, low supernatant turbidities and capillary suction times are achieved even with a prolonged initial settling rate.

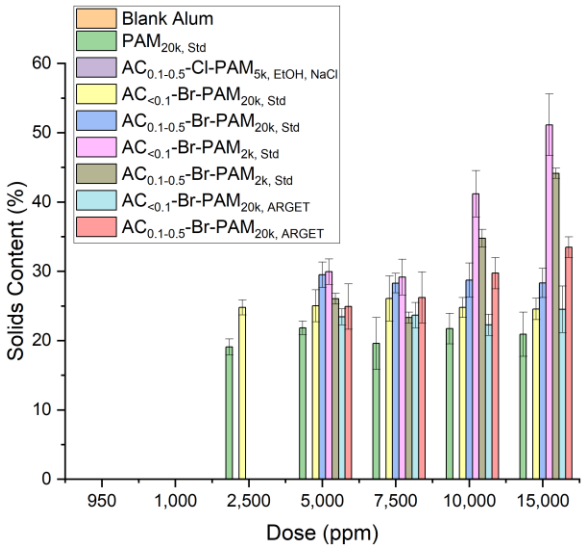

Figure 5.5 Solids contents of flocculated 5 wt% MFT with aluminum sulphate (alum), polyacrylamide (PAM), and polyacrylamide grafted from AC (AC-PAM)

Solids content data is measured on the floc drained for 24 hours using a 1 mm sieve; hence, only flocculants capable of forming flocs greater than 1 mm could be analyzed. AC-PAM

required higher molecular weight PAM brushes near 5,600 g/mol to flocculate at a lower polymer dose of 2,500 ppm, as shown by the performance of $AC_{<0.1}$-Br-$PAM_{20k, Std}$. Moreover, adding hydrophobic AC as a substrate for PAM brushes improves the solids content of the formed flocs. Free PAM increased the solids content of the dilute MFTs from 5 wt% to 19-22 wt%. On the other hand, high molecular weight brush AC-PAM increased the solids content to 22-51 wt%. This is more pronounced at higher doses of 10,000 and 15,000 ppm for $AC_{<0.1 \text{ and } 0.1\text{-}0.5}$-Br-$PAM_{2k, Std}$ where solids contents of 34-51 wt% was achieved due to their higher AC to polymer content of 5.1-5.8 wt% (Figure 5.5).

Flocculation performance between AC particle sizes <0.1 mm and 0.1 – 0.5 mm only had a significant difference in the solids content of their resulting floc. Specifically for $AC_{<0.1 \text{ and } 0.1\text{-}0.5}$-Br-$PAM_{2k, Std}$, due to the higher AC content greater than 5 wt% with similar M_n and M_w. The smaller $AC_{<0.1}$-Br-$PAM_{2k, Std}$, achieved higher solids contents of 29 – 51 wt% while the bigger $AC_{0.1\text{-}0.5}$-Br-$PAM_{2k, Std}$, only reached 23 – 44 wt% at doses 5,000 – 15,000 ppm. The smaller AC particle size could have dispersed better into the tailing solution to prepare denser flocs and achieve better dewatering, hence, a higher solids content. Because of this, research on increasing the hydrodynamic radius of the flocculant to achieve better flocculation performance should focus on increasing the hydrodynamic volume of the PAM and not the particle size of the grafting substrate.[152]

5.4. Conclusions

This chapter examined the flocculation performance of PAM and AC-PAM with a number average molecular weight (M_n) range of 10^5-10^6 g/mol and AC content up to 5 wt% by conducting settling tests. The study found that the effective polymer dosage range of PAM was 2,500 – 15,000 ppm, producing an initial settling rate of 90 – 450 m/hr, a capillary suction time

of 8 – 18 s, supernatant turbidity of 5 – 20 NTU, and solids content of 25 – 26 wt%. On the other hand, AC-PAM with a polymer brush Mn greater than 106 required a higher polymer dosage range of 5,000 – 15,000 ppm, while AC-PAM with a polymer brush Mn 105 g/mol required at least 15,000 ppm. The study also found that higher molecular weight polymer brushes, Mn = 4,900 and 5,600 g/mol, had faster-settling rates of 180 – 410 m/hr due to denser aggregate formed by being able to bridge more particles together using longer polymer chains. AC-PAM with lower molecular weight polymer brushes, Mn = 107 kg/mol, only reached an initial settling rate of 1 m/hr due to its inability to bridge particles. Instead, these are likely undergoing depletion flocculation, as shown by the low supernatant turbidity after settling for 24 hours. Finally, the study found that AC-PAM achieved higher solids contents in the effective polymer dose range as the AC content increased, reaching 29 – 51 wt% using AC-PAM with 5.1 wt% AC. This finding underscores the significant role of AC content in influencing AC-PAM performance in flocculation processes, with the improved solids content hypothesized to occur due to the addition of a hydrophobic AC core when PAM is grafted from the surface of AC.

6. Conclusions

6.1. General Conclusions

This work showcased the successful grafting of polyacrylamide (PAM) from the surface of activated carbon (AC) by surface-initiated atom transfer radical polymerization (SI-ATRP). Prior to the grafting from the surface of AC, the aqueous ATRP of PAM was first evaluated to achieve higher molecular weights with good dispersity and monomer conversions. Various ATRP parameters were explored, including testing activators regenerated by electron transfer (ARGET) ATRP using either a single injection or a slow feeding of the reducing agent, halide salts, cosolvent addition, and different catalyst complexes. The molecular weights and dispersities were determined by SEC, and Raman Spectroscopy determined the monomer conversion. Three different molecular weights, 100, 700, and 1900 kg/mol, with molecular weight dispersities 1.4-1.7, via aqueous ATRP were achieved. Lower molecular weights of 100 kg/mol with low molecular weight dispersities were attained using ethanol as a cosolvent, additional halide salt, an alkyl chloride initiator, and CuCl/Me_6TREN catalyst (Run K). Ultra-high molecular weight PAM with higher molecular weights of 700 and 1,900 kg/mol were attained via standard and ARGET ATRP using Me_6TREN as a ligand and an alkyl bromide initiator (Run N and O). These conditions were then used to graft PAM from the surface of AC with varying AC contents and particle sizes. Both FTIR and XPS of AC-PAM contained numerous peaks corresponding to the functional groups present in PAM. Both standard and ARGET SI-ATRP synthesized high molecular weight PAM brushes with M_n greater than 10^6 g/mol by SEC from <0.1 mm and 0.1 – 0.5 mm AC particle diameters. The standard SI-ATRP had less control over the polymerization, only reaching 5 and 7% mass recovery, but achieved higher experimental M_n of 4,900 and 5,600

kg/mol. ARGET SI-ATRP provided better control, achieving higher mass recoveries of 22 and 37 wt%, with M_n of 3,000 and 1,400 kg/mol at the same high DP of 20,000.

Conducting settling tests on 5 wt% mature fine tailings (MFT) compared the flocculation performance of the synthesized AC-PAMs with different molecular weight brushes, AC contents, and AC particle sizes. Against free polyacrylamide (PAM) with M_n around 10^6 kg/mol, its effective polymer dose range was wider, reaching 2,500 – 15,000 ppm, producing an initial settling rate of 90 – 450 m/hr, a capillary suction time of 8 – 18 s, supernatant turbidity of 5 – 20 NTU, and solids content of 25 – 26 wt%. AC-PAM with a polymer brush Mn greater than 10^6 requires a higher polymer dosage range of 5,000 – 15,000 ppm, while AC-PAM with a polymer brush M_n of 10^5 g/mol requires at least 15,000 ppm. Among AC-PAMs, those with higher molecular weight polymer brushes, with M_n = 4,900 and 5,600 g/mol, have faster-settling rates of 180 – 410 m/hr due to the formation of denser aggregates from being able to bridge more particles together using longer polymer chains. AC-PAM with lower molecular weight polymer brushes, M_n = 105 kg/mol, only reached an initial settling rate of 1 m/hr due to its inability to bridge particles. Instead, these are likely undergoing depletion flocculation, as indicated by the low supernatant turbidity after settling for 24 hours. Finally, AC-PAM achieved higher solids contents in the effective polymer dose range as the AC content increased, reaching 29 – 51 wt% using AC-PAM with 5.1 wt% AC. The improved solids content is hypothesized to occur due to the addition of a hydrophobic AC core when PAM is grafted from the surface of AC.

6.2. Future Work

1. Evaluation of the flocculation performance of high molecular weight AC-PAM for treating full-weight MFT (27-35 wt%). This current work only investigated the flocculation performance using 5wt% MFT. However, the flocculation performance

of full-weight MFT should be investigated for this material's practical use in the existing MFT inventory. This will require flocculation tests outside the established settling tests in this work.

2. Determine if the grafting of AC improves the polymer's leaching into the released water. This could be done by overdosing the tailings with an AC-PAM flocculant and measuring the leached polymer from the released water using HPLC-RID or HPLC-UV.
3. Determine if adding AC improves the quality of the released water from flocculation. This could be examined by measuring the total organic carbon content and concentration of metals in the released water after flocculation.
4. Explore different grafting densities of polyacrylamide brushes from the surface of AC to change the AC content in AC-PAM and evaluate any change in the surface morphology of the grafted PAM. This could be performed by changing the alkyl halide concentrations during their attachment and performing SI-ATRP on them. Additionally, their flocculation performance could be evaluated.
5. Explore the grafting of polyacrylamide copolymers from the surface of AC utilizing SI-ATRP to flocculate mature fine tailings. An example would be synthesizing ionic polyacrylamide with either a quaternary ammonium-containing monomer or acrylic acid and hydrolyzing it to obtain a hydroxide-containing copolymer. A modified SI-ATRP method should be developed to accommodate a new copolymer.

6.3. Contributions to Science

6.3.1. Publications and Patents

- A patent for the synthesis of high molecular weight AC-PAM by SI-ATRP for flocculation applications has been submitted
- A manuscript for synthesizing, characterizing, and evaluating different molecular weights and AC contents of AC-PAM by SI-ATRP for flocculating mature fine tailings is currently being prepared.

6.3.2. Conferences

- Oral presentation at the CSC 2023 in Vancouver, Canada in June 2023
- Oral presentation at the 8th annual International Institute for Environmental Studies (IIES) Science & Policy Workshop and Graduate Student Forum in Chile in December 2023
- Oral presentation at the IUPAC-MACRO 2024 – 50th World Polymer Congress in England in July 2024

Appendix

Supplementary Figures

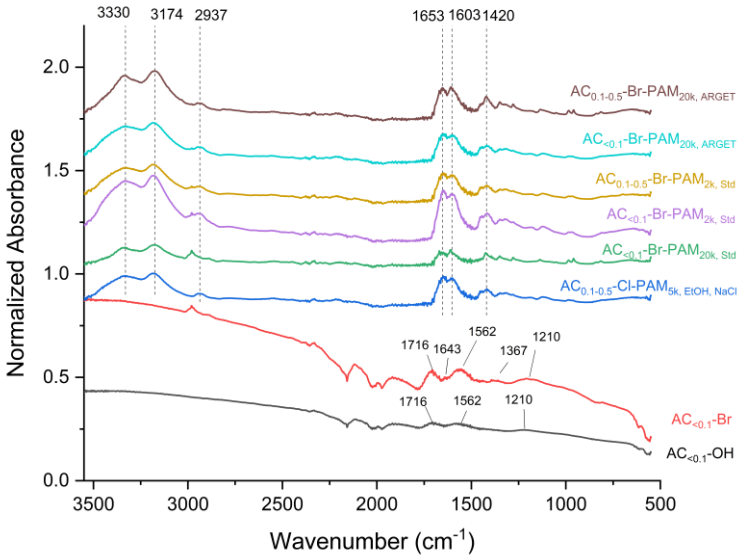

Figure S0.1 FTIR spectra of oxidized AC ($AC_{<0.1}$-OH), bromine initiator grafted AC ($AC_{<0.1}$-Br), polyacrylamide grafted from AC ($AC_{0.1\text{-}0.5}$-Cl-$PAM_{5k,\ EtOH,\ NaCl}$, $AC_{<0.1}$-Br-$PAM_{20k,\ Std}$, $AC_{<0.1}$-Br-$PAM_{2k,\ Std}$, $AC_{0.1\text{-}0.5}$-Br-$PAM_{2k,\ Std}$, $AC_{<0.1}$-Br-$PAM_{20k,\ ARGET}$, and $AC_{0.1\text{-}0.5}$-Br-$PAM_{20k,\ ARGET}$)

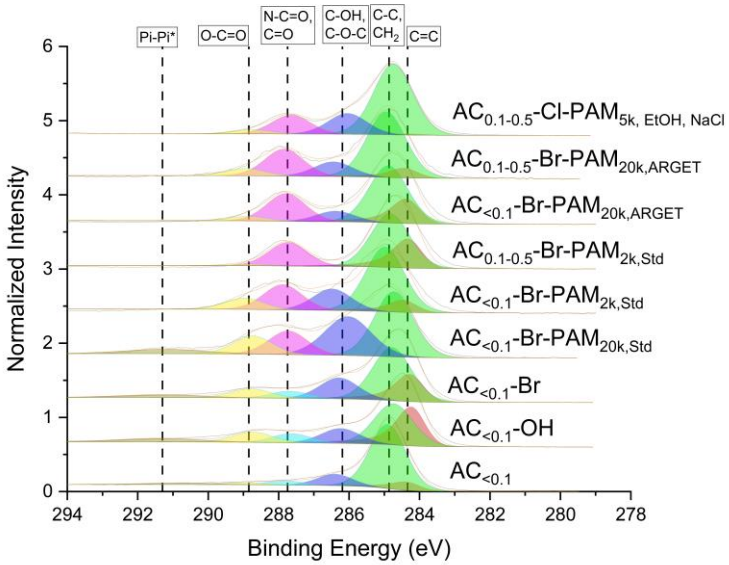

Figure S0.2 High resolution C 1s scans of activated carbon ($AC_{<0.1}$), oxidized AC ($AC_{<0.1}$-OH), bromine initiator grafted AC ($AC_{<0.1}$-Br), and polyacrylamide grafted ACs ($AC_{0.1\text{-}0.5}$-Cl-$PAM_{5k,\ EtOH,\ NaCl}$, $AC_{<0.1}$-Br-$PAM_{20k,\ Std}$, $AC_{<0.1}$-Br-$PAM_{2k,\ Std}$, $AC_{0.1\text{-}0.5}$-Br-$PAM_{2k,\ Std}$, $AC_{<0.1}$-Br-$PAM_{20k,\ ARGET}$, and $AC_{0.1\text{-}0.5}$-Br-$PAM_{20k,\ ARGET}$)

References

(1) BGC Engineering Inc. *Oil Sands Tailings Technology Review*; 2010.

(2) Masliyah, J.; Zhou, Z. J.; Xu, Z.; Czarnecki, J.; Hamza, H. Understanding Water-Based Bitumen Extraction from Athabasca Oil Sands. *Can J Chem Eng* **2004**, *82* (4), 628–654. https://doi.org/10.1002/cjce.5450820403.

(3) Wang, C.; Harbottle, D.; Liu, Q.; Xu, Z. Current State of Fine Mineral Tailings Treatment: A Critical Review on Theory and Practice. *Miner Eng* **2014**, *58*, 113–131. https://doi.org/10.1016/j.mineng.2014.01.018.

(4) Nguyen, B.; Soares, J. B. P. Effect of the Branching Morphology of a Cationic Polymer Flocculant Synthesized by Controlled Reversible-deactivation Radical Polymerization on the Flocculation and Dewatering of Dilute Mature Fine Tailings. *Canadian journal of chemical engineering* **2022**, *100* (4), 790–799. https://doi.org/10.1002/cjce.24329.

(5) Botha, L.; Soares, J. B. P. The Influence of Tailings Composition on Flocculation. *Can J Chem Eng* **2015**, *93* (9), 1514–1523. https://doi.org/10.1002/cjce.22241.

(6) Masliyah, J. H.; Czarnecki, J.; Xu, Z. *Handbook on Theory and Practice on Bitumen Recovery from Athabasca Oil Sands*; Kingsley Knowledge : Cochrane, Alberta, 2011; Vol. 1: Theoretical Basis.

(7) Gumfekar, S. P.; Vajihinejad, V.; Soares, J. B. P. Advanced Polymer Flocculants for Solid-Liquid Separation in Oil Sands Tailings. *Macromol Rapid Commun* **2019**, *40* (1), 1800644. https://doi.org/10.1002/marc.201800644.

(8) Alamgir, A.; Harbottle, D.; Masliyah, J.; Xu, Z. Al-PAM Assisted Filtration System for Abatement of Mature Fine Tailings. *Chem Eng Sci* **2012**, *80*, 91–99. https://doi.org/https://doi.org/10.1016/j.ces.2012.06.010.

(9) BGC Engineering Inc. *Oil Sands Tailings Technology Review OSRIN Report No. TR-1*; Edmonton, 2010.

(10) Vedoy, D. R. L.; Soares, J. B. P. Water-Soluble Polymers for Oil Sands Tailing Treatment: A Review. *Canadian Journal of Chemical Engineering* **2015**, *93* (5), 888–904. https://doi.org/10.1002/cjce.22129.

(11) Matthews, J. G.; Shaw, W. H.; MacKinnon, M. D.; Cuddy, R. G. Development of Composite Tailings Technology at Syncrude. *International Journal of Surface Mining, Reclamation and Environment* **2002**, *16* (1), 24–39. https://doi.org/10.1076/ijsm.16.1.24.3407.

(12) Zhao, H.; Long, J.; Masliyah, J. H.; Xu, Z. Effect of Divalent Cations and Surfactants on Silica−Bitumen Interactions. *Ind Eng Chem Res* **2006**, *45* (22), 7482–7490. https://doi.org/10.1021/ie060348o.

(13) Wang, D.; Wang, D.; Tan, X.; Yeung, A.; Liu, Q. A Review of the Roles of Constituent Minerals and Residual Bitumen in the Solid-Liquid Separation of Oil Sands Tailings. *Journal of Hazardous Materials*. Elsevier B.V. June 5, 2023. https://doi.org/10.1016/j.jhazmat.2023.131178.

(14) Wang, C.; Harbottle, D.; Liu, Q.; Xu, Z. Current State of Fine Mineral Tailings Treatment: A Critical Review on Theory and Practice. *Miner Eng* **2014**, *58*, 113–131. https://doi.org/https://doi.org/10.1016/j.mineng.2014.01.018.

(15) Wang, S.; Alagha, L.; Xu, Z. Adsorption of Organic-Inorganic Hybrid Polymers on Kaolin from Aqueous Solutions. *Colloids Surf A Physicochem Eng Asp* **2014**, *453* (1), 13–20. https://doi.org/10.1016/j.colsurfa.2014.03.069.

(16) Wang, C.; Harbottle, D.; Liu, Q.; Xu, Z. Current State of Fine Mineral Tailings Treatment: A Critical Review on Theory and Practice. *Minerals Engineering*. Elsevier Ltd 2014, pp 113–131. https://doi.org/10.1016/j.mineng.2014.01.018.

(17) Vajihinejad, V.; Gumfekar, S. P.; Bazoubandi, B.; Rostami Najafabadi, Z.; Soares, J. B. P. Water Soluble Polymer Flocculants: Synthesis, Characterization, and Performance Assessment. *Macromol Mater Eng* **2019**, *304* (2), 1800526. https://doi.org/10.1002/mame.201800526.

(18) Vajihinejad, V.; Gumfekar, S. P.; Bazoubandi, B.; Rostami Najafabadi, Z.; Soares, J. B. P. Water Soluble Polymer Flocculants: Synthesis, Characterization, and Performance Assessment. *Macromolecular Materials and Engineering*. Wiley-VCH Verlag February 1, 2019. https://doi.org/10.1002/mame.201800526.

(19) Reis, L. G.; Oliveira, R. S.; Palhares, T. N.; Spinelli, L. S.; Lucas, E. F.; Vedoy, D. R. L.; Asare, E.; Soares, J. B. P. Using Acrylamide/Propylene Oxide Copolymers to Dewater and Densify Mature Fine Tailings. *Miner Eng* **2016**, *95*, 29–39. https://doi.org/10.1016/j.mineng.2016.06.005.

(20) Abdollahi, Z.; Frounchi, M.; Dadbin, S. Synthesis, Characterization and Comparison of PAM, Cationic PDMC and P(AM-Co-DMC) Based on Solution Polymerization. *Journal of Industrial and Engineering Chemistry* **2011**, *17* (3), 580–586. https://doi.org/https://doi.org/10.1016/j.jiec.2010.10.030.

(21) Vajihinejad, V.; Guillermo, R.; Soares, J. B. P. Dewatering Oil Sands Mature Fine Tailings (MFTs) with Poly(Acrylamide-Co-Diallyldimethylammonium Chloride): Effect of Average Molecular Weight and Copolymer Composition. *Ind Eng Chem Res* **2017**, *56* (5), 1256–1266. https://doi.org/10.1021/acs.iecr.6b04348.

(22) Gregory, J.; Barany, S. Adsorption and Flocculation by Polymers and Polymer Mixtures. *Adv Colloid Interface Sci* **2011**, *169* (1), 1–12. https://doi.org/https://doi.org/10.1016/j.cis.2011.06.004.

(23) Long, J.; Li, H.; Xu, Z.; Masliyah, J. H. Role of Colloidal Interactions in Oil Sand Tailings Treatment. *AIChE Journal* **2006**, *52* (1), 371–383. https://doi.org/https://doi.org/10.1002/aic.10603.

(24) Sworska, A.; Laskowski, J. S.; Cymerman, G. Flocculation of the Syncrude Fine Tailings: Part II. Effect of Hydrodynamic Conditions. *Int J Miner Process* **2000**, *60* (2), 153–161. https://doi.org/https://doi.org/10.1016/S0301-7516(00)00013-2.

(25) Tripathy, T.; De, B. Flocculation : A New Way to Treat the Waste Water. *J. Phys. Sci.* **2006**, *10*, 93–127.

(26) Bolto, B.; Gregory, J. Organic Polyelectrolytes in Water Treatment. *Water Res* **2007**, *41* (11), 2301–2324. https://doi.org/https://doi.org/10.1016/j.watres.2007.03.012.

(27) Dao, V. H.; Cameron, N. R.; Saito, K. Synthesis, Properties and Performance of Organic Polymers Employed in Flocculation Applications. *Polym Chem* **2016**, *7* (1), 11–25. https://doi.org/https://doi.org/10.1039/c5py01572c.

(28) Gumfekar, S. P.; Soares, J. B. P. Polymer Reaction Engineering Tools to Design Multifunctional Polymer Flocculants. *Chemosphere (Oxford)* **2018**, *210*, 156–165. https://doi.org/10.1016/j.chemosphere.2018.06.175.

(29) Gumfekar, S. P.; Soares, J. B. P. A Novel Hydrophobically-Modified Polyelectrolyte for Enhanced Dewatering of Clay Suspension. *Chemosphere (Oxford)* **2018**, *194*, 422–431. https://doi.org/10.1016/j.chemosphere.2017.12.009.

(30) Lu, H.; Wang, Y.; Li, L.; Kotsuchibashi, Y.; Narain, R.; Zeng, H. Temperature- and PH-Responsive Benzoboroxole-Based Polymers for Flocculation and Enhanced Dewatering of Fine Particle Suspensions. *ACS Appl Mater Interfaces* **2015**, *7* (49), 27176–27187. https://doi.org/10.1021/acsami.5b09874.

(31) Hripko, R.; Vajihinejad, V.; LopesMotta, F.; Soares, J. B. P. Enhanced Flocculation of Oil Sands Mature Fine Tailings Using Hydrophobically Modified Polyacrylamide Copolymers. *Global Challenges* **2018**, *2* (3), 1700135. https://doi.org/https://doi.org/10.1002/gch2.201700135.

(32) Xu, K.; Wang, H.; Liang, X.; Tan, Y.; Yao, X.; Wang, P. A Novel Hyperbranched Polymeric Flocculant for Waste-Water Treatment. *J Polym Environ* **2018**, *26* (7), 2782–2792. https://doi.org/10.1007/s10924-017-1120-4.

(33) Barra, A.; Santos, J. D. C.; Silva, M. R. F.; Nunes, C.; Ruiz-Hitzky, E.; Gonçalves, I.; Yildirim, S.; Ferreira, P.; Marques, P. A. A. P. Graphene Derivatives in Biopolymer-Based Composites for Food Packaging Applications. *Nanomaterials* **2020**, *10* (10), 1–32. https://doi.org/10.3390/nano10102077.

(34) Kopeć, M.; Spanjers, J.; Scavo, E.; Ernens, D.; Duvigneau, J.; Julius Vancso, G. Surface-Initiated ATRP from Polydopamine-Modified TiO2 Nanoparticles. *Eur Polym J* **2018**, *106*, 291–296. https://doi.org/10.1016/J.EURPOLYMJ.2018.07.033.

(35) Averick, S.; Simakova, A.; Park, S.; Konkolewicz, D.; Magenau, A. J. D.; Mehl, R. A.; Matyjaszewski, K. ATRP under Biologically Relevant Conditions: Grafting from a Protein. *ACS Macro Lett* **2012**, *1* (1), 6–10. https://doi.org/10.1021/MZ200020C/SUPPL_FILE/MZ200020C_SI_001.PDF.

(36) Contreras, C. B.; Weibel, D. E.; Strumia, M. C. Polystyrene Brushes/TiO2 Nanoparticles Prepared via SI-ATRP on Polypropylene and Its Superhydrophobicity. *Journal of polymer research* **2021**, *28* (4). https://doi.org/10.1007/s10965-021-02462-9.

(37) Xie, X.; Gao, H.; Luo, X.; Su, T.; Zhang, Y.; Qin, Z. Polyethyleneimine Modified Activated Carbon for Adsorption of Cd(II) in Aqueous Solution. *J Environ Chem Eng* **2019**, *7* (3), 103183. https://doi.org/10.1016/j.jece.2019.103183.

(38) Sun, S.; Wu, P. A One-Step Strategy for Thermal- and PH-Responsive Graphene Oxide Interpenetrating Polymer Hydrogel Networks. *J Mater Chem* **2011**, *21* (12), 4095–4097. https://doi.org/10.1039/c1jm10276a.

(39) Bousquet, A.; Awada, H.; Hiorns, R. C.; Dagron-Lartigau, C.; Billon, L. Conjugated-Polymer Grafting on Inorganic and Organic Substrates: A New Trend in Organic Electronic Materials. *Prog Polym Sci* **2014**, *39* (11), 1847–1877. https://doi.org/https://doi.org/10.1016/j.progpolymsci.2014.03.003.

(40) Wu, T.; Efimenko, K.; Genzer, J. Combinatorial Study of the Mushroom-to-Brush Crossover in Surface Anchored Polyacrylamide. *J Am Chem Soc* **2002**, *124* (32), 9394–9395. https://doi.org/10.1021/JA027412N/ASSET/IMAGES/LARGE/JA027412NF00002.JPEG.

(41) Zhang, H.; Du, Z.; Jiang, Y.; Yu, Q. Preparation and Characterization of Grafting Polyacrylamide from PET Films by SI-ATRP via Water-Borne System. *J Appl Polym Sci* **2012**, *126* (6), 1941–1955. https://doi.org/10.1002/APP.36865.

(42) Matyjaszewski, K. Atom Transfer Radical Polymerization (ATRP): Current Status and Future Perspectives. *Macromolecules* **2012**, *45* (10), 4015–4039. https://doi.org/10.1021/ma3001719.

(43) Braunecker, W. A.; Matyjaszewski, K. Controlled/Living Radical Polymerization: Features, Developments, and Perspectives. *Progress in Polymer Science (Oxford)* **2007**, *32* (1), 93–146. https://doi.org/10.1016/j.progpolymsci.2006.11.002.

(44) Matyjaszewski, K. Controlled Radical Polymerization: State-of-the-Art in 2011. *ACS Symposium Series* **2012**, *1100*, 1–13. https://doi.org/10.1021/bk-2012-1100.ch001.

(45) Matyjaszewski, K.; Xia, J. Atom Transfer Radical Polymerization. *Chem Rev* **2001**, *101* (9), 2921–2990. https://doi.org/10.1021/cr940534g.

(46) V. Tsarevsky, N.; Matyjaszewski, K. "Green" Atom Transfer Radical Polymerization: From Process Design to Preparation of Well-Defined

Environmentally Friendly Polymeric Materials. *Chem Rev* **2007**, *107* (6), 2270–2299. https://doi.org/10.1021/cr050947p.

(47) Lorandi, F.; Fantin, M.; Matyjaszewski, K. Atom Transfer Radical Polymerization: A Mechanistic Perspective. *J Am Chem Soc* **2022**, *144* (34), 15413–15430. https://doi.org/10.1021/JACS.2C05364/ASSET/IMAGES/LARGE/JA2C05364_0017.JPEG.

(48) Wang, J.-S.; Matyjaszewski, K. Controlled/"living" Radical Polymerization. Atom Transfer Radical Polymerization in the Presence of Transition-Metal Complexes. *J Am Chem Soc* **2002**, *117* (20), 5614–5615. https://doi.org/10.1021/ja00125a035.

(49) Qiu, J.; Charleux, B.; Matyjaszewski, K. Controlled/Living Radical Polymerization in Aqueous Media: Homogeneous and Heterogeneous Systems. *Prog Polym Sci* **2001**, *26* (10), 2083–2134. https://doi.org/10.1016/S0079-6700(01)00033-8.

(50) Khabibullin, A.; Mastan, E.; Matyjaszewski, K.; Zhu, S. Surface-Initiated Atom Transfer Radical Polymerization. In *Controlled Radical Polymerization at and from Solid Surfaces*; Vana, P., Ed.; Springer International Publishing: Cham, 2016; pp 29–76. https://doi.org/10.1007/12_2015_311.

(51) Moad, G.; Rizzardo, E.; Thang, S. H. Living Radical Polymerization by the RAFT Process. *Aust J Chem* **2005**, *58* (6), 379–410.

(52) Lai, J. T.; Filla, D.; Shea, R. Functional Polymers from Novel Carboxyl-Terminated Trithiocarbonates as Highly Efficient RAFT Agents. *Macromolecules* **2002**, *35* (18), 6754–6756. https://doi.org/10.1021/ma020362m.

(53) Chiefari, J.; Chong, Y. K. (Bill); Ercole, F.; Krstina, J.; Jeffery, J.; Le, T. P. T.; Mayadunne, R. T. A.; Meijs, G. F.; Moad, C. L.; Moad, G.; Rizzardo, E.; Thang, S. H. Living Free-Radical Polymerization by Reversible Addition−Fragmentation Chain Transfer: The RAFT Process. *Macromolecules* **1998**, *31* (16), 5559–5562. https://doi.org/10.1021/ma9804951.

(54) Moad, G.; Rizzardo, E.; Thang, S. H. Radical Addition–Fragmentation Chemistry in Polymer Synthesis. *Polymer (Guildf)* **2008**, *49* (5), 1079–1131.

(55) Tebben, L.; Studer, A. Nitroxides: Applications in Synthesis and in Polymer Chemistry. *Angewandte Chemie International Edition* **2011**, *50* (22), 5034–5068. https://doi.org/https://doi.org/10.1002/anie.201002547.

(56) Sciannamea, V.; Jérôme, R.; Detrembleur, C. In-Situ Nitroxide-Mediated Radical Polymerization (NMP) Processes: Their Understanding and Optimization. *Chem Rev* **2008**, *108* (3), 1104–1126. https://doi.org/10.1021/cr0680540.

(57) Benoit, D.; Chaplinski, V.; Braslau, R.; Hawker, C. J. Development of a Universal Alkoxyamine for "Living" Free Radical Polymerizations. *J Am Chem Soc* **1999**, *121* (16), 3904–3920. https://doi.org/10.1021/ja984013c.

(58) Nicolas, J.; Guillaneuf, Y.; Lefay, C.; Bertin, D.; Gigmes, D.; Charleux, B. Nitroxide-Mediated Polymerization. *Prog Polym Sci* **2013**, *38* (1), 63–235. https://doi.org/https://doi.org/10.1016/j.progpolymsci.2012.06.002.

(59) Hawker, C. J.; Bosman, A. W.; Harth, E. New Polymer Synthesis by Nitroxide Mediated Living Radical Polymerizations. *Chem Rev* **2001**, *101* (12), 3661–3688. https://doi.org/10.1021/cr990119u.

(60) Greszta, D.; Mardare, D.; Matyjaszewski, K. “Living” Radical Polymerization. 1. Possibilities and Limitations. *Macromolecules* **1994**, *27* (3), 638–644. https://doi.org/10.1021/ma00081a002.

(61) Goto, A.; Fukuda, T. Kinetics of Living Radical Polymerization. *Prog Polym Sci* **2004**, *29* (4), 329–385.

(62) Matyjaszewski, K. Lifetimes of Polystyrene Chains in Atom Transfer Radical Polymerization. *Macromolecules* **1999**, *32* (26), 9051–9053.

(63) Krys, P.; Matyjaszewski, K. Kinetics of Atom Transfer Radical Polymerization. *Eur Polym J* **2017**, *89* (January), 482–523. https://doi.org/10.1016/j.eurpolymj.2017.02.034.

(64) Wang, J.-S.; Matyjaszewski, K. Controlled /“ Living ” Radical Polymerization . Atom Transfer Radical Polymerization in the Presence of Pi-Cl. *J. Am. Chem. Soc.* **1995**, *117* (6), 5614–5615.

(65) V. Tsarevsky, N.; Pintauer, T.; Matyjaszewski, K. Deactivation Efficiency and Degree of Control over Polymerization in ATRP in Protic Solvents. *Macromolecules* **2004**, *37* (26), 9768–9778. https://doi.org/10.1021/ma048438x.

(66) Tang, W.; Tsarevsky, N. V.; Matyjaszewski, K. Determination of Equilibrium Constants for Atom Transfer Radical Polymerization. *J Am Chem Soc* **2006**, *128* (5), 1598–1604. https://doi.org/10.1021/JA0558591/SUPPL_FILE/JA0558591SI20051207_064651.PDF.

(67) Tsarevsky, N. V.; Braunecker, W. A.; Matyjaszewski, K. Electron Transfer Reactions Relevant to Atom Transfer Radical Polymerization. *J Organomet Chem* **2007**, *692* (15), 3212–3222. https://doi.org/10.1016/J.JORGANCHEM.2007.01.051.

(68) Fantin, M.; Isse, A. A.; Gennaro, A.; Matyjaszewski, K. Understanding the Fundamentals of Aqueous ATRP and Defining Conditions for Better Control. *Macromolecules* **2015**, *48* (19), 6862–6875. https://doi.org/10.1021/acs.macromol.5b01454.

(69) Simakova, A.; Averick, S. E.; Konkolewicz, D.; Matyjaszewski, K. Aqueous ARGET ATRP. *Macromolecules* **2012**, *45* (16), 6371–6379. https://doi.org/10.1021/ma301303b.

(70) Burdyńska, J.; Cho, H. Y.; Mueller, L.; Matyjaszewski, K. Synthesis of Star Polymers Using ARGET ATRP. *Macromolecules* **2010**, *43* (22), 9227–9229. https://doi.org/10.1021/ma101971z.

(71) Szczepaniak, G.; Fu, L.; Jafari, H.; Kapil, K.; Matyjaszewski, K. Making ATRP More Practical: Oxygen Tolerance. *Acc Chem Res* **2021**, *54* (7), 1779–1790. https://doi.org/10.1021/acs.accounts.1c00032.

(72) A. Braunecker, W.; V. Tsarevsky, N.; Gennaro, A.; Matyjaszewski, K. Thermodynamic Components of the Atom Transfer Radical Polymerization Equilibrium: Quantifying Solvent Effects. *Macromolecules* **2009**, *42* (17), 6348–6360. https://doi.org/10.1021/ma901094s.

(73) Matyjaszewski, K.; Hongchen, D.; Jakubowski, W.; Pietrasik, J.; Kusumo, A. Grafting from Surfaces for "Everyone": ARGET ATRP in the Presence of Air. *Langmuir* **2007**, *23* (8), 4528–4531. https://doi.org/10.1021/la063402e.

(74) Tsarevsky, N. V.; Braunecker, W. A.; Vacca, A.; Gans, P.; Matyjaszewski, K. Competitive Equilibria in Atom Transfer Radical Polymerization. *Macromol Symp* **2007**, *248* (1), 60–70. https://doi.org/10.1002/MASY.200750207.

(75) Tang, W.; Kwak, Y.; Braunecker, W.; V. Tsarevsky, N.; L. Coote, M.; Matyjaszewski, K. Understanding Atom Transfer Radical Polymerization: Effect of Ligand and Initiator Structures on the Equilibrium Constants. *J Am Chem Soc* **2008**, *130* (32), 10702–10713. https://doi.org/10.1021/ja802290a.

(76) Wang, Z.; Yan, J.; Liu, T.; Wei, Q.; Li, S.; Olszewski, M.; Wu, J.; Sobieski, J.; Fantin, M.; Bockstaller, M. R.; Matyjaszewski, K. Control of Dispersity and Grafting Density of Particle Brushes by Variation of ATRP Catalyst Concentration. *ACS Macro Lett* **2019**, *8* (7), 859–864. https://doi.org/10.1021/acsmacrolett.9b00405.

(77) Matyjaszewski, K.; J. Miller, P.; Shukla, N.; Immaraporn, B.; Gelman, A.; B. Luokala, B.; M. Siclovan, T.; Kickelbick, G.; Vallant, T.; Hoffmann, H.; Pakula, T. Polymers at Interfaces: Using Atom Transfer Radical Polymerization in the Controlled Growth of Homopolymers and Block Copolymers from Silicon Surfaces in the Absence of Untethered Sacrificial Initiator. *Macromolecules* **1999**, *32* (26), 8716–8724. https://doi.org/10.1021/ma991146p.

(78) Gillies, M. B.; Matyjaszewski, K.; Norrby, P.-O.; Pintauer, T.; Poli, R.; Richard, P. A DFT Study of R−X Bond Dissociation Enthalpies of Relevance to the Initiation Process of Atom Transfer Radical Polymerization. *Macromolecules* **2003**, *36* (22), 8551–8559. https://doi.org/10.1021/ma0351672.

(79) Pintauer, T.; Reinöhl, U.; Feth, M.; Bertagnolli, H.; Matyjaszewski, K. Extended X-Ray Absorption Fine Structure Study of Copper(I) and Copper(II) Complexes in Atom Transfer Radical Polymerization. *Eur J Inorg Chem* **2003**, *2003* (11), 2082–2094. https://doi.org/https://doi.org/10.1002/ejic.200200503.

(80) Tang, W.; Matyjaszewski, K. Effects of Initiator Structure on Activation Rate Constants in ATRP. *Macromolecules* **2007**, *40* (6), 1858–1863. https://doi.org/10.1021/ma062897b.

(81) Arshadi, M.; Yamdagni, R.; Kebarle, P. Hydration of the Halide Negative Ions in the Gas Phase. II. Comparison of Hydration Energies for the Alkali Positive and Halide Negative Ions. *J Phys Chem* **1970**, *74* (7), 1475–1482. https://doi.org/10.1021/j100702a014.

(82) Pintauer, T.; McKenzie, B.; Matyjaszewski, K. Determination of the Equilibrium Constant for Bromide Dissociation from ATRP Active Cu(II) Complexes and Its Effect on the Overall Catalyst Activity. *ABSTRACTS OF PAPERS OF THE AMERICAN CHEMICAL SOCIETY* **2002**, *224*, U441–U441.

(83) Fundeanu, I.; van der Mei, H. C.; Schouten, A. J.; Busscher, H. J. Polyacrylamide Brush Coatings Preventing Microbial Adhesion to Silicone Rubber. *Colloids Surf B*

Biointerfaces **2008**, *64* (2), 297–301. https://doi.org/10.1016/J.COLSURFB.2008.02.005.

(84) Xiao, D.; Wirth, M. J. Kinetics of Surface-Initiated Atom Transfer Radical Polymerization of Acrylamide on Silica. *Macromolecules* **2002**, *35* (8), 2919–2925. https://doi.org/10.1021/MA011313X/ASSET/IMAGES/LARGE/MA011313XF00006.JPEG.

(85) Sun, Y.; Du, H.; Deng, Y.; Lan, Y.; Feng, C. Preparation of Polyacrylamide via Surface-Initiated Electrochemical-Mediated Atom Transfer Radical Polymerization (SI-EATRP) for Pb2+ Sensing. *Journal of Solid State Electrochemistry* **2016**, *20* (1), 105–113. https://doi.org/10.1007/S10008-015-3008-3/TABLES/2.

(86) Lilge, I.; Schönherr, H. Control of Cell Attachment and Spreading on Poly(Acrylamide) Brushes with Varied Grafting Density. *Langmuir* **2016**, *32* (3), 838–847. https://doi.org/10.1021/ACS.LANGMUIR.5B04168/ASSET/IMAGES/LARGE/LA-2015-04168N_0011.JPEG.

(87) Pinchasik, B.-E.; Tauer, K.; Möhwald, H.; Skirtach B-E Pinchasik, A. G.; Möhwald, H.; Tauer, K.; Skirtach, A. G. Polymer Brush Gradients by Adjusting the Functional Density Through Temperature Gradient. *Adv Mater Interfaces* **2014**, *1* (2), 1300056. https://doi.org/10.1002/ADMI.201300056.

(88) Kong, X.; Kawai, T.; Abe, J.; Iyoda, T. Amphiphilic Polymer Brushes Grown from the Silicon Surface by Atom Transfer Radical Polymerization. *Macromolecules* **2001**, *34* (6), 1837–1844.

https://doi.org/10.1021/MA001152H/ASSET/IMAGES/LARGE/MA001152HF00009.JPEG.

(89) Tsukagoshi, T.; Kondo, Y.; Yoshino, N. Protein Adsorption on Polymer-Modified Silica Particle Surface. *Colloids Surf B Biointerfaces* **2007**, *54* (1), 101–107. https://doi.org/10.1016/J.COLSURFB.2006.10.004.

(90) Chakraborty, S.; Bishnoi, S. W.; Pérez-Luna, V. H. Gold Nanoparticles with Poly(N-Isopropylacrylamide) Formed via Surface Initiated Atom Transfer Free Radical Polymerization Exhibit Unusually Slow Aggregation Kinetics. *The Journal of Physical Chemistry C* **2010**, *114* (13), 5947–5955. https://doi.org/10.1021/jp910417g.

(91) Wu, L.; Glebe, U.; Böker, A. Synthesis of Hybrid Silica Nanoparticles Densely Grafted with Thermo and PH Dual-Responsive Brushes via Surface-Initiated ATRP. *Macromolecules* **2016**, *49* (24), 9586–9596. https://doi.org/10.1021/acs.macromol.6b01792.

(92) Tan, L.; Liu, B.; Siemensmeyer, K.; Glebe, U.; Böker, A. Synthesis of Thermo-Responsive Nanocomposites of Superparamagnetic Cobalt Nanoparticles/Poly(N-Isopropylacrylamide). *J Colloid Interface Sci* **2018**, *526*, 124–134. https://doi.org/https://doi.org/10.1016/j.jcis.2018.04.074.

(93) Wu, L.; Glebe, U.; Böker, A. Synthesis of Hybrid Silica Nanoparticles Densely Grafted with Thermo and PH Dual-Responsive Brushes via Surface-Initiated ATRP. *Macromolecules* **2016**, *49* (24), 9586–9596. https://doi.org/10.1021/acs.macromol.6b01792.

(94) Wang, J.; Pu, Q.; Ning, P.; Lu, S. Activated Carbon-Based Composites for Capturing CO2: A Review. *Greenhouse Gases: Science and Technology* **2021**, *11* (2), 377–393. https://doi.org/10.1002/ghg.2051.

(95) González-García, C. M.; González-Martín, M. L.; Denoyel, R.; Gallardo-Moreno, A. M.; Labajos-Broncano, L.; Bruque, J. M. Ionic Surfactant Adsorption onto Activated Carbons. *J Colloid Interface Sci* **2004**, *278* (2), 257–264. https://doi.org/10.1016/j.jcis.2004.06.012.

(96) Rashidi, N. A.; Yusup, S. An Overview of Activated Carbons Utilization for the Post-Combustion Carbon Dioxide Capture. *Journal of CO2 Utilization* **2016**, *13*, 1–16. https://doi.org/https://doi.org/10.1016/j.jcou.2015.11.002.

(97) Abd, A. A.; Othman, M. R.; Kim, J. *A Review on Application of Activated Carbons for Carbon Dioxide Capture: Present Performance, Preparation, and Surface Modification for Further Improvement*; Environmental Science and Pollution Research, 2021; Vol. 28. https://doi.org/10.1007/s11356-021-15121-9.

(98) Celzard, A.; Fierro, V.; Marêché, J. F.; Furdin, G. Advanced Preparative Strategies for Activated Carbons Designed for the Adsorptive Storage of Hydrogen. *Adsorption Science & Technology* **2007**, *25* (3–4), 129–142. https://doi.org/10.1260/026361707782398254.

(99) Gan, Y. X. Activated Carbon from Biomass Sustainable Sources. *C (Basel)* **2021**, *7* (2), 39. https://doi.org/10.3390/c7020039.

(100) Marsh, H.; Rodríguez-Reinoso, F. CHAPTER 2 - Activated Carbon (Origins). In *Activated Carbon*; Marsh, H., Rodríguez-Reinoso, F., Eds.; Elsevier Science Ltd:

Oxford, 2006; pp 13–86. https://doi.org/https://doi.org/10.1016/B978-008044463-5/50016-9.

(101) Bansal, R. C.; Goyal, M. *Activated Carbon Adsorption*; CRC Press, 2005. https://doi.org/10.1201/9781420028812.

(102) Daud, W. M. A. W.; Houshamnd, A. H. Textural Characteristics, Surface Chemistry and Oxidation of Activated Carbon. *Journal of Natural Gas Chemistry*. Elsevier B.V. 2010, pp 267–279. https://doi.org/10.1016/S1003-9953(09)60066-9.

(103) Rivera-Utrilla, J.; Sánchez-Polo, M.; Gómez-Serrano, V.; Álvarez, P. M.; Alvim-Ferraz, M. C. M.; Dias, J. M. Activated Carbon Modifications to Enhance Its Water Treatment Applications. An Overview. *J Hazard Mater* **2011**, *187* (1), 1–23. https://doi.org/https://doi.org/10.1016/j.jhazmat.2011.01.033.

(104) Lan, J.; Wang, B.; Bo, C.; Gong, B.; Ou, J. Progress on Fabrication and Application of Activated Carbon Sphere in Recent Decade. *Journal of Industrial and Engineering Chemistry* **2023**, *120*, 47–72. https://doi.org/10.1016/J.JIEC.2022.12.045.

(105) Teare, M.; Burrowes, A.; Baturin-Pollock, C.; Rokosh, D.; Evans, C.; Gigantelli, P.; Marsh, R. ST98-2012: Alberta's Energy Reserves 2011 and Supply/Demand Outlook 2012–2021. *Calgary, Alberta: Energy Resources Conservation Board* **2012**.

(106) Puente-Ornelas, R.; Lizcano-Zulaica, C. J.; Guzmán, A. M.; Zambrano, P. C.; Das-Roy, T. K. Dissolution of Refractories for Gasification Process of Petroleum Coke

for the Steel Industry. *Fuel* **2012**, *93*, 581–588. https://doi.org/https://doi.org/10.1016/j.fuel.2011.08.039.

(107) Fisher, K. S.; Vreugdenhil, A. J. Adsorption of Chromium (VI) Using an Activated Carbon Derived from Petroleum Coke Feedstock. *Int J Mol Sci* **2022**, *23* (24). https://doi.org/10.3390/ijms232416172.

(108) Strong, O. K. L.; Nazari, E.; Roy, T.; Scotland, K.; Pede, P. R.; Vreugdenhil, A. J. Transforming Micropores to Mesopores by Heat Cycling KOH Activated Petcoke for Improved Kinetics of Adsorption of Naphthenic Acids. *Heliyon* **2023**, *9* (2), e13500. https://doi.org/https://doi.org/10.1016/j.heliyon.2023.e13500.

(109) Fisher, K. S.; Vreugdenhil, A. J. Metal-Impregnated Petroleum Coke-Derived Activated Carbon for the Adsorption of Arsenic in Acidic Waters. *ACS Omega* **2023**, *8* (32), 29083–29100. https://doi.org/10.1021/acsomega.3c02078.

(110) Liu, Y.; Miao, X.; Zhu, J.; Zhang, Z.; Cheng, Z.; Zhu, X.; Liu, Y.; Miao, X.; Zhu, J.; Zhang, Z.; Cheng, Z.; Zhu, X. Polymer-Grafted Modification of Activated Carbon by Surface-Initiated AGET ATRP. *Macromol Chem Phys* **2012**, *213* (8), 868–877. https://doi.org/10.1002/MACP.201100668.

(111) Liu, P.; Wang, T. Surface-Initiated Atom Transfer Radical Polymerization of Hydroxyethyl Acrylate from Activated Carbon Powder with Homogenized Surface Groups. *Surface Review and Letters* **2007**, *14* (2), 269–275. https://doi.org/10.1142/S0218625X07009359.

(112) Bégin, S. J.; Scotland, K. M.; Pede, P. R.; Vreugdenhil, A. J. Polyacrylamide Grafted Activated Carbon by Surface-Initiated AGET ATRP for the Flocculation of

MFT. *Macromol Chem Phys* **2023**, *224* (22). https://doi.org/10.1002/macp.202300223.

(113) Striegel, A.; Yau, W. W.; Kirkland, J. J.; Bly, D. D. *Modern Size-Exclusion Liquid Chromatography: Practice of Gel Permeation and Gel Filtration Chromatography*; John Wiley & Sons, 2009.

(114) Hoffmann, G. G. *Infrared and Raman Spectroscopy*; DeGruyter STEM, 2023.

(115) Gupta, M. K.; Bansil, R. Laser Raman Spectroscopy of Polyacrylamide. *Journal of Polymer Science: Polymer Physics Edition* **1981**, *19* (2), 353–360. https://doi.org/https://doi.org/10.1002/pol.1981.180190214.

(116) van der Heide, P. *X-Ray Photoelectron Spectroscopy: An Introduction to Principles and Practices*; Wiley, 2012.

(117) Albert Einstein. On a Heuristic Point of View about the Creation and Conversion of Light . *Ann. Phys.* **1905**, *31*, 132–148.

(118) Bulmer, J. T.; Starr, J. Syncrude Analytical Methods for Oil Sand and Bitumen Processing. **1979**.

(119) Mikkelsen, L. H. The Shear Sensitivity of Activated Sludge: Relations to Filterability, Rheology and Surface Chemistry. *Colloids Surf A Physicochem Eng Asp* **2001**, *182* (1), 1–14. https://doi.org/https://doi.org/10.1016/S0927-7757(00)00772-X.

(120) Turchiuli, C.; Fargues, C. Influence of Structural Properties of Alum and Ferric Flocs on Sludge Dewaterability. *Chemical Engineering Journal* **2004**, *103* (1), 123–131. https://doi.org/https://doi.org/10.1016/j.cej.2004.05.013.

(121) Chen, C.-S.; Lau, Y. Y.; Mercer, S. M.; Robert, T.; Horton, J. H.; Jessop, P. G. The Effect of Switchable Water Additives on Clay Settling. *ChemSusChem* **2013**, *6* (1), 132–140. https://doi.org/https://doi.org/10.1002/cssc.201200465.

(122) Li, J.; Jiao, S.; Zhong, L.; Pan, J.; Ma, Q. Optimizing Coagulation and Flocculation Process for Kaolinite Suspension with Chitosan. *Colloids Surf A Physicochem Eng Asp* **2013**, *428*, 100–110. https://doi.org/https://doi.org/10.1016/j.colsurfa.2013.03.034.

(123) Lu, L.; Pan, Z.; Hao, N.; Peng, W. A Novel Acrylamide-Free Flocculant and Its Application for Sludge Dewatering. *Water Res* **2014**, *57*, 304–312. https://doi.org/https://doi.org/10.1016/j.watres.2014.03.047.

(124) Sworska, A.; Laskowski, J. S.; Cymerman, G. Flocculation of the Syncrude Fine Tailings: Part II. Effect of Hydrodynamic Conditions. *Int J Miner Process* **2000**, *60* (2), 153–161. https://doi.org/https://doi.org/10.1016/S0301-7516(00)00013-2.

(125) Koza, C. R.; Norton, G. A.; van Leeuwen, J. (Hans). Dewatering Investigations on Fungal Biomass Grown in Thin Stillage from a Dry-Mill Corn Ethanol Plant. *Biomass Bioenergy* **2017**, *97*, 65–69. https://doi.org/https://doi.org/10.1016/j.biombioe.2016.12.011.

(126) Thompson, D. K.; Motta, F. L.; Soares, J. B. P. Investigation on the Flocculation of Oil Sands Mature Fine Tailings with Alkoxysilanes. *Miner Eng* **2017**, *111*, 90–99. https://doi.org/10.1016/j.mineng.2017.06.008.

(127) Grand View Research. *GVR Report Cover Polyacrylamide Market Size, Share & Trends Analysis Report By Product (Cationic, Anionic), By Application (Water Treatment, Oil & Gas), By Region (Asia Pacific, North America), And Segment Forecasts, 2023 - 2030*; 2022. https://www.grandviewresearch.com/industry-analysis/polyacrylamide-market# (accessed 2024-07-31).

(128) Raju, J.; Roberts, J.; Taylor, M.; Patry, D.; Chomyshyn, E.; Caldwell, D.; Cooke, G.; Mehta, R. Toxicological Effects of Short-Term Dietary Acrylamide Exposure in Male F344 Rats. *Environ Toxicol Pharmacol* **2015**, *39* (1), 85–92. https://doi.org/10.1016/J.ETAP.2014.11.009.

(129) Yu, F.; Fu, R.; Xie, Y.; Chen, W. Isolation and Characterization of Polyacrylamide-Degrading Bacteria from Dewatered Sludge. *International Journal of Environmental Research and Public Health 2015, Vol. 12, Pages 4214-4230* **2015**, *12* (4), 4214–4230. https://doi.org/10.3390/IJERPH120404214.

(130) Liu, J.; Ren, J.; Xu, R.; Yu, B.; Wang, J. Biodegradation of Partially Hydrolyzed Polyacrylamide by Immobilized Bacteria Isolated from HPAM-Containing Wastewater. *Environ Prog Sustain Energy* **2016**, *35* (5), 1344–1352. https://doi.org/https://doi.org/10.1002/ep.12354.

(131) Maćczak, P.; Kaczmarek, H.; Ziegler-Borowska, M. Recent Achievements in Polymer Bio-Based Flocculants for Water Treatment. *Materials* **2020**, *13* (18). https://doi.org/10.3390/MA13183951.

(132) Jiang, X.; Li, Y.; Tang, X.; Jiang, J.; He, Q.; Xiong, Z.; Zheng, H. Biopolymer-Based Flocculants: A Review of Recent Technologies. *Environ Sci Pollut Res Int* **2021**, *28* (34), 46934. https://doi.org/10.1007/S11356-021-15299-Y.

(133) Pal, S.; Ghorai, S.; Dash, M. K.; Ghosh, S.; Udayabhanu, G. Flocculation Properties of Polyacrylamide Grafted Carboxymethyl Guar Gum (CMG-g-PAM) Synthesised by Conventional and Microwave Assisted Method. *J Hazard Mater* **2011**, *192* (3), 1580–1588. https://doi.org/10.1016/J.JHAZMAT.2011.06.083.

(134) Das, R.; Ghorai, S.; Pal, S. Flocculation Characteristics of Polyacrylamide Grafted Hydroxypropyl Methyl Cellulose: An Efficient Biodegradable Flocculant. *Chemical Engineering Journal* **2013**, *229*, 144–152. https://doi.org/10.1016/J.CEJ.2013.05.104.

(135) Scotland, K. M.; Bégin, S.; Strong, O. K. L.; Pede, P. R.; Vreugdenhil, A. J. The Development of a Novel Non-Leaching Flocculant, Derived from Activated Carbon and Polyacrylamide. *Canadian Journal of Chemical Engineering* **2023**. https://doi.org/10.1002/cjce.25040.

(136) Siyam, T. Development of Acrylamide Polymers for the Treatment of Waste Water. *Des Monomers Polym* **2001**, *4* (2), 107–168. https://doi.org/10.1163/156855500300203377.

(137) Zoppe, J. O.; Ataman, N. C.; Mocny, P.; Wang, J.; Moraes, J.; Klok, H. A. Surface-Initiated Controlled Radical Polymerization: State-of-the-Art, Opportunities, and Challenges in Surface and Interface Engineering with Polymer Brushes. *Chem Rev* **2017**, *117* (3), 1105–1318. https://doi.org/10.1021/acs.chemrev.6b00314.

(138) Jones, G. R.; Anastasaki, A.; Whitfield, R.; Engelis, N.; Liarou, E.; Haddleton, D. M. Copper-Mediated Reversible Deactivation Radical Polymerization in Aqueous Media. *Angewandte Chemie International Edition* **2018**, *57* (33), 10468–10482. https://doi.org/https://doi.org/10.1002/anie.201802091.

(139) Teodorescu, M.; Matyjaszewski, K. Atom Transfer Radical Polymerization of (Meth)Acrylamides. *Macromolecules* **1999**, *32* (15), 4826–4831. https://doi.org/10.1021/ma990175x.

(140) Wever, D. A. Z.; Polgar, L. M.; Stuart, M. C. A.; Picchioni, F.; Broekhuis, A. A. Polymer Molecular Architecture As a Tool for Controlling the Rheological Properties of Aqueous Polyacrylamide Solutions for Enhanced Oil Recovery. *Ind Eng Chem Res* **2013**, *52* (47), 16993–17005. https://doi.org/10.1021/ie403045y.

(141) Liu, Y.; Miao, X.; Zhu, J.; Zhang, Z.; Cheng, Z.; Zhu, X. Polymer-Grafted Modification of Activated Carbon by Surface-Initiated AGET ATRP. *Macromol Chem Phys* **2012**, *213* (8), 868–877. https://doi.org/10.1002/macp.201100668.

(142) Zhang, H.; Du, Z.; Jiang, Y.; Yu, Q. Preparation and Characterization of Grafting Polyacrylamide from PET Films by SI-ATRP via Water-Borne System. *J Appl Polym Sci* **2012**, *126* (6), 1941–1955. https://doi.org/https://doi.org/10.1002/app.36865.

(143) Mastan, E.; Xi, L.; Zhu, S. Factors Affecting Grafting Density in Surface-Initiated ATRP: A Simulation Study. *Macromol Theory Simul* **2016**, *25* (3), 220–228. https://doi.org/10.1002/mats.201500081.

(144) Masliyah, J.; Zhou, Z. J.; Xu, Z.; Czarnecki, J.; Hamza, H. Understanding Water-Based Bitumen Extraction from Athabasca Oil Sands. *Can J Chem Eng* **2004**, *82* (4), 628–654. https://doi.org/10.1002/cjce.5450820403.

(145) Saborimanesh, N. Toward Sustainable Remediation of Oil Sands Fine Tailings-A Review. *J Environ Manage* **2021**, *288*, 112418. https://doi.org/https://doi.org/10.1016/j.jenvman.2021.112418.

(146) Alberta Energy Regulator. *Directive 085: Fluid Tailings Management for Oil Sands Mining Projects*; 2022.

(147) Vajihinejad, V.; Guillermo, R.; Soares, J. B. P. Dewatering Oil Sands Mature Fine Tailings (MFTs) with Poly(Acrylamide-Co-Diallyldimethylammonium Chloride): Effect of Average Molecular Weight and Copolymer Composition. *Ind Eng Chem Res* **2017**, *56* (5), 1256–1266. https://doi.org/10.1021/acs.iecr.6b04348.

(148) Fellows, C. M.; Doherty, W. O. S. Insights into Bridging Flocculation. *Macromolecular Symposium* **2006**, *231*, 1–10. https://doi.org/10.1002/masy.200551301.

(149) Hunter, J. *Comprehensive Treatise of Electrochemistry*, 1st ed.; Yeager, E., Bockris, J. O., Conway, B. E., Eds.; Plenum Press: New York, 1980; Vol. 6.

(150) Fan, Y.; Ma, X.; Dong, X.; Feng, Z.; Dong, Y. Characterisation of Floc Size, Effective Density and Sedimentation under Various Flocculation Mechanisms. *Water Science and Technology* **2020**, *82* (7), 1261–1271. https://doi.org/10.2166/wst.2020.385.

(151) Gumfekar, S. P.; Soares, J. B. P. Polymer Reaction Engineering Tools to Design Multifunctional Polymer Flocculants. *Chemosphere* **2018**, *210*, 156–165. https://doi.org/10.1016/j.chemosphere.2018.06.175.

(152) Das, R.; Ghorai, S.; Pal, S. Flocculation Characteristics of Polyacrylamide Grafted Hydroxypropyl Methyl Cellulose: An Efficient Biodegradable Flocculant. *Chemical Engineering Journal* **2013**, *229*, 144–152. https://doi.org/https://doi.org/10.1016/j.cej.2013.05.104.

(153) Vajihinejad, V.; Gumfekar, S. P.; Dixon, D. V.; Silva, M. A.; Soares, J. B. P. Enhanced Dewatering of Oil Sands Tailings by a Novel Water-Soluble Cationic Polymer. *Sep Purif Technol* **2021**, *260*. https://doi.org/10.1016/j.seppur.2020.118183.

(154) Li, Y.; Kaminsky, H.; Revington, A.; Sadighian, A. *A PROTOCOL TO ASSESS AND SCREEN NEW FLOCCULANT FOR SUNCOR'S PASS PROGRAM PLANNING*; 2022.